# LASER DYNAMICS OF A MODE-LOCKED THULIUM/HOLMIUM FIBER LASER IN THE SOLITONIC AND THE STRETCHED PULSE REGIMES

by

RAJESH KADEL

M.S., Tribhuvan University, 2001
M.S., Kansas State University, 2008

AN ABSTRACT OF A DISSERTATION

submitted in partial fulfillment of the requirements for the degree

DOCTOR OF PHILOSOPHY

Department of Physics
College of Arts and Sciences

KANSAS STATE UNIVERSITY
Manhattan, Kansas

2014

# Abstract

Mode-locked lasers that produce short optical pulses in the mid-infrared wavelength region have been sought out for a wide range of applications such as free space communication, molecular spectroscopy, medical diagnostics, and remote sensing. Here, a thulium and holmium (Tm/Ho) co-doped fiber laser that mode-locks in both the solitonic and stretched-pulse regimes is used to produce ultra-short pulses in the 2 μm region. Nonlinear polarization rotation technique is used where fiber nonlinearity is responsible to mode-lock the laser. The anomalous group velocity dispersion of both the single mode and gain fibers used limit the laser operation in the solitonic regime where spectral bandwidth is 10 nm and hence the pulse duration is limited to 996 fs. In order to increase the spectral bandwidth and hence get the shorter pulses the anomalous dispersion of these fibers has to compensate using normal group velocity dispersion fiber in the laser cavity.

High numerical aperture fibers, which have normal group velocity dispersion around 2 μm due to its large and positive waveguide dispersion, can be used to compensate the anomalous dispersion of the gain and single mode fibers. We used a high numerical aperture fiber called UHNA4 in the laser cavity in order to compensate the anomalous dispersion of other fibers and mode-locked the laser in stretched pulse regime. The spectral bandwidth of the laser increased to 31 nm with corresponding pulse duration of 450 fs measured from the interferometric autocorrelation. The laser dynamics of the Tm/Ho co-doped fiber laser is also studied while going from the stretched-pulse to solitonic regime by fiber cut-back measurements of normal dispersion fiber. It was clearly observed that both the spectral bandwidth and the pulse duration changed significantly going from one region to the other.

# LASER DYNAMICS OF A MODE-LOCKED THULIUM/HOLMIUM FIBER LASER IN THE SOLITONIC AND THE STRETCHED PULSE REGIMES

by

RAJESH KADEL

M.S., Tribhuvan University, 2001
M.S., Kansas State University, 2008

A DISSERTATION

submitted in partial fulfillment of the requirements for the degree

DOCTOR OF PHILOSOPHY

Department of Physics
College of Arts and Sciences

KANSAS STATE UNIVERSITY
Manhattan, Kansas

2014

Approved by:

Major Professor
Brian R. Washburn

# Copyright

# Abstract

Mode-locked lasers that produce short optical pulses in the mid-infrared wavelength region have been sought out for a wide range of applications such as free space communication, molecular spectroscopy, medical diagnostics, and remote sensing. Here, a thulium and holmium co-doped fiber laser that mode-locks in both the solitonic and stretched-pulse regimes is used to produce ultra-short pulses in the 2 μm region. Nonlinear polarization rotation technique is used where fiber nonlinearity is responsible to mode-lock the laser. The anomalous group velocity dispersion of both the single mode and gain fibers used limit the laser operation in the solitonic regime where spectral bandwidth is 10 nm and hence the pulse duration is limited to 996 fs. In order to increase the spectral bandwidth and hence get the shorter pulses the anomalous dispersion of these fibers has to compensate using normal group velocity dispersion fiber in the laser cavity.

High numerical aperture fibers, which have normal group velocity dispersion around 2 μm due to its large and positive waveguide dispersion, can be used to compensate the anomalous dispersion of the gain and single mode fibers. We used a high numerical aperture fiber called UHNA4 in the laser cavity in order to compensate the anomalous dispersion of other fibers and mode-locked the laser in stretched pulse regime. The spectral bandwidth of the laser increased to 31 nm with corresponding pulse duration of 450 fs measured from the interferometric autocorrelation. The laser dynamics of the Tm/Ho co-doped fiber laser is also studied while going from the stretched-pulse to solitonic regime by fiber cut-back measurements of normal dispersion fiber. It was clearly observed that both the spectral bandwidth and the pulse duration changed significantly going from one region to the other.

# Table of Contents

# List of Figures

# List of Tables

# Acknowledgements

First and foremost, I would like to express my sincere gratitude and thanks to my research advisor Professor Dr. Brian Washburn for giving me the opportunity to work in such an exciting research area. Your wisdom, knowledge and generosity have guided me throughout my research and graduate studies. Thank you for your continuous support and encouragement. Without your support, this thesis could not be completed. It is my pleasure and honor to thank Dr. Kristan Corwin for her numerous helpful advices and insightful discussion on each and every work of this thesis. She is one of the nicest people I have ever met. I would like to thank my graduate committee members: Dr. Carlos Trallero, Prof. Andrew Rys for the invaluable time and suggestions. I would also like to thank Prof. Daniel Swenson for being an outside chairperson of my graduate committee.

I am thankful to all the faculty members and staffs of Physics department for your direct or indirect support during my graduate studies. I would like to thank both former and current members of the Washburn and Corwin group. Especially, I would like to thank Dr. Jinkang Lim and Dr. Andrew Jones for helping me to learn some of the experimental skills. I always love to talk with them. I also thank to my nearest and dearest lab mates: Dr. Karl Tillman, Dr. Kevin Knabe, Dr. Will Hageman, Wu Shun, Chenchen Wang, May Ebbeni, Neda Dadashzadeh, Turghun Matniyaz, Marry Harner, and Hu Xiaohong for your helpfulness and ever-smiling faces!

I would like to thank my friends and seniors from Nepalese community of Manhattan, especially: Dr. Khem Acharya, Dr. Rajesh Thapa, Dr. Mukta Bhandari, Dr. Shambhu Ghimire,

Dr. Rajan Dhaubhadel, Dr. Deepak Shrestha, and Dr. Shruti Shrestha for your support and encouragement during my graduate study and stay in Manhattan.

My very special thanks go to my parents and family for their constant guidance and encouragements throughout my life. I would like to thank my wife Sudha for your everlasting love and support in my journey of life. Finally, thanks to my lovely daughter Seijal for making me a cheerful dad.

# Chapter 1 - Introduction

Optical fibers exhibit many properties that are extremely useful for the production of both pulsed and continuous wave lasers. For example, an optical fiber can guide light in well-defined spatial mode with low loss over long distances, which is a desirable feature for a laser cavity. Additionally, the fiber can serve as a host to rare-earth dopants which can serve as the laser gain. And finally, the fiber exhibits nonlinear optical effects that can serve as a self-gating mechanism for the production of ultrashort pulse trains. All these properties together make optical fibers the ideal medium for producing high power, high bandwidth ultrashort pulse trains. Since the fiber lasers are compact, robust, alignment-free operation, efficient heat dissipation and low-cost maintenance, they are considered as serious competitors over the traditional solid state and gas (such as Nd:YAG, $CO_2$) lasers. The earliest form of fiber laser was demonstrated by E. Snitzer and his colleagues [1]. The fiber lasers can be operated in continuous-wave as well as in pulsed mode with an output of one or more pulses per round-trip. Pulsed lasers, which are the focus of this thesis, have a variety of important applications in areas of fundamental research as well as in medical and industrial fields, depending on the wavelength and pulse width.

In a fiber laser, the active gain medium is a length of fiber whose core doped with rare-earth cations such as neodymium ($Nd^{3+}$), praseodymium ($Pr^{3+}$), ytterbium ($Yb^{3+}$), erbium ($Er^{3+}$), thulium ($Tm^{3+}$) and holmium ($Ho^{3+}$). The lasing wavelength from the fiber lasers depend on both the rare-earth cations doped in the core and the host materials. The emission spectrum of the fiber lasers can cover from ultra-violet to mid-infrared as shown in Figure 1.1. When Nd-, Er-, Tm-, Pr-, or Ho-doped in the fluorozicronate (ZBLAN) glass fiber the emission wavelength ranges from the ultra-violet to visible regime by up-conversion effects [2-5]. Yb-, or Nd-doped

silica fiber emits the light around 1 µm [6, 7]. Er-doped silica fiber lasers provide the emission wavelength around 1.5 µm [8]. Since this wavelength is located in the telecommunication window, Er-doped fiber lasers have been extensively studied in past years. When Tm-, or Ho-doped silica or germinate fibers, the emission wavelength covers around 2 µm [9-11] . Emission of wavelength longer than 2 µm is always challenging due to lack of either doping element or as host materials that can guide the light at longer wavelengths. The infrared transmission in the glass is controlled by the phonon density of states i.e. the longest emitting wavelength from the fiber laser is always shorter than its maximum transmissible wavelength because the phonon density of states determines the radiative efficiencies of the fluorescence transition of rare-earth cations [12].

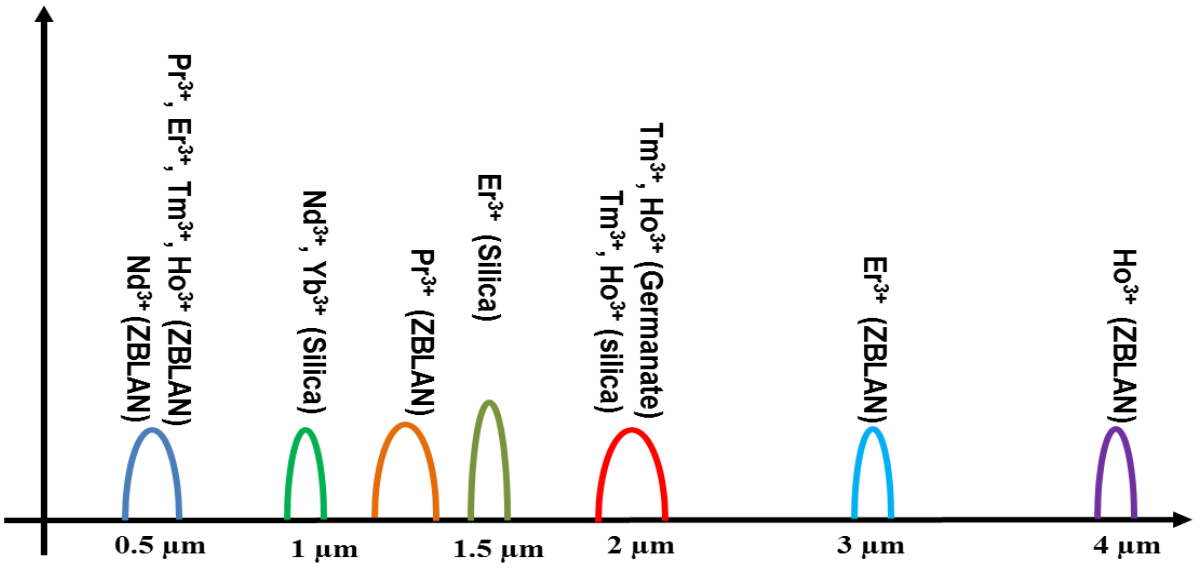


**Figure 1.1 Fluorescence wavelength of the rare-earth cations laser transitions doped in different types of host glasses. The lasing wavelength depends both on the rare-earth cations and the host materials.**

Due to high single pass gain and broad gain spectral bandwidths, rare-earth doped fibers are attractive gain medium for mode-locked fiber lasers to generate ultrashort pulses. Various mode-locking techniques were implemented in these rare-earth doped fiber lasers in order to generate ultrashort and high peak power pulses that can cover a wide range of wavelengths from ultra-violet to mid-infrared.

## 1.1 Near Infrared Pulsed Fiber Lasers

Ultrashort pulses are generated in a laser by locking the longitudinal cavity modes of the laser cavity together and this is process known as mode-locking. When an active or nonlinear pulse-forming element is incorporated inside the laser cavity the mode-locking can be achieved and the details of mode-locking will be discussed in Chapter 2. The output of such a laser is a train of pulses, each of ~100 fs duration separated by ~ 10 ns. Fiber based ultrafast pulse sources have been intensively studied after the first demonstration of ultrashort pulse generation in optical fibers in 1990 [13, 14]. A variety of mode-locking mechanisms have been developed in order to generate the optical pulses in different wavelength regimes. Mainly, ultrashort pulses are created either by active mode-locking or passive mode-locking. In active mode-locking, a fast shutter is used inside the laser cavity and it can produce the optical pulses with pulse durations of ~ 100 ps or longer. Hence, in order to generate ultrashort pulses passive mode-locking is preferred in which a fiber nonlinearity is used to create the effect known as self-amplitude modulation (SAM), where the pulse modulates its own amplitude via the nonlinearity and creating a train of ultrashort pulses. Passive mode-locking in fiber lasers can be obtained by various methods as will be described in Chapter 2 of this thesis. The most commonly used method is Kerr-type mode-locking where a nonlinear interferometer inside the laser cavity acts

as a saturable absorber [15]. This method is known as nonlinear polarization evolution (NPE) which depends on the nonlinear interference between two polarization modes. In fiber lasers, the most common approach to generate ultrashort pulses is soliton mode-locking where the net cavity dispersion is negative and is balanced by the nonlinear effects of the fiber triggered by the high intensity pulse itself. The pulse duration in the soliton mode-locking is set by the condition $Z_p \leq 3Z_0$ [16], where $Z_0$ is the soliton period and $Z_p$ is the cavity length. A cavity length of 50 cm is needed to achieve 100 fs pulse duration in order to satisfy above condition. Thus, it is very hard to have such as short cavity length in the fiber laser and also not easy to compensate the dispersion and nonlinearity. To overcome such limitations associated with the soliton mode-locking there is another approach of mode-locking where alternate segments of normal and anomalous dispersion fibers were put inside the cavity such that the pulse maintains the minimum duration only over small sections of the cavity and hence experiences significantly less nonlinear effects. This type of laser configuration is known as stretched-pulse and will be discussed in Chapter 5.

A mode-locked erbium-doped fiber laser near 1.5 μm was demonstrated with pulse duration of 4 ps in 1989 [17]. There is strong need to generate ultrashort pulse for a number of applications such as frequency metrology [18]. A number of techniques had been developed and implemented in order to achieve the shortest pulse possible. I. N. Duling III demonstrated an all-fiber ring soliton mode-locked laser with pulse duration of 2 ps using a nonlinear-optical fiber loop mirror [15]. Mode-locking with nonlinear polarization rotation (NPR), 452 fs pulse was generated from an erbium-doped fiber laser [19]. Later a 77 fs pulse was generated from a stretched-pulse mode-locked all-fiber ring laser by dispersion compensation inside the laser cavity [20]. To the date, the shortest pulse duration form the mode-locked erbium-doped fiber

laser is 37.4 fs at center wavelength near 1550 nm [21]. A broad (~200 nm) spectrum with ~20 fs pulse duration is generated form a Yb-doped fiber laser near 1 μm using highly nonlinear photonic crystal fiber (PCF) as normal dispersion fiber inside the laser cavity [22].

All the works mention above can generate the ultrashort pulses in the near infrared (NIR). As discussed earlier, the emission wavelength from the rare-earth doped fibers can cover wide range of wavelength and hence these well-developed techniques can be used to generate ultrashort pulses in other regions especially the mid-infrared.

## 1.2 Creating Pulsed Fiber Lasers in the Mid-Infrared

Extending the laser wavelength into the mid-infrared (MIR) spectral region has necessitated the use of fluoride glass fiber due to its low phonon energy and high loss of the fused silica fiber at longer wavelengths. Laser emission around 2.7 μm can be obtained when Er-, or Ho- is doped in to the fluoride glass [23-25] . A Ho-doped fluoride fiber laser could provide emission around 3.9 μm under cryogenic conditions [26]. This is the longest wavelength emitted from a fiber laser till now. Due to the poor physical properties of the fluoride glasses, it is a significant challenge to get high output power from fluoride fiber lasers. The maximum output power from fluoride fiber lasers is 24 W at 2.7 μm [24].

Longer wavelength emission could be possible in other ways, such as quantum cascade laser [27], gas laser [18] and nonlinear phenomena where nonlinear effects are exploited to transfer energy from the visible or near-infrared region to the mid-infrared region. $\chi^{(2)}$ (second order susceptibility) is responsible for the nonlinear effects of the bulk materials. MIR generation in bulk materials can be done either with an optical parametric amplifier (OPA) [28] or an optical

parametric oscillator (OPO) [29] based on difference frequency generation (DFG). The efficiency of these processes depends not only on the strength of the nonlinearity but also on the phase-matching condition of the corresponding optical waves. The phase-matching condition in the bulk materials (second order effect) can be achieved by the introduction of a short periodic region in which the sign of $\chi^{(2)}$ alternates. Since the bulk OPA or OPO's are expensive and alignment sensitive, there is always trends towards making fiber based sources due to its excellent beam quality. In nonlinear fiber optics, the mid-infrared generation can be achieved by Raman effects [30], fiber-based optical parametric processes [31], and supercontinuum generation. Fiber-based optical parametric processes operate through four-wave-mixing (FWM) with a pump wavelength close to zero dispersion wavelength (ZDW) of the fiber and are mediated by the $\chi^{(3)}$ nonlinearity of the glass and the phase-matching is continuous and wide, so signal gain occurs both near and far from the pump wavelength. Highly nonlinear fiber is used for FWM to generate MIR and will be discussed in Appendix B. ZBLAN fibers can also be used for mid-infrared supercontinuum generation when optically pumped by a pulsed laser [32].

The MIR laser sources discussed above are mainly in the form of continuous wave. It is very challenging to build a mode-locked fiber laser in the MIR region due to unviability of the gain fiber and optical elements needed to mode-lock the laser. To date there are only a few mode-locked lasers available in the MIR region, most of them are in solid state form. Using Kerr lens effect mode-locked femtosecond $Cr^{2+}$:ZnSe laser at 2.42 μm with pulse duration of 95 fs at repetition rate of 94.3 MHz has been demonstrated [33]. MIR pulses in the form of a frequency comb can be generated from difference frequency generation [34-39].

In this dissertation, I mainly focus on 2 μm light generation from a Tm/Ho co-doped silica fiber laser and the mode-locking in different pulse regimes in order to generate ultrashort pulses.

## 1.3 Mode-Locked Tm and Tm/Ho Doped Fiber Lasers

In the recent years, there has been a lot of interest in studying lasers operating near 2 μm because it lies in the so called "eye safe" wavelength region and it has a wide range of applications such as in medicine [40-42] , LIDAR [43], MIR generation [44] etc. Emission around 2 μm regions can be achieved when rare-earth elements thulium and holmium are doped in different host crystals and cores of the glass fibers. The first thulium laser at 2 μm was demonstrated when Tm:YAG was pumped by flash lamps in 1965 [45]. But many different host materials can be used to emit 2 μm light from thulium and holmium such as: Tm: $YAlO_3$, Tm:YLF [46], Tm: $Y_2O_3$ [47], Tm: LuAG [48], Ho: YAG [49].

These crystals based 2 μm laser sources are bulky and very hard to work with it. In order to make portable and compact lasers, thulium and holmium cations are incorporated into the core of the optical fibers to demonstrate the fiber laser. The main advantage of the Tm-and Ho-doped fiber lasers is that its emission can cover the gap between the band of $Nd^{3+}$ and $Er^{3+}$. When $Tm^{3+}$ ions are doped into the fused-silica glass fiber, the emission wavelength ranges from 1.7 to 2.1 μm [50]. When fluoride glass is used instead as the host material the emission wavelength can be extended to 2.3 μm [51] due to an increase in the number of metastable upper states which provide the additional transitions. Since the fluoride fibers are hard to handle due to their

physical properties, most of the work is done on silica fibers where Tm-or Ho-ions are doped into the core of the fiber.

Thulium or thulium/holmium co-doped silica fibers are better choices as a laser gain medium to generate 2 μm light due to their widest and broad fluorescence spectrum (1.7 to 2.1 μm) compared to other rare-earth ions. This indicates that ultrashort, high peak power pulse generation is possible. After demonstration of the first thulium continuous-wave fiber laser by D. C. Hanna *et al.* in 1988 [9], the first passively mode-locked thulium fiber laser is reported by L. E. Nelson *et al*. in 1995 [52] in which the pulse energy was limited to tens of picojoules. A number of attempts have been implemented in recent years in order to get the short pulse duration and hence the high pulse energy. Sharp *et al*. reported a soliton thulium-doped fiber laser with short cavity length and achieved 190 fs pulse width [53]. In both the cases, the laser is operating in the solitonic regime and hence the pulse energy is limited due to formation of spectral sidebands. Since a short pulse laser has a number of potential applications such as molecular spectroscopy, it is important to achieve the shortest pulse possible. The ultrashort pulse can be achieved by dispersion management inside the laser cavity. The details of dispersion management will be discussed in Chapters 3 and 4.

## 1.4 Thesis Problem Statement

Lasers have a number of applications such as free space optical communications, remote sensing, LIDAR, and standoff chemical detection. All these applications require propagation of laser light in the atmosphere. So it is highly desire to have a laser which is eye safe and hence 2 μm laser is a good candidate for these applications since this wavelength is absorbed by the

vitreous part of the eye and cannot reach to the retina and also lies in the atmospheric transparency window. Also, a number of atmospheric gases, e.g. $H_2O$, $CO_2$, $N_2O$, have absorption lines in the 2 µm region. Therefore, both continuous and pulsed 2 µm lasers can be used to detect and analyze these gases. Especially, pulsed lasers are the best candidates for the spectroscopy since they contains a large number of spectral components within its bandwidth and hence can detect a number of molecules in a single shot.

Wavelengths near the 2 µm range have strong absorption in water, which is the main constituent of biological tissue, and hence have minimal penetration depth in tissue as shown in Figure 1.2. So, substantial heating of small area of the tissue is achieved and makes the 2 µm laser a promising candidate for highly precise cutting of biological tissue. 2 µm lasers would be ideal sources for surgery since they can suppress the bleeding during laser cutting due to coagulation effects.

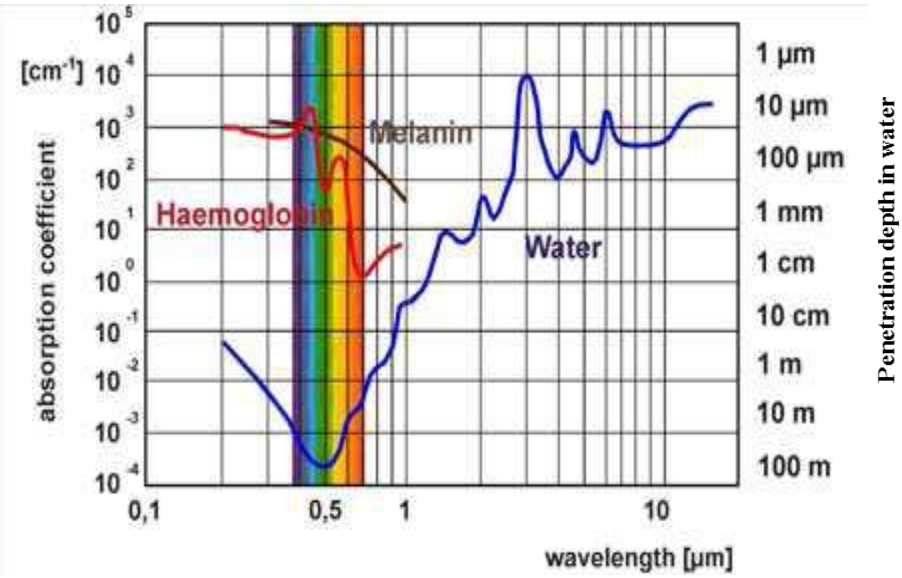


**Figure 1.2 Absorption and penetration depth in water and other biological tissue constituents for different wavelengths. This figure is taken from Ref.[54].**

Other possible applications of 2 µm lasers are nonlinear frequency conversion and supercontinuum generation in the MIR. Pulsed thulium doped fiber lasers can also be used to obtain the MIR by nonlinear frequency conversion processes [55]. High-energy multi-cycle infrared pulses near 2 µm generated via optical parametric amplification can be used to increase the high-harmonic cut-off energy [56]. For all of these practical applications, it is very important to have a compact, portable and cheap laser near 2 µm with high output energy. So the mode-locked Tm/Ho co-doped fiber laser is an excellent candidate to fulfill these requirements.

For the purpose, I performed the passively mode-locking of a thulium/holmium co-doped fiber laser in an all-fiber format to realize a compact and robust laser to achieve ultrashort pulses near 2 µm. The laser is mode-locked in two different regimes called solitonic and stretched-pulse by managing the intracavity dispersion. This laser could be extended to a phase-stabilized comb near 2 µm as described in ref [57] and used for mid-infrared supercontinuum in ZBLAN fiber that is ongoing project in the laboratory. I also investigated the laser dynamics of a pulsed Tm/Ho co-doped fiber laser when mode-locked in both the solitonic and stretched-pulsed regime. An experiment on optical parametric amplification was also performed with highly nonlinear fiber as nonlinear material for the MIR generation which will be discussed in Appendix B.

## 1.5 Importance of This Thesis

Continuous and pulsed laser sources in the mid-infrared region (3-12 µm) have long been sought after for many applications such as medical diagnostics [58], molecular identification [59], or gas monitoring [60]. In this region large numbers of molecules have characteristic vibrational transitions as shown in Figure 1.3. While continuous mid-infrared lasers have been

produced by molecular gas lasers or by quantum cascade lasers, high repetition frequency pulsed mid-infrared lasers have been more elusive. Due to the success of using direct frequency comb-based spectroscopy in the visible and near-infrared [61], there is a strong desire to push phase-stabilized frequency combs to the mid-infrared region from 2.5 to 12 μm. Visible and near-infrared combs are generated by phase-stabilized mode-locked lasers that produce femtosecond duration pulses at repetition frequencies in the megahertz. Such combs have been produced using solid-state lasers such as Ti:sapphire or Cr:forsterite; and by rare-earth doped fiber lasers. These lasers have wide bandwidths and are thus able to produce short duration, high peak power pulses. The frequency combs from these lasers can be extended to wavelengths outside their gain bandwidth using fiber nonlinearities [62].

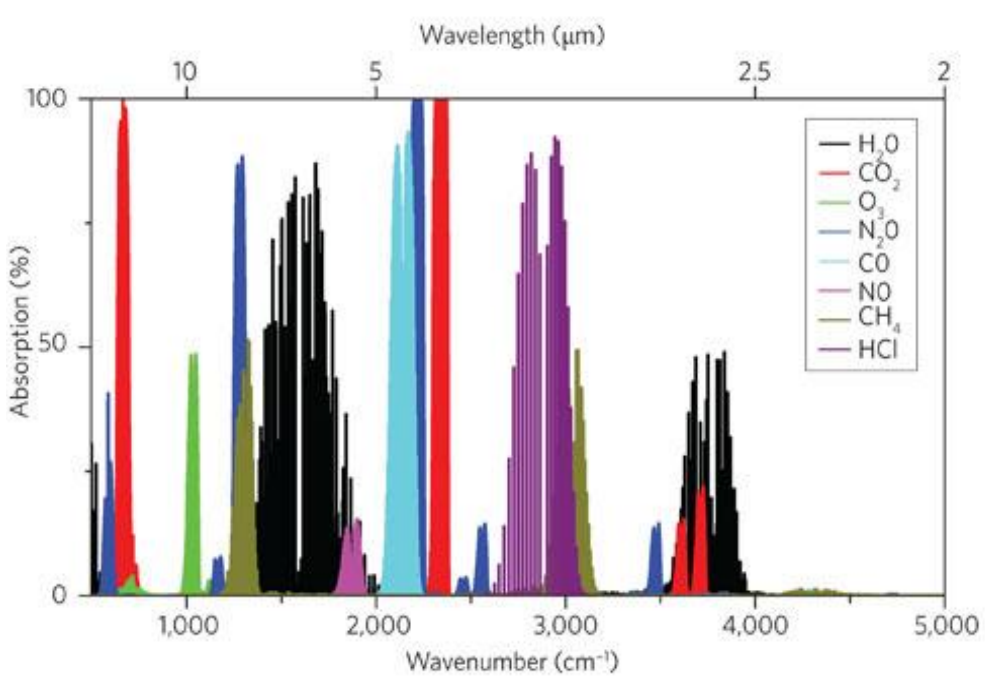


**Figure 1.3 Molecular mid-infrared fingerprints. Absorption at the line center for the main isotopologue of various gaseous molecules in the wavelength region of 2-20 μm. This figure is taken from Ref. [63].**

Unfortunately there are few lasers that can produce a mid-infrared frequency comb directly. Solid-state lasers produce frequency combs in the visible and near-infrared, and these combs can be extended into the mid-infrared using difference frequency generation [63, 64]. An alternative method is to use mode-locked fiber laser-based combs and extend it to the mid-infrared using nonlinear effects such as self-phase modulation (SPM). Mode-locked erbium doped fiber (EDF) lasers are the natural choice since they have been shown to generate combs out to 2.3 μm in highly nonlinear fibers, limited only by the strong IR absorption of fused silica [65]. Hence the thulium or thulium/holmium co-doped fiber lasers are the better choice than EDF lasers since they laser near 2 μm and have broad bandwidth (~200 nm) that can support short, high peak power pulses. These pulses could generate a supercontinuum in fluoride (ZBLAN) fiber to extend the comb into the MIR. Recently, a phase-stabilized Tm-doped fiber laser-based comb with supercontinuum extending to 3 μm has been demonstrated [57].In their work, the authors were able to generate octave-spanning supercontinuum from periodically poled $LiNbO_3$ (PPLN) when pumped by 70 fs pulses centered at 2 μm generated from a Tm oscillator as shown in Figure 1.4(a). The measured $f_{CEO}$ beat signals between $f$-2$f$, 2$f$-3f, and 3$f$-4$f$ spectral components are as shown in Figure 1.4(b).

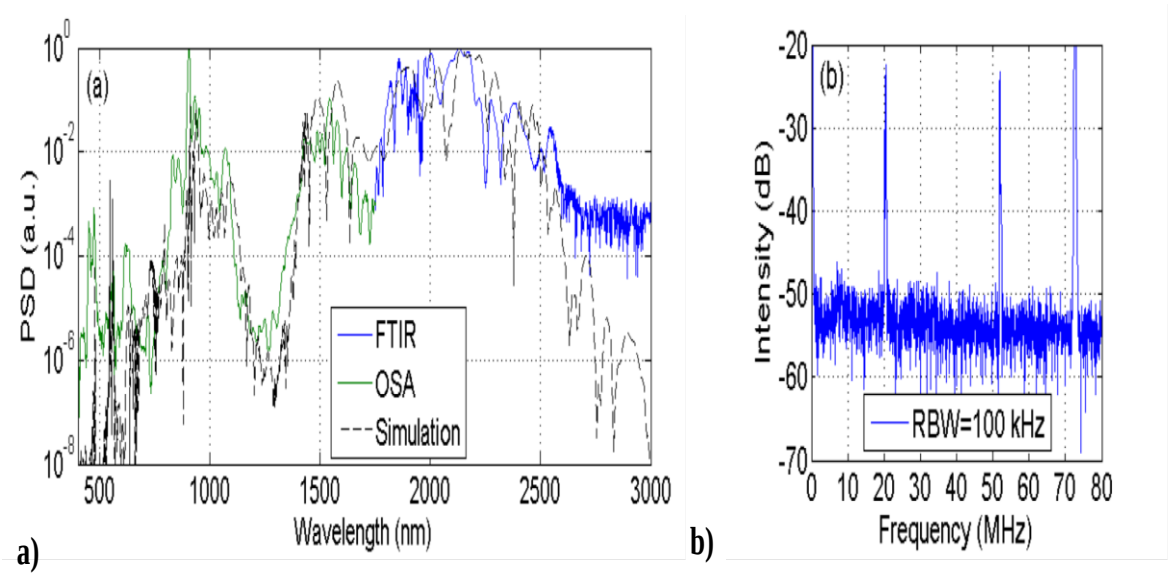


**Figure 1.4 (a) Power spectral density of the PPLN-waveguide supercontinuum (22.11 μm QPM period), operating at 1.8 W input power. (b) RF spectrum at 796nm (filtered via a grating spectrometer) measured on silicon APD, showing $f_{CEO}$ at 62.5 MHz and the repetition rate at 72 MHz. This figure is taken from Ref. [57].**

## 1.6 Thesis Outline

In this dissertation, I report the ultrashort pulse generation near 2 μm in all-fiber format by using thulium/holmium co-doped fiber as a gain medium. The structure of the dissertation is arranged in the following way:

In Chapter 2, I will discuss the mode-locking of the laser and the theory of mode-locking of the laser in two different regimes. Then I will talk about the important optical properties of fibers and briefly introduce the different mode-locking mechanisms used in fiber lasers to generate ultrashort pulses. Then I will discuss rare-earth doped fibers especially thulium and holmium co-doped fiber.

In Chapter 3, I will discuss the solitonic operation of a mode-locked thulium/holmium co-doped fiber laser. Then I will discuss the intra-cavity dispersion management of the laser using a number of possible normal group velocity dispersion (GVD) fibers to increase the spectral bandwidth. This chapter also discusses the mode-locking of the laser at two different center wavelengths.

In Chapter 4, the external pulse compression of a 2 μm pulse using photonic crystal fiber is discussed. The intra-cavity dispersion of the laser is compensated using high numerical (NA) fiber and the stretched pulse operation of the laser is demonstrated. I will also discuss the laser dynamics of the thulium/holmium co-doped fiber laser going from solitonic to stretched-pulse regime by changing the cavity dispersion.

In Chapter 5, this thesis will be summarized, and future work towards realizing the 2 μm phase-stabilized comb and mid-infrared supercontinuum generation in ZBLAN fiber will be proposed.

# Chapter 2 - Mode-Locking of Rare-Earth Doped Fiber Laser

## 2.1 Introduction

.Fiber lasers were made possible in the 1960s when trivalent rare-earth ions were doped into the glass hosts [66]. The optical fibers used to generate near and mid infrared lasers are mainly made up of oxide or fluoride glass where rare-earth cations such as erbium ($Er^{3+}$) [67, 68], ytterbium ($Yb^{3+}$) [69], neodymium ($Nd^{3+}$) [70], thulium ($Tm^{3+}$) [9, 50, 71] and holmium ($Ho^{3+}$) [72] are doped in the core of the fiber. The emission wavelength can be tuned by using different dopants and or a different host medium of the fiber. The emission wavelength with the different rare-earth cations doped in different host media is shown in Table 2.1. As seen from the Table 2.1, when different rare-earth elements are doped into the silicate glass the longest wavelength that can generate is around 2.1 μm. But, when a fluoride glass is used as a host material and the same categories of rare-earth elements are doped, the emitted wavelength can be extended almost close to 4 μm.

These rare-earth doped fibers have a large gain bandwidth near their corresponding emission wavelength regions and hence are very good candidate for the ultrashort pulse generation via mode-locking. The detail of mode-locking will be discussed in Section 2.4. The ultrashort pulse generation and propagation of these fibers depend on their properties such as gain, dispersion, and nonlinearity of the fiber. The control of dispersion along with fiber nonlinearity is very important during the mode-locking of the fiber laser to obtain the short and high energy pulses from the laser cavity.

**Table 2-1 Emission wavelength for different rare-earth cation doped fibers in different host materials. The emission wavelengths lie between 1 to 4 μm depending on the host and doping materials.**

| Rare earth cation | Host medium | Emission wavelength (μm) |
|---|---|---|
| Neodymium | Silicate glass | 1.03-1.1 |
| Ytterbium | Silicate glass | 1.0-1.1 |
| Erbium | Silicate glass | 1.5-1.6 |
| Erbium | Fluoride glass | 2.7 |
| Thulium | Silicate glass | 1.7-2.1 |
| Thulium | Fluoride glass | 1.45-1.53 |
| Holmium | Silicate glass | 2.1 |
| Holmium | Fluoride glass | 2.9, 3.22, 3.95 |

In this chapter, I will discuss the mode-locking mechanism of the fiber lasers and discuss the optical properties of the fibers and different rare-earth doped fibers used to generate near and mid infrared light. In Section 2.2, I will talk about the mode-locking mechanism of the laser. In Section 2.3, I will discuss the mode-locking theory used to generate ultrashort pulses from the laser. In Section 2.4, the optical properties of the fibers such as dispersion and nonlinearity are shown to play an important role in generation and propagation of the ultrashort pulses. Section 2.4 also discusses the different rare-earth doped fibers and mode-locking mechanism that can be used to generate ultrashort pulses at different wavelength regions.

## 2.2 Mode-Locking of a Laser

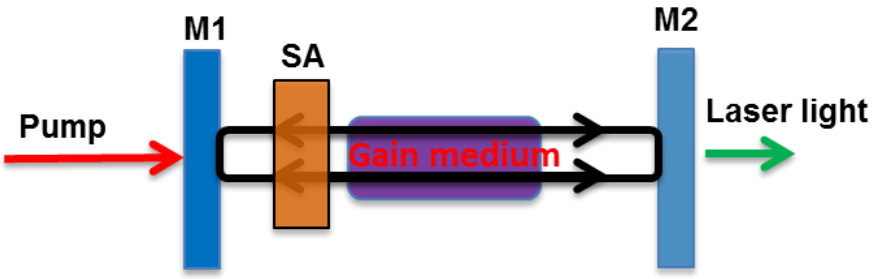


**Figure 2.1 Basic configuration of a laser cavity for ultrashort pulse generation. M1 (high reflector) and M2 (output coupler); mirrors, SA; saturable absorber.**

Mode-locking is a technique to generate ultrashort pulses from the laser. The basic configuration of the laser is shown in Figure 2.1, which consists of two mirrors M1; a high reflector at lasing wavelength and M2; acts as an output coupler with a gain medium placed between them. The gain medium is optically pumped from one side and the newly generated light called lase is coupled out from the other side. The light generated inside the laser cavity bounced back and forth between the mirrors number of times in such a way that the light will interfere both constructively and destructively so that standing waves will form inside the cavity called the longitudinal modes. The laser can support large number of longitudinal modes within their gain bandwidth of the gain medium. For the laser cavity of length of 1 m there will be ~$10^6$ longitudinal modes at wavelength of 2 μm.

In simple laser configuration, these longitudinal modes will oscillate independently without any fixed relationship between each other and interfere in such way that a constant intensity will be observed at the output as shown in Figure 2.2 (a), where only couples of independent longitudinal modes are shown. When there is large number of longitudinal modes

presents in the laser cavity the output becomes constant. This configuration of the laser is known as continuous-wave (CW) operation. But when these modes forced to oscillate with fixed relation by putting any active or passive components inside the laser cavity, then these modes will periodically interfere constructively producing intense burst at the output called pulse as shown in Figure 2.2 (b). Then the laser is said to be mode-locked in other words the laser is in pulse operation.

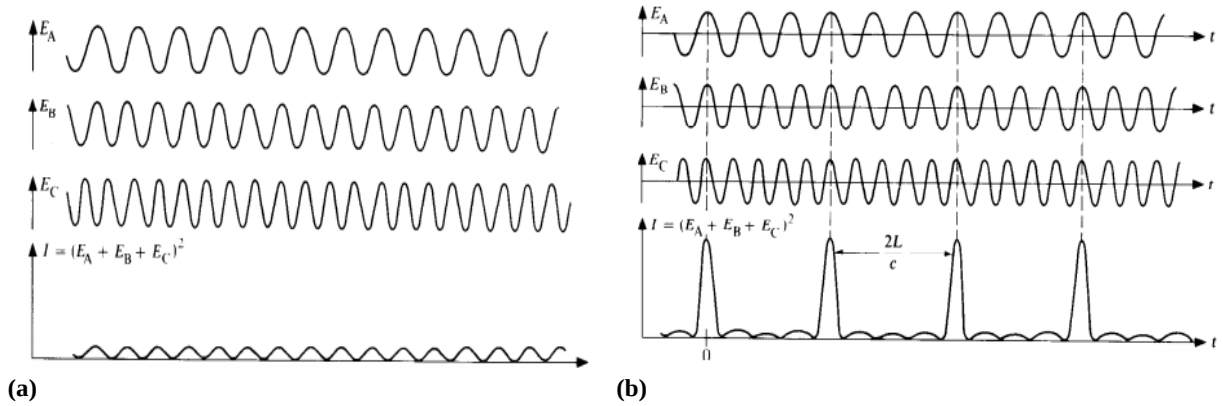


**(a)** **(b)**

**Figure 2.2 a) Continuous-wave operation; the output of the laser is constant b) Pulsed operation; the output of the laser will be intense burst and the separation of each peak round trip time of the laser cavity.**

## 2.3 Theory of Mode-Locked Laser-The Haus Master Equation

The mode-locked laser consists of number of elements in addition to group velocity dispersion (GVD) and self-phase modulation (SPM) such as linear loss and phase shift, dispersive gain, self-amplitude modulation (SAM) and saturable absorption as shown in

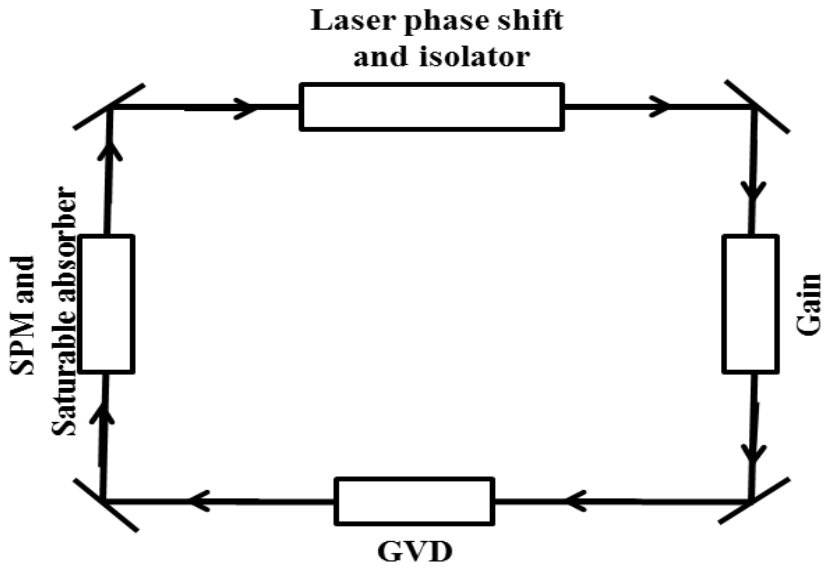


**Figure 2.3 Schematic of the ring laser cavity design with gain, gain dispersion, GVD, SPM, fast saturable absorber, and linear loss and phase shift. The laser is mode-locked using the saturable absorber.**

Figure 2.3. When the mode-locked pulse experiences the only small changes per pass (both linear and nonlinear), these effects may be included in the Master equation [73]

$$\left[(g-l)+\left(\frac{g}{\Omega_g^2}+iD\right)\frac{d^2}{dt^2}+(\gamma-i\delta)|u|^2\right]u=i\psi u, \tag{2.1}$$

where *u(t)* is the complex amplitude of the slowly varying temporal envelope, *l* is the linear loss per pass, *g* is the laser gain, $\Omega_g$ is the gain bandwidth, $\gamma|u|^2$ represents the SAM, and ψ is the net linear phase shift. Eq. (2.1) sets the sum of all the changes equal to net phase-shift ψ around the loop. The contribution of the GVD is represented by the parameter D which is equivalent to the net cavity dispersion and is given by

$$D=\frac{1}{2}\beta_2 L_D, \tag{2.2}$$

where $L_D$ is the dispersion length. While the SPM contribution is represented by $\delta = 2\pi n_2 L_{NL}/\lambda A_{eff}$, where $L_{NL}$ is the nonlinear length, and $n_2$ is the nonlinear index, $\lambda$ is the wavelength, and $A_{eff}$ is the effective modal area. $\gamma$ in Eq. (2.1) is inversely proportional to the loss saturation intensity and must be positive so that higher intensities see lower loss.

### *2.3.1 Solitonic Operation*

When the laser is operating in the net anomalous GVD regime, the positive Kerr effect (SPM) and negative GVD can compensate each other, it is possible to form chirp-free pulses (*$\beta$=0)* and hence behave soliton-like. So, the laser can be mode-locked by combined effect of GVD and SPM and the laser is operating in solitonic regime. In such a case, the Master equation (2.1) has an exact steady-state solution [74]

$$u(t) = A_0 \left[ sech\left(\frac{t}{\tau}\right)\right]^{(1+i\beta)}, \tag{2.3}$$

where $A_0$ is the pulse amplitude, $\tau$ is the normalized pulse width ($\tau = 0.567\tau_{FWHM}$), and $\beta$ is the chirp parameter which depends on *D* and $\delta$.

The pulse energy, *W*, of the soliton is given from the soliton area theorem

$$W = 2|A_0|^2\tau, \tag{2.4}$$

and is limited since the peak power or pulse width of the laser is limited. When a pulse passing through NPR mode-locking, the gain in energy is given in terms of SAM as

$$\int_{-\infty}^{\infty} dt|u|^2 \sin(\gamma|u|^2), \tag{2.5}$$

Using Eq. (2.2) with $\beta=0$ the maximum energy gained would be $\gamma|A_0|^2 \cong 0.6\pi$. This indicates that the peak power of the soliton is limited. So, if the pump power is increased to obtain the high peak power of the soliton, it will reach the maximum limit imposed by the NPR saturation and then the single pulse will break up into multiple pulses per cavity round-trip.

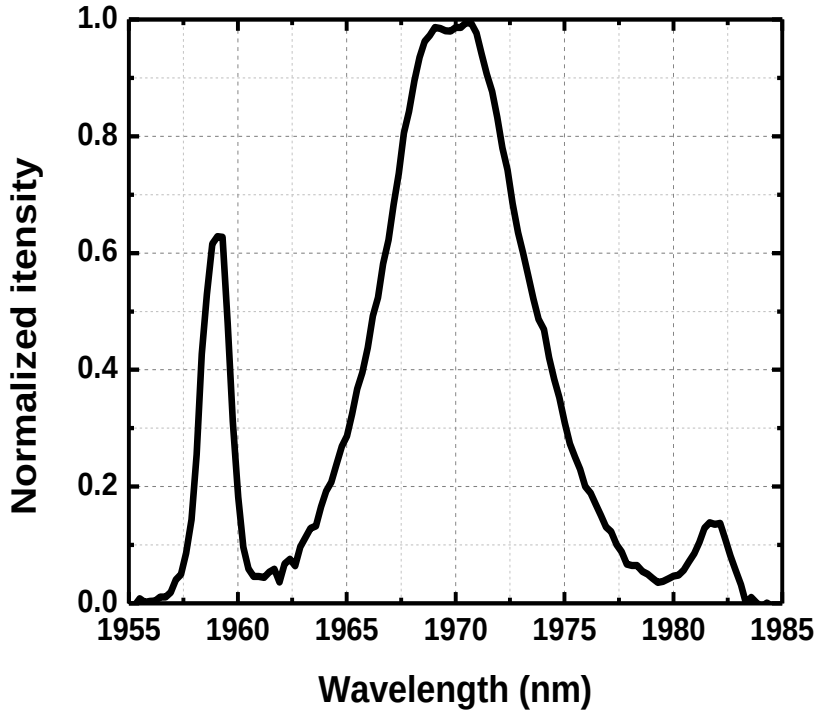


**Figure 2.4 A typical mode-locked spectrum of the solitonic pulse fiber laser.**

Also, the soliton-like nature of the pulses can be verified by observing the spectral sidebands on the mode-locked spectrum of the solitonic fiber lasers as shown in Figure 2.4. The frequency offest of the sideband from the peak of the soliton spectrum is given when there is a phase matching between each frequency component and the dispersive wave generated at each period (fiber length)

$$\Delta\omega = \pm\frac{1}{\tau}\sqrt{m\frac{8Z_0}{Z_p} - 1}, \tag{2.6}$$

where m is an integer, $Z_0$ is the soliton period, and $Z_p$ is the perturbation length (length of the fiber in the laser). At these phase-matched frequencies, the dispersive radiation builds up and causes the sideband of order m in the mode-locked spectrum.

### *2.3.2 Stretched-Pulse Operation*

When there is imbalance between the GVD in the laser cavity in other words when the laser cavity has sections of normal and anomalous GVD then there is change in the pulse shape per round trip. This change of the pulse per pass can be represented by the operator

$$iD\frac{d}{dt} = i\left(\frac{\beta_{2p}L_p}{2} - \left|\frac{\beta_{2n}L_n}{2}\right|\right)\frac{d}{dt}, \tag{2.7}$$

where $\beta_{2,s}$ are the GVD, $L_s$ is the length of the fiber, and the subscripts p and n denote the normal and anomalous GVD respectively. This imbalance of the ring cavity causes asymmetric change of the pulse in the two parts of the ring and affects the SAM and SPM parameters. The accumulated nonlinear phase shift is evaluated using a zeroth-order approximation for the expanding and contracting pulse in Figure 4.1. If net cavity GVD is positive then the laser is said to be mode-locked in the stretched-pulse regime. The Master equation for this case can be obtained by a Taylor series expansion of the pulse in time with assumption of small change per pass, which leads to Master equation

$$\left[(g-l) + \left(\frac{g}{\Omega_g^2} + iD\right)\frac{d^2}{dt^2} + \gamma_0|A_0|^2\left(1-\mu\frac{t^2}{\tau_0^2}\right) - i\delta_0|A_0|^2\left(1-\mu\frac{t^2}{\tau_0^2}\right)\right]u(t) = -i\psi u(t), \tag{2.8}$$

where $\mu < 1$ is the curvature of the parabolic time dependence obtained from the Gaussian solution to order $t^2$.

The Master equation (2.7) has the Gaussian-pulse solution

$$u(t) = A_0 \exp\left(-a\frac{t^2}{2}\right), \tag{2.9}$$

where *a* is the complex parameter and is obtained by balancing terms in Eq. (2.10). The Gaussian pulse shape is an approximation to the actual pulse shape and hence the actual pulse shape is Gaussian in the high-intensity portion of the pulse and is exponential in the wings where the nonlinearity ceases to act on the pulse.

This theory of mode-locking is specially developed while working in erbium doped fiber laser in 1990s but it can be equally valid for other kinds of fiber lasers due to similar kind of optical properties associated with them and the laser cavity is also designed in the similar way. The fiber nonlinearity along with its dispersion plays an important role in mode-locking of a fiber laser in order to generate ultrashort pulses. In next section, I will discuss the properties of the optical fiber such as dispersion and nonlinearity.

Since the goal of this work is to generate ultrashort pulses near 2 μm in all fiber format, I will focus discussion on mode-locking of the fiber laser.

## 2.4 Mode-Locking of Fiber Laser

As discussed in previous section, the laser can be mode-locked via combined action of dispersion and nonlinearity associated with the optical elements used. In fiber lasers, both the

dispersion and nonlinearity associated with the fibers. So in this section, I will discuss the optical properties of the fibers and different techniques used to mode-lock the fiber lasers.

### *2.4.1 Properties of Optical Fibers*

Optical fibers are excellent waveguides and the light is guided inside it by total internal reflection (TIR) since the refractive index of the core is higher than the cladding. The general picture of the propagation of the light inside the step index fiber is as shown in Figure 2.5. These fibers can be well characterize by defining a so-called V parameter also known as normalized frequency, that determines the number of modes supported by the fibers, defined as

$$V = k_0 a (n_1^2 - n_2^2)^{1/2} = \frac{2\pi a}{\lambda} NA, \tag{2.10}$$

where $k_0 = 2\pi/\lambda$, $a$ is the core radius, and λ is the wavelength of light. $n_1$ and $n_2$ are the refractive indices of the core and cladding of the fiber ($n_1 > n_2$). $NA = (n_1^2 - n_2^2)^{1/2}$ is called the numerical aperture of the fiber. If V < 2.405, the step-index fibers can support the single mode and are called single-mode fibers (SMF). For SMF, the relative core-cladding index difference ($\Delta = \frac{n_1 - n_2}{n_1}$) is ≈0.003 which requires $a$ < 5 μm.

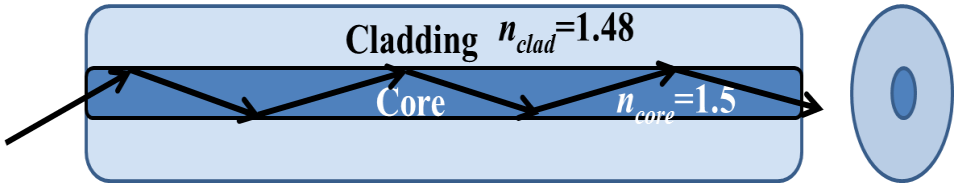


**Figure 2.5 Structure of the step-index optical fiber. The light is guided inside the fiber by total internal reflection.**

#### *2.4.1.1 Dispersion of Optical Fibers*

While designing a mode-locked fiber laser and amplifiers it is very important to understand the dispersion of the fibers used. The dispersion in the fiber depends both on the materials of which it is made and the waveguide properties like core size, and difference in refractive indices between core and cladding. For a fiber with core index $n_1$ and cladding index $n_2$, the propagation constant, $\beta$ of any mode is limited within the interval $n_1 k \geq \beta \geq n_2 k$, where $k=2\pi/\lambda$ is the vacuum wavenumber [75] and is given by

$$\beta(\omega) = \frac{n(\omega)\omega}{c} \tag{2.11}$$

where c is the speed of light, ω is the frequency of the light and n(ω) is the effective index of refraction and is given by the combination of both material and waveguide dispersion. The waveguide of the optical fiber modifies the overall index of refraction. To account for this, the normalized propagation constant b(V) as a function of normalized frequency (Eq. (2.10)) needs to be computed. The normalized propagation constant is given as [75]

$$b(\omega) = \frac{\beta^2/k^2 - n_2^2}{n_1^2 - n_2^2} \tag{2.12}$$

In the weakly guide approximation i.e. when the most of the power is guided inside the core of the fiber and the index difference between core and cladding is very small then the expression for the propagation constant can be expressed as

$$\beta(\omega) = n_2 k[1 + b(\omega)\Delta n] \tag{2.13}$$

where the normalized propagation constant can be expressed in terms of normalized frequency as [75]

$$b(\omega) = 1 - \left(\frac{1+\sqrt{2}}{1+\sqrt[4]{4+V(\omega)^4}}\right)^2 \tag{2.14}$$

Comparing Eqs. (2.11) and (2.13), the expression for the net index of refraction of the fiber can be obtained

$$n(\omega) = n_2[1 + b(\omega)\Delta n] \tag{2.15}$$

where $n_2$ corresponds to the material dispersion of the fiber and the second term on the right hand side corresponds to the waveguide dispersion. Since the material dispersion is also frequency dependent, the general form of Eq. (2.15) in weakly guiding approximation will be

$$n(\omega) = n_0(\omega)[1 + b(\omega)\Delta n] \tag{2.16}$$

where $n_0(\omega)$ is the index of refraction of the core for given material.

#### *2.4.1.1.1 Material Dispersion*

The wavelength and hence frequency dependence of the index of refraction $n(\lambda)$ of the medium can be calculated by using the Sellmeier equation as

$$n_0(\lambda) = \sqrt{1 + \sum_{i=1}^{m} \frac{A_j\lambda^2}{\lambda^2 - B_m^2}} \approx \sqrt{1 + \frac{A_1\lambda^2}{\lambda^2 - B_1^2} + \frac{A_2\lambda^2}{\lambda^2 - B_2^2} + \frac{A_3\lambda^2}{\lambda^2 - B_3^2}}\,, \tag{2.17}$$

where $A_j$ and $B_j$ are the Sellmeier coefficients which depend on the medium, and λ is in μm. The index of refraction and group velocity dispersion can be calculated based on the Sellmeier equation. Since for most of the optical fibers the host medium is fused silica, the

Sellmeier coefficients are $A_1$=0.6961663, $A_2$=0.4079426, $A_3$=0.8974794, $B_1$=0.00467914826, $B_2$=0.135120631, and $B_3$=9.79340025[76]. The refractive index of the core is higher than the air which decreased the speed of light in the medium since $v_p = c/n$, where $c$ is the speed of light in the vacuum and n is the refractive index of the medium. $v_p$ is called the phase velocity of the light but the speed of the pulse when it propagates inside the fibers is given by

$$v_g = \frac{d\omega}{dk}, \tag{2.18}$$

called the group velocity of the pulse or wave packet. In vacuum, the phase velocity and group velocity are equal. Since the refractive index depends on the wavelength, the dispersion relation ($\omega = vk$ ) can be written as

$$\omega = vk = \left(\frac{c}{n(\lambda)}\right)\frac{2\pi}{\lambda}, \tag{2.19}$$

where k is the wave-vector. Substituting this in Eq. (2.18)

$$v_g = \frac{c}{n - \lambda\frac{dn}{d\lambda}} = \frac{c}{N_g}, \tag{2.20}$$

where $N_g = n - \lambda\frac{dn}{d\lambda}$ is the group index, the ratio of the vacuum velocity of light to the group velocity in the medium.

#### *2.4.1.1.2 Waveguide Dispersion*

In a fiber, there is another dispersion that arises from waveguide effect called the waveguide dispersion. The dispersive wave experiences different amount of phase shift due to waveguide dispersion than the material dispersion. Waveguide dispersion originates from the

frequency-dependent distribution of wave vectors and it plays an important role in waveguides, which have small effective mode area. The waveguide dispersion can be calculated using Eq. (2.14).

Since the waveguide dispersion depends on the geometry of the waveguide, the total dispersion can be tuned by changing the structure of the fiber. The change in the total dispersion of the different fibers will be discussed in Chapter 5.

#### *2.4.1.1.3 Group Velocity Dispersion*

The group velocity dispersion (GVD) of the fibers plays an important role in the pulse propagation in the fiber lasers since each frequency component travels with different speed due to frequency dependence of the index of refraction. Hence the pulse gets spreadout and distorted. Now to calculate the GVD of the fiber, start with the propagation constant defined in Eq. (2.13). The $\beta(\omega)$ can be expanded as a Taylor series in ω

$$\beta(\omega) = \beta_0 + \beta_1(\omega - \omega_0) + \frac{1}{2}\beta_2(\omega - \omega_0)^2 + \frac{1}{6}\beta_3(\omega - \omega_0)^3 + \cdots \tag{2.21}$$

where $\beta_1 = \left(\frac{\partial\beta(\omega)}{\partial\omega}\right)_{\omega=\omega_0}$, $\beta_2 = \left(\frac{\partial^2\beta(\omega)}{\partial\omega^2}\right)_{\omega=\omega_0}$, and $\beta_3 = \left(\frac{\partial^3\beta(\omega)}{\partial\omega^3}\right)_{\omega=\omega_0}$. $\beta_2$ is called the second order dispersion or GVD. GVD plays an important role in pulse propagation in the fiber. $\omega_0$ is the carrier angular frequency. These coefficients can be expressed in terms of the net refractive index of the fiber as

$$\beta_1 = \frac{d\beta(\omega)}{d\omega} = \frac{N_g}{c} = \frac{1}{c}\left(n + \omega\frac{dn}{d\omega}\right)$$

$$\beta_2 = \frac{d^2\beta(\omega)}{d\omega^2} = \frac{1}{c}\left(2\frac{dn}{d\omega} + \omega\frac{d^2n}{d\omega^2}\right), \tag{2.22}$$

which means by knowing the net index of refraction of the fiber the GVD can be calculated.

For fused silica fiber, the GVD is computed and then plotted with respect to wavelength as shown in Figure 2.6. As seen from the graph GVD vanishes at wavelength $\sim 1370\, nm$ called zero-dispersion wavelength $\lambda_D$ where the pulse can propagate without change in its shape. From this point, the lower wavelength (or higher frequency) side GVD has positive values called the normal GVD, and the higher wavelength (or lower frequency) side GVD has negative values called anomalous GVD. In the normal GVD regime, the shorter wavelengths ($\lambda < \lambda_D$) travel slower than the longer wavelengths ($\lambda > \lambda_D$), and in anomalous GVD regime longer wavelengths travel slower than shorter wavelengths. The fiber manufacturer provides the D(λ) values instead of GVD and they can be related with

$$D(\lambda) = -\frac{2\pi c}{\lambda^2}\beta_2, \tag{2.23}$$

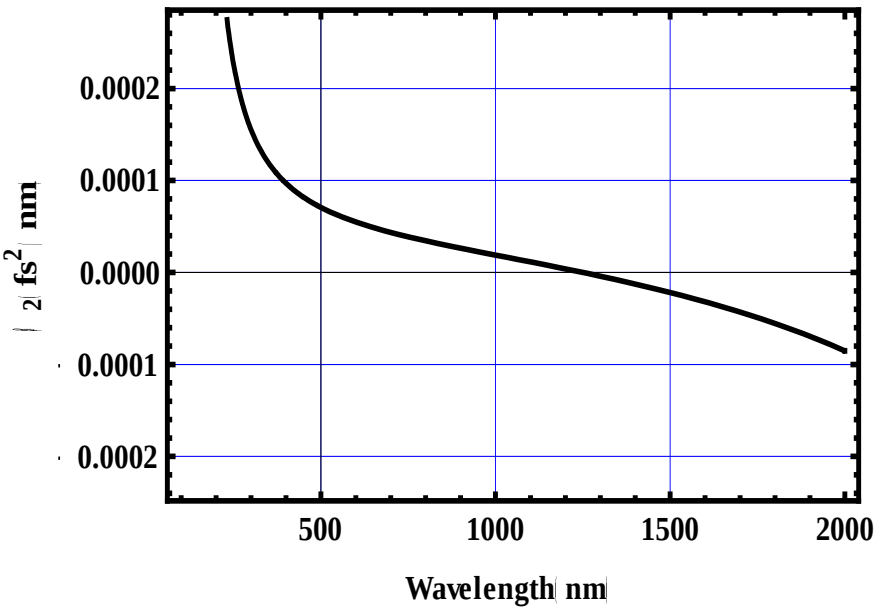


**Figure 2.6 Group velocity dispersion of Corning SMF-28. The GVD of the SMF was computed using the manufacture's core size, the Sellmeier coefficients, and the weakly guiding approximation.**

In optical fiber, the higher order dispersion, especially third order dispersion (TOD), also plays an important role in pulse propagation and ultrashort pulse generation during the mode-locking of lasers. The TOD is given as

$$\beta_3 = \frac{d^3\beta(\omega)}{d\omega^3} = \frac{1}{c}\left(3\frac{d^2n}{d\omega^2} + \omega\frac{d^3n}{d\omega^3}\right) \tag{2.24}$$

#### *2.4.1.1.4 Dispersion Length*

When the pulse is propagating in the fibers it is useful to define a quantity for dispersion called dispersion length as

$$L_D = \frac{T_0^2}{|\beta_2|}, \tag{2.25}$$

where $T_0$ is the initial pulse width. When a Gaussian pulse propagates by length $L_D$ the pulse gets broadened by a factor of $\sqrt{2}$. It can be seen from this equation that the pulse will spread faster if $\beta_2$ is larger and the initial pulse width is short. For each case the dispersion length is small. The pulse broadening becomes significant after the dispersion length.

#### *2.4.1.1.5 Gain Dispersion*

The two types of dispersions discussed in above the section are associated with the fiber when no gain materials are doped into the core. If some gain materials such as rare-earth cations are present in the core of the fiber, then there will be another kind of dispersion associated with it called the gain dispersion and arises because of the change in the refractive index due to an absorption features of the materials i.e. whenever there is the absorption feature in the materials, there will be a corresponding change in the refractive index. This can be

explained from the Kramers-Kronig relation and the gain-induced refractive index change is given by [77]

$$\delta n(\omega) = \Gamma_s \frac{1}{2nL} \int_0^L \chi'(\omega, z) dz \tag{2.26}$$

where $\Gamma_s$ is the mode/doped core overlap factor, L is the length of the fiber, and $\chi'$ is the real part of a complex atomic susceptibility ($\chi = \chi' - i\chi''$) generated due to the presence of activator (rare-earth) ions. Hence it is required that rare-earth dopants must be taken into account while making the oscillator and amplifier containing these elements. It is observed that the gain-dependent dispersion can completely compensate the bulk material dispersion for relatively low concentration [78]. In this work, I haven't taken account of gain-dispersion while designing the laser at 2 μm.

#### *2.4.1.2 Fiber Nonlinearity*

The response of any dielectric medium to an intense electro-magnetic field becomes nonlinear due to the anharmonic motion of bound electrons of the medium under the influence of strong applied field. So in nonlinear optics, the total polarization, $\tilde{P}(r, \omega)$ induced by the electric dipoles can be expressed in terms of a power series in the electric field.

$$\tilde{P}(r, \omega) = \varepsilon_0 \left[ \chi^{(1)}(\omega) E + \chi^{(2)}(\omega) : EE + \chi^{(3)}(\omega) \vdots EEE + \cdots \right], \tag{2.27}$$

where $\varepsilon_0$ is the permittivity in free space and $\chi^{(j)}(\omega)$ is the electric susceptibility tensor of the *j*th order and rank *j+1*. The first term in Eq. (2.27) represents the linear polarization related with the refractive index and the absorption of the material, which is dominant term in the total polarization. The remaining terms is responsible for the nonlinear effects such as second

harmonic generation and sum frequency generation. [79]. The optical fiber made with fused silica in general lacks inversion symmetry, so $\chi^{(2)}$ vanishes and the optical fibers therefore do exhibit second order nonlinear effect. Hence $\chi^{(3)}$ is the lowest nonlinear effect in the fiber and is responsible for the third harmonic generation, four-wave mixing and nonlinear refraction [79]. The most nonlinear effect in optical fiber is therefore originated from nonlinear refraction i.e. the dependence of the refractive index with the intensity of the light known as the Kerr effect. The total refractive index in the presence of the applied electric field can be written as

$$\tilde{n}(\omega, |E|^2) = n(\omega) + n_2|E|^2, \tag{2.28}$$

where $n(\omega)$ is the linear part of the refractive index of the material given by Eq. (2.18), $|E|^2 = I$ is the intensity of the applied field inside the fiber, and $n_2$ is the coefficient of nonlinear refractive index and can be related with the real part of $\chi^{(3)}$ as

$$n_2 = \frac{3}{8n} Re\left[\chi^{(3)}_{xxxx}\right], \tag{2.29}$$

To get this expression it is assumed that the electric field is linearly polarized and only one component contributes to the refractive index. The intensity dependence of the refractive index ($n_2$) is responsible for the many nonlinear effects such as self-phase modulation (SPM) and cross-phase modulation (XPM). The nonlinear refractive index of the fused silica fiber is about $3\times 10^{-20}$ $m^2/W$. Even this value is smaller than that of other nonlinear dielectric media; these optical fibers show a nonlinear effect because the light is confined in a very narrow core.

The SPM is completely degenerate four wave mixing and experiences the self-induced phase shift by the applied electric field during the propagation inside the fibers. The total phase shift induced is given as

$$\varphi(\omega, I) = \tilde{n}(\omega, I)k_0 z = [n(\omega) + n_2 I]k_0 z, \tag{2.30}$$

where $k_0 = {}^{2\pi}/_{\lambda}$ is the propagation constant and $z$ is the length of the fiber. The first term is due to linear refractive index known as linear phase shift and the second term is intensity dependent nonlinear phase shift due to SPM. The SPM is responsible for the spectral broadening of ultrashort pulses [80] as shown in Figure 2.7 and the formation of optical solitons in the anomalous dispersion regime of the fibers [81].The XPM describes the nonlinear phase shift of one optical field induced by another field and is responsible for the asymmetric spectral broadening of co-propagating optical pulses.

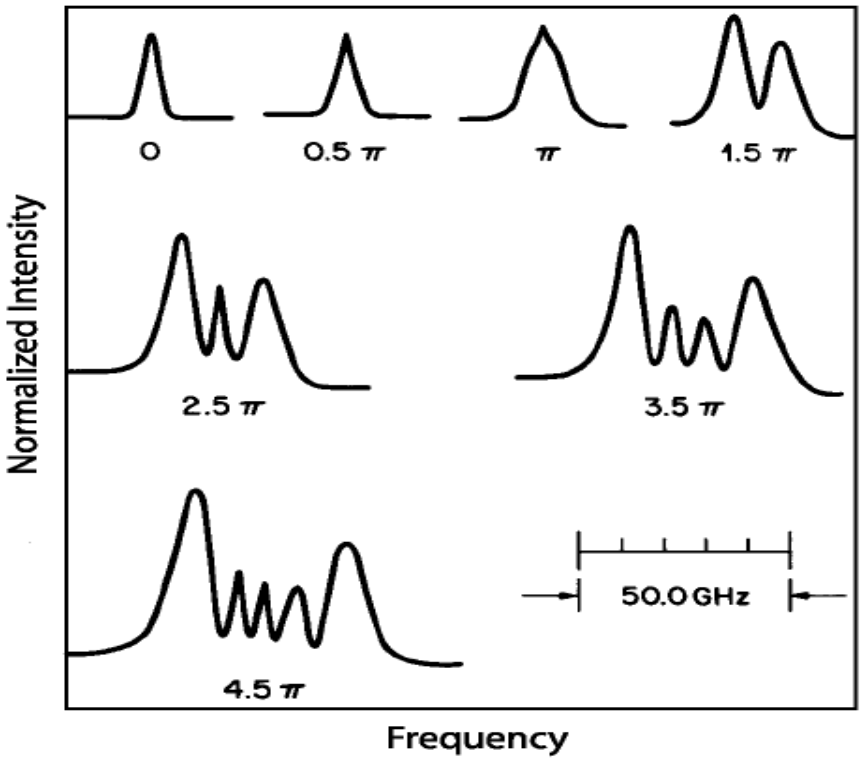


**Figure 2.7 Experimentally observed output spectra from a 3.35 μm silica-core fiber of length 99 m for a nearly Gaussian pulse shape. Spectra are labeled by a maximum phase shift which is proportional to the peak power. This figure is reproduced from Ref. [80].**

#### *2.4.1.2.1 Nonlinear Length*

Similar to the dispersion length, the nonlinear length in the fiber can be defined as

$$L_{NL} = \frac{1}{\gamma P_0}, \tag{2.31}$$

where $P_0$ is the peak power at the beginning of the fiber and γ is the effective nonlinear coefficient of the fiber, defined as

$$\gamma = \frac{n_2 \omega_0}{c \pi r^2}, \tag{2.32}$$

where $\omega_0$ is the frequency of the light and $r$ is the mode field radius of the fiber. Physically, the nonlinear length is defined as the effective propagation distance of the fiber over which the nonlinear phase shift becomes 1 radian.

The dispersion length $L_D$ and the nonlinear length $L_{NL}$ together provide the length scale for the pulse propagation in the fiber. When $L_D/L_{NL} << 1$, the pulse propagation then is governed by GVD that produces changes in the pulse shape and when $L_D/L_{NL} >> 1$, the pulse propagation is then governed by SPM that produces changes in the pulse spectrum. But when $L_D/L_{NL} \approx 1$, both GVD and SPM act together, leading to a qualitatively different behavior. When the fiber has anomalous dispersion ($\beta_2 < 0$), then the fiber can support optical solitons; the pulse shape does not change while propagating in the fiber. But when the fiber has normal dispersion ($\beta_2 > 0$), then the pulse can be compressed using both GVD and SPM.

As discussed in Chapter 1, different rare-earth cations can be doped inside core of the fiber and can generate light at different wavelength regions. In next section, I will discuss the different rare-earth doped fibers and their emission wavelengths.

### *2.4.2 Gain Fibers*

A variety of rare-earth cations can be doped into the core of the fiber which acts as a gain medium in fiber lasers. The lasing wavelength depends on the fluorescence transition of the rare-earth cations doped in the core of the fiber. Depending on the dopants and host material, the lasing wavelength covers wide range of the many important wavelengths in the near and mid-infrared regions. Among them neodymium, erbium, thulium and holmium are the most common rare earth cations used in a silicate host. The low loss and physical strength of silicate glasses have made them remarkably useful host materials for rare-earth cations in the wavelength region 1-2.2 μm. Unfortunately, it is hard to extend the emission wavelength beyond this region in a silicate host due to high loss.

#### *2.4.2.1 Erbium Doped Fiber*

Optical fibers with Erbium atoms doped in the core can generate light in the near infrared region around 1.55 μm. This emission wavelength is particularly of use for telecommunications since the low loss wavelength for single mode optical fiber is near 1.5 μm. The general picture of energy transition in erbium-doped silicate glass is as shown in Figure 2.8. The relaxation time of the erbium atom is long (~ 1 ms) allowing us to consider it as a three level system for lasing.

The erbium ion has two strong absorption lines at 980 nm and 1480 nm and these two wavelengths are used for most of the erbium doped lasers and amplifiers. The spectral emission near 1550 nm is due to the transition between $^4I_{13/2} \rightarrow {}^4I_{15/2}$. The erbium-doped fiber has a broad spectral bandwidth over 50 nm near 1550 nm.

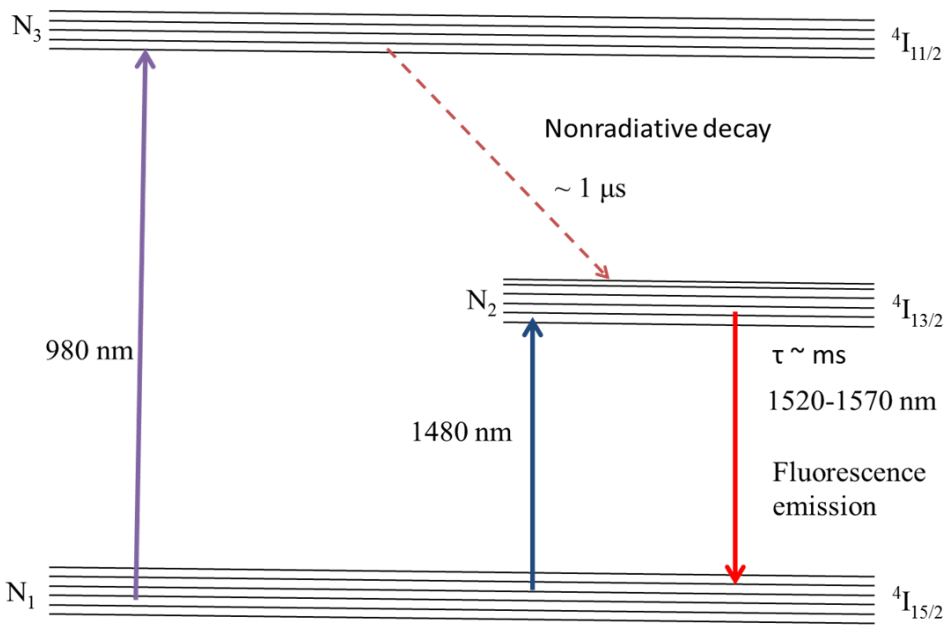


**Figure 2.8 Schematic of the energy level diagram of erbium in approximation of a three level system with possible pump and lasing wavelengths. Two pumping wavelengths 980 nm and 1480 nm can be used to lase light around 1560 nm from the transition between $^4I_{13/2} \rightarrow {}^4I_{15/2}$.**

### *2.4.2.2 Ytterbium Doped Fiber*

The other possible fiber to generate light in the near infrared region is ytterbium doped fiber. The energy level diagram of the ytterbium when doped in silicate is as shown in Figure 2.9. It has a very simple structure with two levels with laser emission occurs between $^2F_{7/2} \rightarrow {}^2F_{5/2}$ when pump by 940 nm wavelength. The upper state has lifetime in the order of 1-2 ms. The lasing wavelength is around 1030 nm.

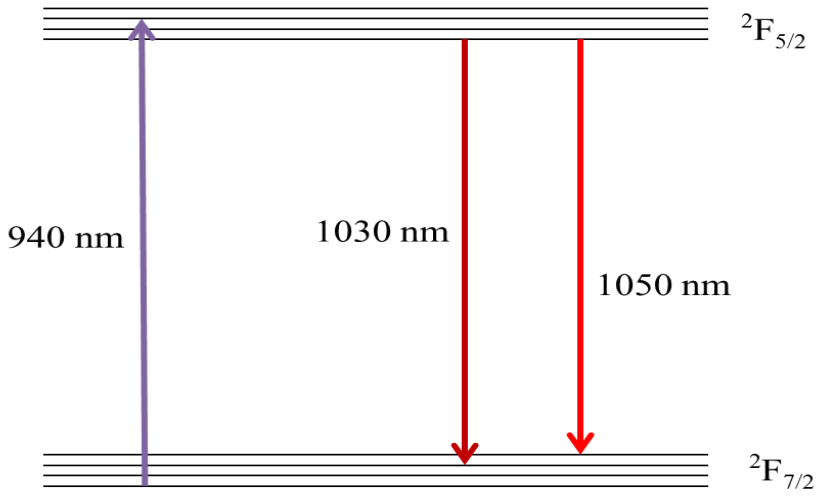


**Figure 2.9 Schematic of the energy level diagram of ytterbium ions in Yb:YAG with possible pump and lasing wavelengths. 940 nm is used as a pump source and the transition between $^2F_{7/2} \rightarrow {}^2F_{5/2}$ will lase at a wavelength around 1030 nm.**

### *2.4.2.3 Thulium Doped Fiber*

In order to extend the emission wavelength into the mid infrared region > 2 μm, one has to use either different rare-earth cations doped in fused silica or different host materials. It is a significant challenge to extend emission wavelength beyond 1.5 μm due to some physical properties associated with the glass such as low values for background absorption, thermal conductivity and glass transition temperature. The emission wavelength in the glass is controlled by the phonon density of states. The longest emitting wavelength is always shorter than its maximum transmissible wavelength because the phonon density of states determines the radiative efficiencies of the fluorescence transition in the rare-earth cations. Transition metal can be used as a dopant in the glass to lase at long wavelengths. Since the transition metals have large emission probabilities compared with rare-earth cations, therefore they have very short energy lifetimes.

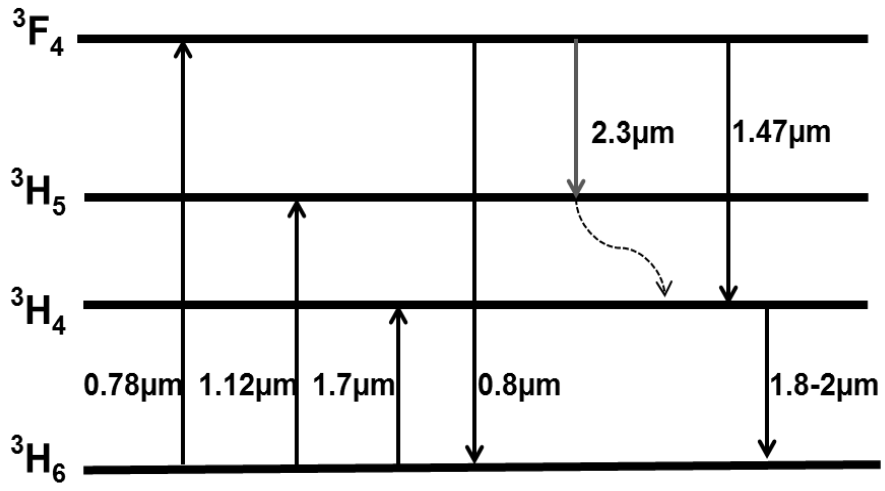


**Figure 2.10 Schematic of the energy level diagram of thulium ions doped in fused silica glass with possible pump and lasing wavelengths. A variety of pumping wavelengths 0.78 μm, 1.12 μm and 1.17 μm can be used to emit the wavelengths ranging from 0.8 μm to 2 μm. Lasing at 2 μm is due to the transition between $^3H_4 \rightarrow {}^3H_6$.**

When thulium ion is doped into the fused silica glass the laser wavelength can be extended up to 2.1 μm. The typical energy level diagram of the thulium (Tm) ion with possible laser transition is shown in Figure 2.10. Lasing near 2 μm in the pure Tm doped fiber occurs between the $^3H_4 \rightarrow {}^3H_6$ sates when pumped around 1.56 μm. The spectral bandwidth of the thulium doped fiber covers a very large range from 1.7 – 2.1 μm. This can support short, high peak power pulses near 2 μm.

### *2.4.2.4 Thulium/Holmium Co-Doped Fiber*

The lasing wavelength can further extend to longer wavelength ~ 2.2 μm when holmium (Ho) ion is doped in the fused silica glass along with the thulium. The energy level diagram of Tm/Ho co-doped fiber with possible transitions is as shown in Figure 2.11. The approach of co-doping $Ho^{3+}$ ions along with the $Tm^{3+}$ in fused silica is to achieve lasing on the transition

$^5I_7$-$^5I_8$ of $Ho^{3+}$ [11] due to energy transfer mechanisms through $Tm^{3+}$ excitation. If the $Tm^{3+}$ concentration is sufficiently high there is energy transfer from $^3H_4$ $Tm^{3+}$ ions to $^5I_7$ $Ho^{3+}$ ions leading to population inversion. The doping Tm:Ho ratio will determine the transparency level of the laser transition and the threshold power. It is believed that the high ratios will ensure that enough $Ho^{3+}$ ions will be sufficiently excited to exceed the transparency level of the laser transition for a given pump power and hence decrease the thresholds [82]. For long length of the Tm/Ho fiber the fluorescence is attributed to $Ho^{3+}$ and the total spectral bandwidth can be extended significantly.

The details of the thulium and thulium/holmium co-doped fibers used to generate ultrashort pulses near 2 μm region will be discussed in Chapter 3.

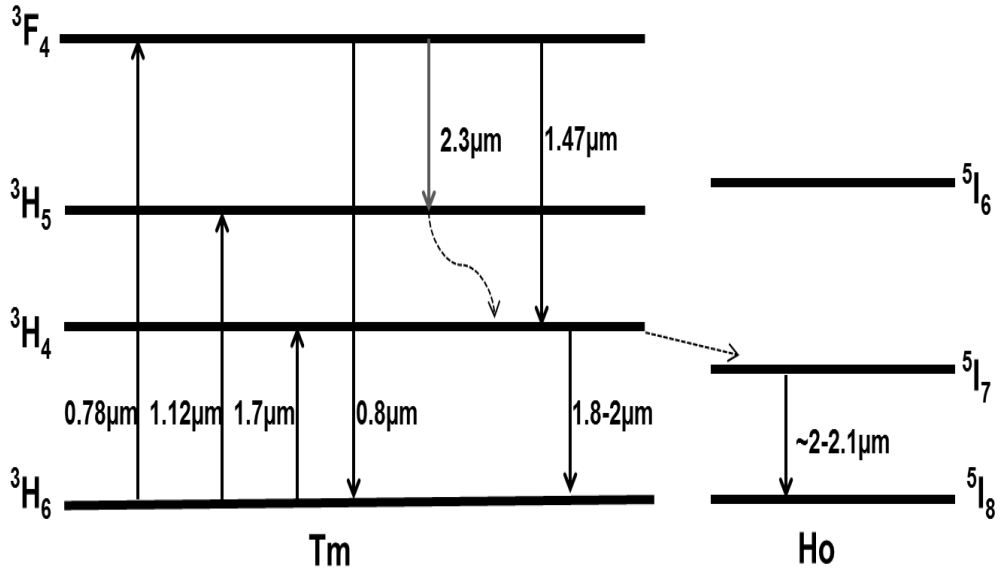


**Figure 2.11 Schematic of the energy level diagram of thulium and holmium ions doped in fused silica glass with possible pump and lasing wavelengths. Due to doping of Ho ions in the fiber, the lasing wavelength can be extended up to 2.1 μm.**

### *2.4.3 Self Amplitude Modulation in Fibers- Passive Mode-Locking*

Fiber lasers can be mode-locked both actively and passively. In passive mode-locking the laser is mode-locked without using any active component inside the laser cavity where the laser is able to produce ultrashort pulses by self-amplitude modulation (SAM) due the nonlinearity of the fiber which modulates the cavity loss. When an intense optical pulse propagate inside the fiber the SPM leads to SAM due to combined effect of dispersion and nonlinearity of the fiber. Passive mode-locking in fiber lasers can be achieved using three methods: saturable absorbers, nonlinear amplifying loop mirror, and nonlinear polarization rotation (polarization additive pulse mode-locking or Kerr mode-locking).

#### *2.4.3.1 Mode-Locking With Saturable Absorber*

Various kinds of semiconductor saturable absorbers can be used in the fiber laser for mode-locking. Semiconductor saturable absorber mirror (SESAM), saturable Bragg reflector (SBR), and carbon nanotubes as a saturable absorber have been widely used because of their readiness for passive mode-locking. Mode-locking of erbium-doped fiber lasers and frequency combs using single wall carbon nanotubes (SWCNT) as a saturable absorber is studied extensively in Ref. [83]. The main advantage of mode-locking with a saturable absorber is that one can obtain high repetition frequency (> 100 MHz) fiber laser which is very useful for optical frequency metrology. But, the spectral width and the output power are limited in this technique due to thermal damage at high power [83].

### *2.4.3.2 Nonlinear Amplifying Loop Mirror*

In 1990, a fiber laser was mode-locked using a nonlinear amplifying loop mirror (NALM) with sub-picosecond pulse duration [84] for the first time. The NALM relied on the Kerr effect and employed in a figure eight fiber laser (F8L) as shown in Figure 2.12. It consists of two fiber rings; the left ring is a main resonator and the right ring is a nonlinear amplifying loop mirror. The electric field coming out from the left ring is split into two parts by 50/50 splitter placed in between. In the right loop, one electric field propagates in the clockwise direction and the other in the counterclockwise direction. Since the gain fiber is placed asymmetrically in NALM, different amount of phase shift occurs between the two fields given by

$$\delta\varphi_c = \frac{\pi}{\lambda_s} n_2 g I_s L$$

$$\delta\varphi_{cc} = \frac{\pi}{\lambda_s} n_2 I_s L, \tag{2.33}$$

where $\varphi_c$ and $\varphi_{cc}$are the nonlinear phase shift of the electric field propagating in the clockwise- and counter clockwise direction respectively, $\lambda_s$ is the signal wavelength, $n_2$ is the nonlinear index of refraction, $I_s$ is the signal intensity, and $g$ is the gain coefficient of the gain fiber. When there is a proper phase bias, the NALM transmits higher intensities while reflecting the lower intensities and hence the laser is mode-locked.

As we know the NALM relies on the Kerr effect i.e. the nonlinear process, it can produce ultrashort pulses. Pulses as short as 50 fs can be generated by an erbium-doped fiber laser with a NALM [85]. But there are few disadvantages in this technique. The main disadvantage is that the

repetition rate is always lower since it has two rings and requires relatively long lengths of fiber. The other disadvantage is that it has tendency to operate with bursts of multiple pulses due to long cavity length and has not shown self-starting mode-locking.

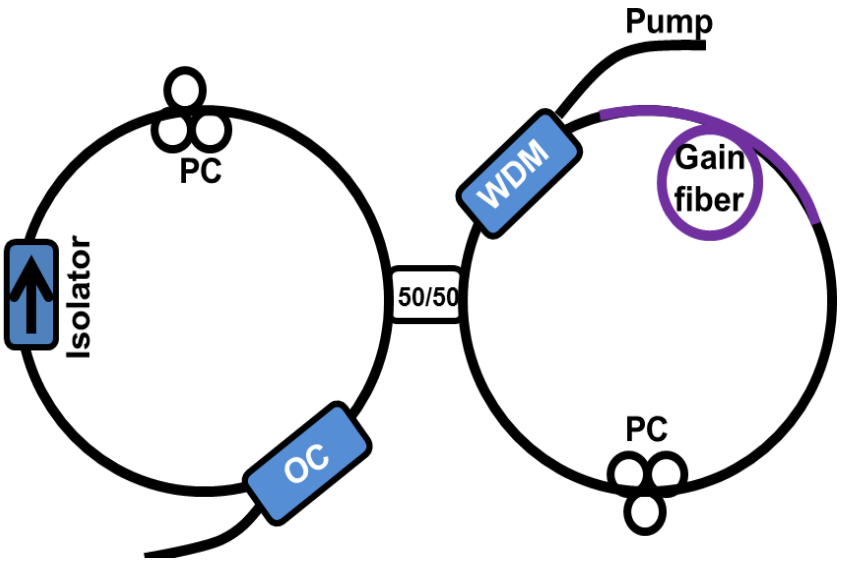


**Figure 2.12 Schematic of the figure eight ring laser using a nonlinear amplifying loop mirror (NALM) saturable absorber [86]. WDM: wavelength division multiplexer, PC: polarization controller, OC: output coupler. Isolator allows unidirectional propagation of light.**

### *2.4.3.3 Nonlinear Polarization Rotation*

Nonlinear polarization rotation (NPR) also known as polarization additive pulse mode-locking (P-APM) is a passive mode-locking technique used in a fiber lasers which depends on the intensity dependent rotation of an elliptical polarization state in the fiber. This technique of mode-locking in erbium-doped fiber laser has been studied by K. Tamura [87]. Figure 2.13 shows the basic idea how the nonlinear polarization rotation can be used in conjunction with the

bulk system to obtain an artificial saturable absorber and to mode-lock the laser. When linearly polarized light is incident on the polarizer, it sets the polarization and converts it into elliptical polarization after the quarter (λ/4)-wave plate. The elliptically polarized light experiences the intensity dependent rotation of the polarization ellipse axes when propagating through the Kerr medium because the intensity of each axis experiences different amounts of nonlinear phase shift for each axis. That causes the light to rotate it axis, known as nonlinear polarization rotation. At the output of the Kerr medium, the half (λ/2)-wave plate is set in such way that the pulse with high peak power passes through the polarizer while low peak power gets blocked and hence we get the ultrashort pulses.

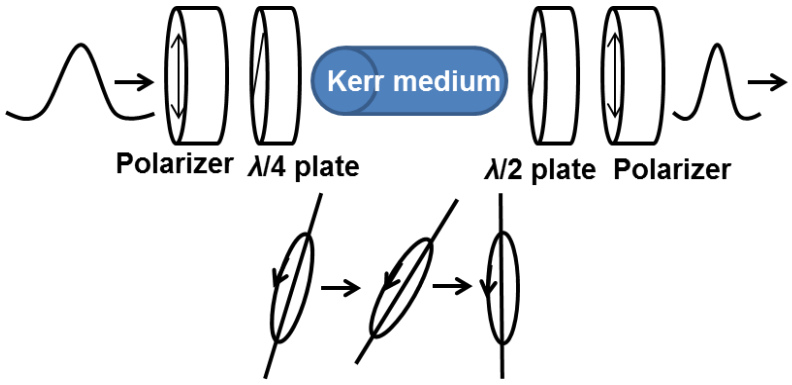


**Figure 2.13 Schematic of the nonlinear polarization rotation (NPR) for an artificial saturable absorber.**

This mode-locking mechanism can be employed in all fiber formats as shown in Figure 2.14. Initially, the light is linearly polarized at position (1) set by the polarizer. The polarization controller PC1 changes the linear polarization light into elliptical at position (2). When this elliptically polarized light passes through the length of fiber, it experiences the rotation of its axis due to the Kerr effect. The second polarization controller PC2 [position (4)] is set in such a way that it only allows passes the light polarized in a particular direction having

high peak intensity. In this way, we create an artificial saturable absorber (absorbs the low intensity light but transmits the high intensity light) and hence the laser is mode-locked.

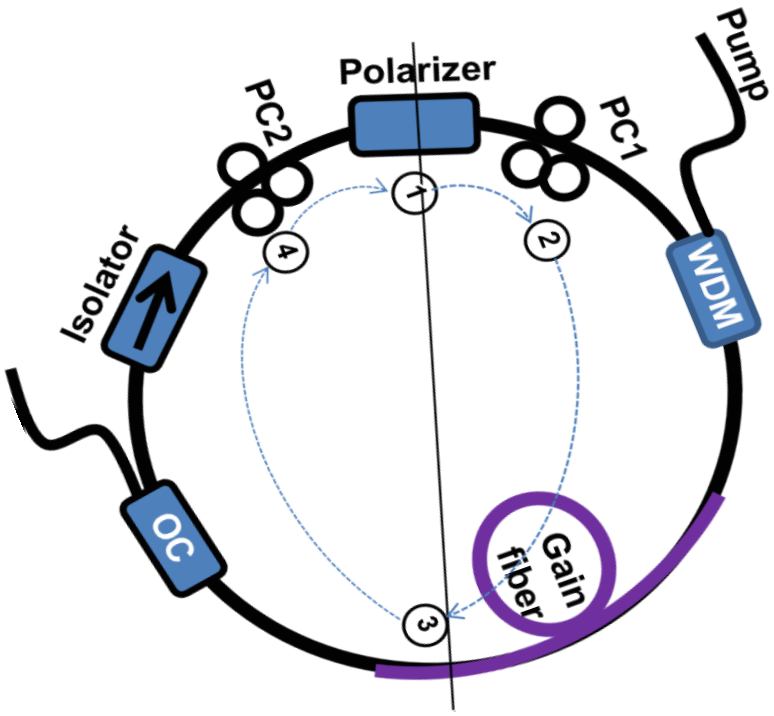


**Figure 2.14 Schematic of the fiber ring laser using a nonlinear polarization rotation (NPR) saturable absorber. WDM: wavelength division multiplexer, PC: polarization controller, OC: output coupler. Isolator allows unidirectional propagation of light. This figure is reproduced from Ref.[83].**

The nonlinear polarization rotation is extremely fast because it relies on the self-phase modulation from the Kerr effect in the fiber and hence there is no practical limit of the pulse width. But, there is a limit on the repetition rate of the mode-locked laser. It is very hard to achieve the higher repetition frequency because the intra-cavity energy will be small for the shorter length of the fiber.

In this research, nonlinear polarization rotation is used to mode-lock the thulium/holmium co-doped fiber laser and will be discussed in Chapters 4 and 5.

## 2.5 Summary

In this Chapter, I discussed the properties of different rare-earth doped optical fibers, where the emission spectrum covers a wide range of wavelengths from 1 - 2 μm depending on the dopants and the host materials. I also reviewed the optical properties of the single-mode fiber, GVD and the fiber nonlinearity that is responsible for SPM. Pulse propagation inside the fiber is characterized by the combination of GVD and SPM. When there is a balance between GVD and SPM, the soliton will form in the fiber whose shape does not change during the propagation through the length of the fiber

I discussed the mode-locking mechanism of the fiber laser in order to generate the ultra-short pulses. The passive mode-locking can be achieved by using different techniques such as saturable absorber (SESAM, SWCNT, and SBR), nonlinear amplifying loop mirror and nonlinear polarization rotation. I will focus on the mode-locking of thulium and holmium co-doped fiber lasers using NPR in Chapters 3 and 4.

As discussed in Chapter 1, the goal is to generate the mid-infrared light. To achieve this, I first use optical parametric process in the nonlinear fiber which relied on the SPM, will be discussed in Appendix B.

# Chapter 3 - Solitonic Operation of Mode-Locked Thulium/Holmium Co-Doped Fiber Laser

## 3.1 Introduction

As discussed in Chapter 1, a pulsed 2 μm laser is a good candidate as a pump source for the mid-infrared supercontinuum generation in fluoride fibers. Thulium (Tm) or thulium/holmium (Tm/Ho) co-doped fiber lasers are a better choice compared to erbium to produce mid-infrared (> 2 μm) frequency combs directly since they lase near 2 μm and have a broad spectral bandwidth (1.7 – 2.1 μm) that can support short, high peak power pulses. Previously, a Tm-doped passively mod-locked fiber laser with nonlinear polarization rotation and spectral filtering as a mode-locking mechanism was reported by Nelson [52].

In this chapter, I will discuss the passive mode-locking of the Tm/Ho co-doped fiber laser in all fiber formats using the technique of nonlinear polarization rotation as discussed in Chapter 2. The lasing wavelength for the fiber depends on the pump wavelength and the absorption of the fiber itself. The use of Tm/Ho co-doped fiber in our research is to generate light near 2 μm region where commercially available erbium doped fiber amplifier (EDFA) near 1560 nm can be used as a pump source. I will also discuss the intracavity dispersion compensation in order to get the large spectral bandwidth and hence the short pulse duration and high peak power. High peak power is required for the supercontinuum generation to generate mid-IR light.

## 3.2 Absorption and Emission of Tm/Ho Co-Doped Fiber

The Tm/Ho co-doped fiber that used to generate 2 μm light is Coractive TH512. According to manufacturer's specification, it has concentration of 2900 part per million (ppm) by wt. Tm and < 400 ppm. Wt. Ho (7.25:1 Tm/Ho ratio) with core diameter of 9 ± 1 μm, cladding diameter of 124.7 ± 1.0 μm, and a numerical aperture of 0.16 ± 0.02. The core absorption is > 120 dB/m at 790 nm. The pumping scheme in order to generate 2 μm light depends on the absorption feature of the fiber. As seen in Figure 3.1 [11], a wide range of pump sources can be used to generate 2 μm light from the Tm or Tm/Ho co-doped fiber.

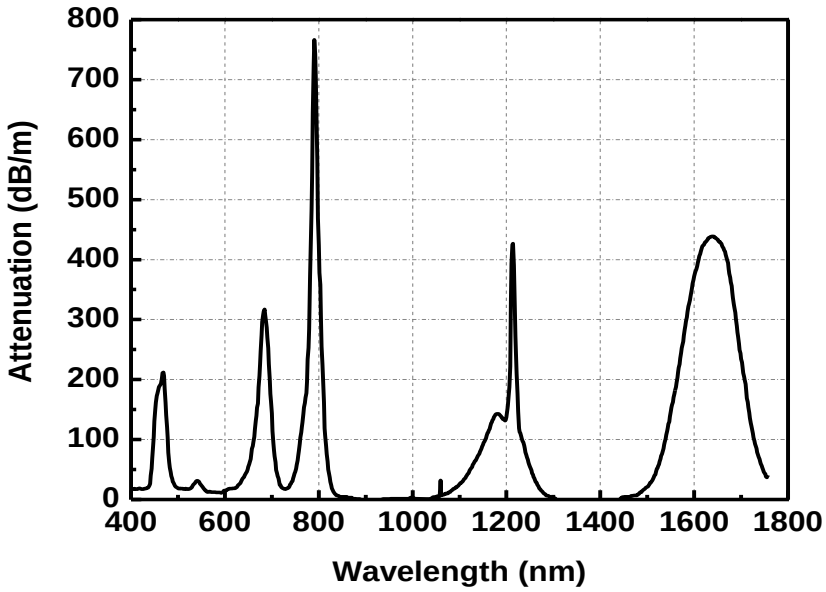


**Figure 3.1 Attenuation spectrum of the Tm/Ho co-doped fiber. This graph is reproduced from Ref. [11].**

In this experiment, the EDFA near 1560 nm is used as a pump source because high power EDFAs are easily available at this wavelength. So the attenuation of our Tm/Ho co-doped fiber at 1560 nm as function of input power is measured and plotted as shown in Figure 3.2. The

length of the fiber used was 0.5 m. At low input power, the measured loss is about 11 dB/m which is very close to the manufacturer's specification. As the input power is increased the loss through the fiber decreased for the given length of the fiber because for the given length of the fiber when pump power is increased the fiber gets saturated and cannot absorb light anymore.

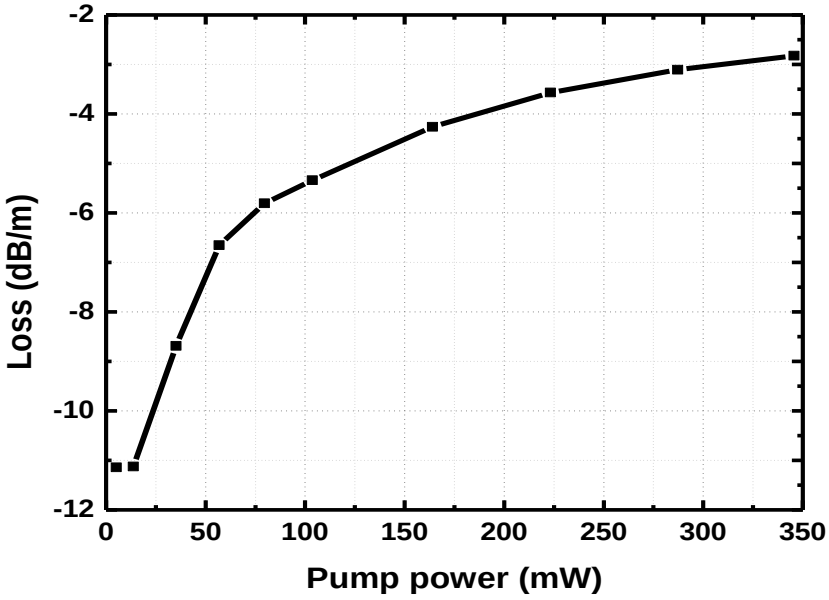


**Figure 3.2 Attenuation of Tm/Ho co-doped fiber at wavelength 1560 nm. 0.5m length of Tm/Ho co-doped fiber is used and output power is measured for each given input power.**

The amplified spontaneous emission (ASE) is measured after 1 m of the Tm/Ho co-doped fiber when it is pumped by the amplified 1560 nm light and it is shown in Figure 3.3. As seen from the figure, the ASE covered the wide range of spectral bandwidth from 1900 nm to 2100 nm with the peak around 1.96 μm. So, the Tm/Ho co-doped fiber can support large spectral bandwidth, and narrow pulses laser near 2 μm. The center wavelength of the laser cavity can shift around the peak absorption when there is loss in the cavity, due to the insertion losses of different fiber optic components (WDM, isolator, output coupler), and fiber splicing. This is because the pump power is increased to compensate the loss and consequently leads to a change

in the frequency dependent gain, producing gain filtering [88]. The laser can lase when the gain of the fiber is greater than the loss of the cavity.

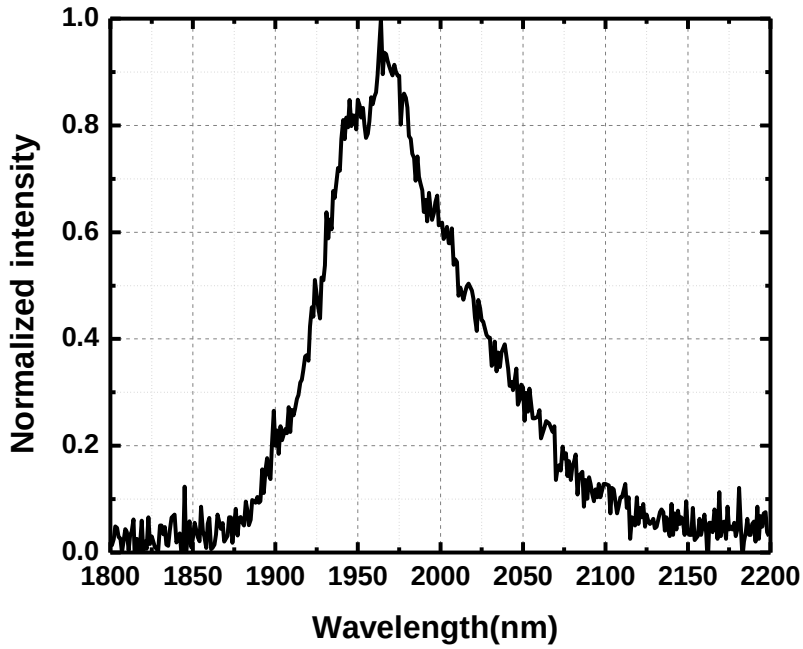


**Figure 3.3 Amplified spontaneous emissions (ASE) of Tm/Ho co-doped fiber when pumped by 1560 nm. The ASE is measured after 1 m of fiber. The ASE covers about 200 nm of bandwidth with a peak around 1.96 μm.**

Previously it has been reported that when the Tm/Ho co-doped fiber is pumped at 820 nm the spectral bandwidth even wider than pumping near 1560 nm [11]. The emission spectrum from 0.5 m of the Tm/Ho co-doped fiber and 2 m of the Tm doped fiber is as shown in Figure 3.4. The blue curve is for Tm/Ho co-doped fiber and red curve is for singly Tm doped fiber. From graph it is seen that the Tm/Ho co-doped fiber exhibit two emission bands when pumped with 820 nm which is absorbed by the ${}^3H_6 \rightarrow {}^3F_4$ transition of $Tm^{3+}$ as shown in Figure 2.4. The near band near 1.95 μm is corresponding to transition between ${}^3H_4 \rightarrow {}^3H_6$ of $Tm^{3+}$ and the other band near 2 μm is corresponding to transition between ${}^5I_7 \rightarrow {}^5I_8$ of $Ho^{3+}$ [72,

89]. This indicated that there is energy transfer from $^3H_4$ manifold of $Tm^{3+}$ to the $^5I_7$ manifold of $Ho^{3+}$. It is believed that the efficiency, pump threshold, and the lasing wavelength depend on the doping ratios of thulium and holmium. In general higher the Tm-to-Ho ratio lower the pump threshold and higher the efficiency because enough $Ho^{3+}$ ions will be sufficiently excited to exceed the transparency level of the laser transition [82]. Also for the longer length of the Tm/Ho co-doped fiber the emission of longer wavelengths is primarily due to the $Ho^{3+}$ fluorescence.

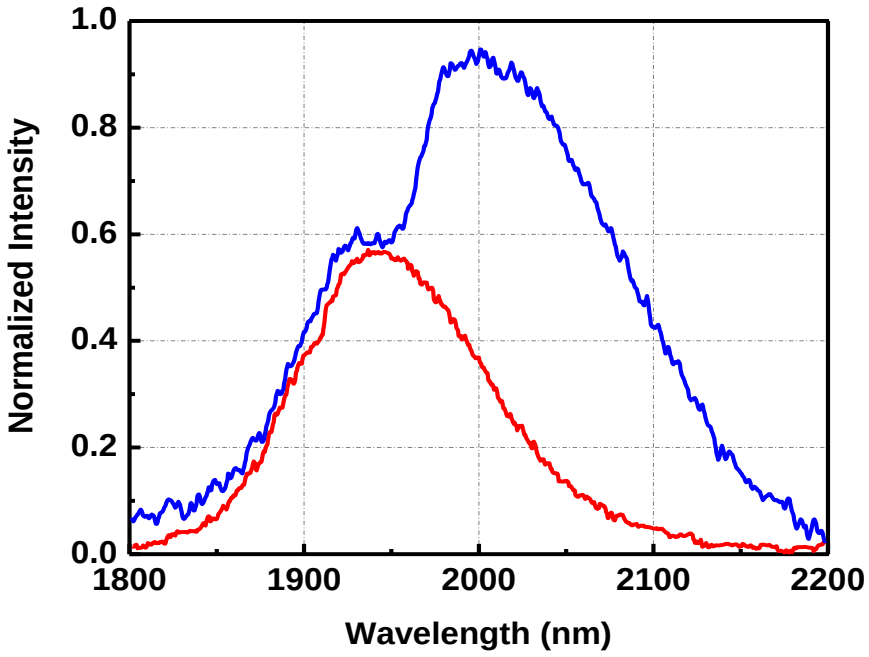


**Figure 3.4 Emission spectra from the end of the fiber of 50 cm when pumped at 821 nm. This Figure is reproduced form Ref. [11].**

## 3.3 Pump Laser Source

As I discussed in the previous section, 1560 nm can be used as a pump source to generate light at 2 μm from Tm/Ho co-doped fiber. An erbium doped fiber amplifier seeded with

a 1560 nm laser diode is chosen as a pump source. The power versus current characteristic of the 1560 nm laser diode used to seed the EDFA is as shown in Figure 3.5. The maximum power that the laser diode can put out is around 10 mW when the pump current is 100 mA.

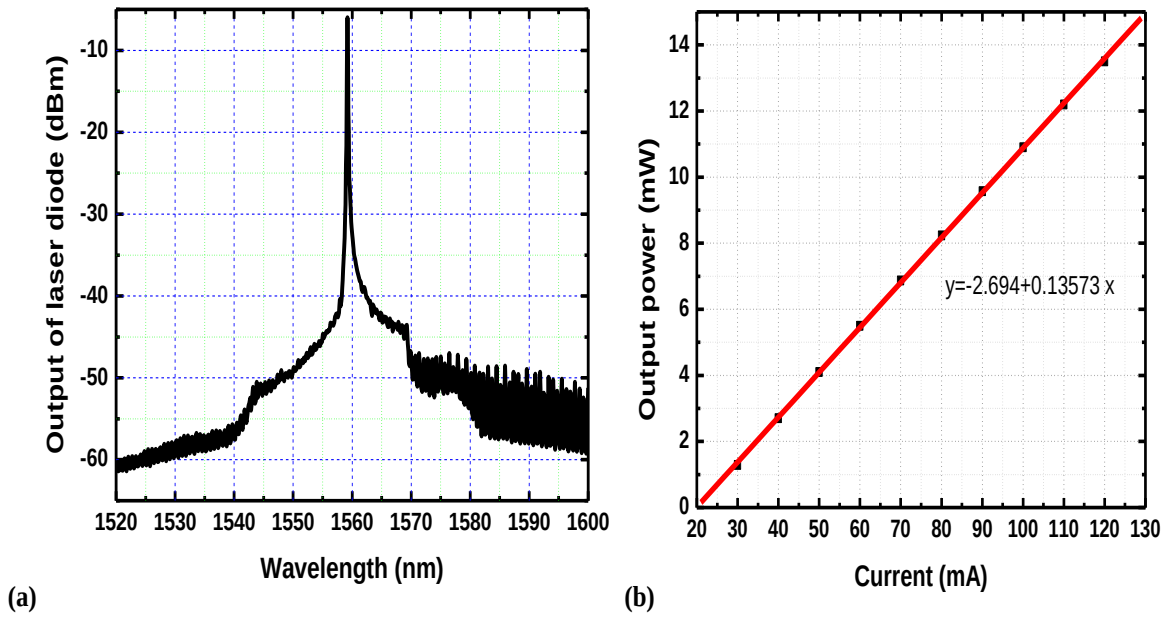


**Figure 3.5 Power versus current characteristic curve of the 1560 nm laser diode. The spectrum of the laser diode is measured from the optical spectrum analyzer.**

The signal from the laser diode is amplified using an EDFA. The output spectrum of the EDFA (a) along with the power at 1560 nm with respect to the current of the amplifier (b) is shown in Figure 3.6. Most of the amplified power is at 1560 nm and the maximum output is about 600 mW at 500mA of the pump current.

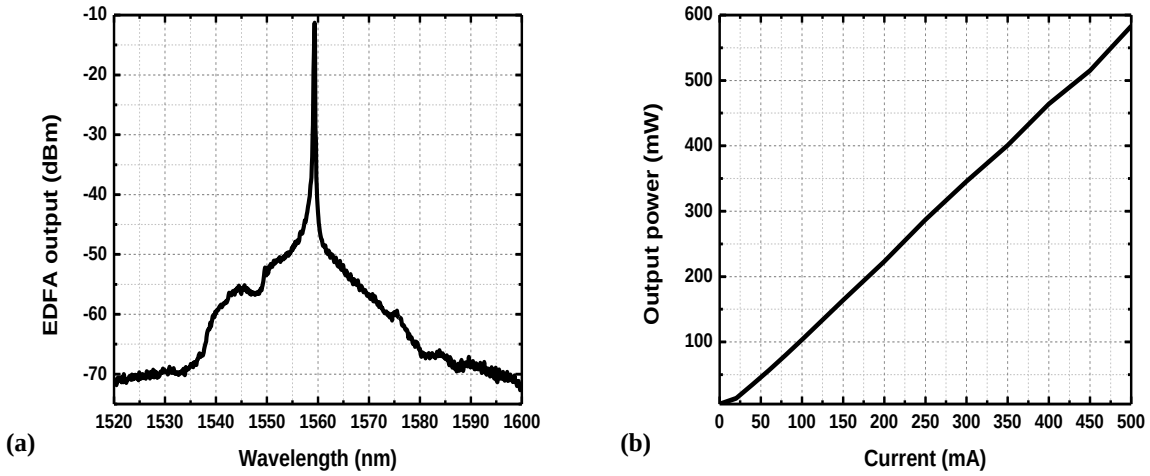


**Figure 3.6 Output of the erbium doped fiber amplifier (EDFA) (a) spectrum and (b) output power vs. pump current at 1560 nm. The spectrum of the laser diode is measured from the optical spectrum analyzer.**

## 3.4 Mode-Locking of Tm/Ho Co-doped Fiber Laser

As discussed in Chapter 2, the laser is mode-locked via the nonlinear polarization rotation technique. Initially, c-band optical components, such as output coupler and polarization sensitive isolator, except the wavelength division multiplexer (WDM) are used since the 2 μm WDM was not commercially available when the experiment was first started.

### *3.4.1 Fiber Laser Design*

The experimental design of our Tm/Ho co-doped fiber laser is shown in Figure 3.7. The 1.56 μm laser is used to pump the gain fiber. The EDFA is used to amplify the signal from the distributed feedback laser. An amplified signal more than 200 mW is coupled into the laser cavity through a 1.55/2 μm WDM to pump the Tm/Ho co-doped fiber.

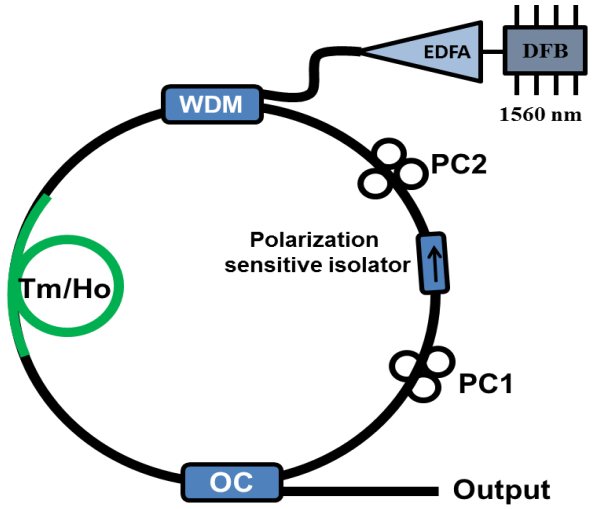


**Figure 3.7 Schematic of the Tm/Ho co-doped fiber laser ring cavity. DFB, distributed feedback laser; EDFA, erbium doped fiber amplifier: WDM, wavelength division multiplexer; OC, output coupler; PC, polarization controller [90].**

From the measurement in Section 3.2, it is observed that the absorption at 1.56 μm is ~11 dB/m. A c-band polarization sensitive isolator manufactured by AFW technology along with two polarization controllers PC1 and PC2 before and after it are used for passive mode-locking via nonlinear polarization rotation. A long section of 6 m Corning SMF-28, including all the pigtails of the various optical components, is used to get a sufficient amount of nonlinear phase shift per round trip in the cavity. A c-band 70/30 fiber coupler is used as the output coupler. 30% of the light is taken as output to characterize the laser where 70% is feedback to the laser cavity. The laser's spectral output is measured by using a monochrometer; pulse trains are detected by a 15 MHz HgTe photodetector and the pulse width is measured by the interferometric autocorrelation.

### *3.4.2 Laser Performance*

Mode-locking was initially obtained when there was 4 m of Tm/Ho co-doped fiber and 7 m of SMF in the cavity by adjusting the pump power and the two polarization controllers PC1 and PC2. To monitor the mode-locking an electronic spectrum analyzer (ESA) is used. A clean and stable ESA spectrum is seen with signal to noise ratio of around 40 dB when the laser is mode-locked. A typical output spectrum of the mode-locked laser measured from the monochrometer is as shown in Figure 3.8. The center wavelength of the spectrum is around 2.04 μm with full width half-maximum (FWHM) of 9 nm.

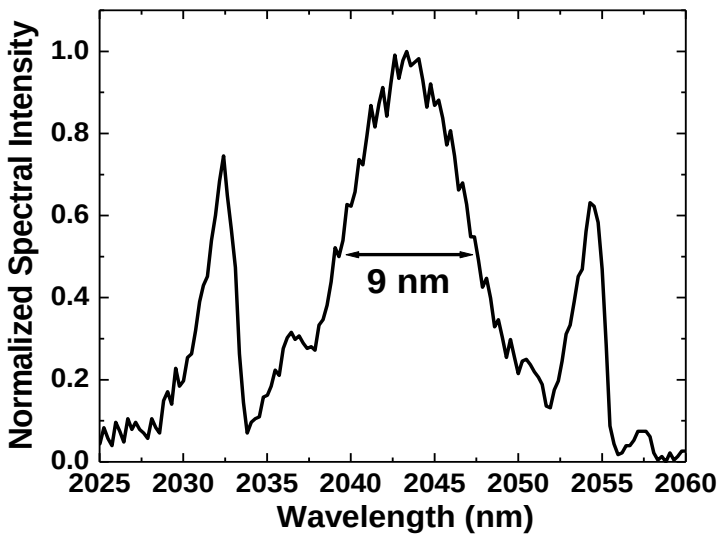


**Figure 3.8 Mode-locked spectrum of Tm/Ho co-doped fiber laser for 4 m of Tm/Ho co-doped fiber when pumped by 1.56 μm laser with 7 m of SMF in the laser cavity [90]. The full width half-maximum is 9 nm centered around 2.04 μm.**

Since the group velocity dispersion (GVD or $\beta_2$) of both the Tm/Ho co-doped fiber and SMF used inside the laser cavity have anomalous GVD and hence the net cavity dispersion, defined as the product of GVD and fiber length ($\beta_2$L), is negative. The negative net cavity

dispersion was verified by the observation of the solitonic resonance sideband known as Kelly sideband [91]. This indicates that the laser is operating in the solitonic regime. These sidebands form due to the periodic perturbation of linearly propagating dispersive waves generated inside the laser cavity on successive round trips. The dispersive waves will interfere destructively except at those wavelengths for which the differential phase between the soliton and the dispersive wave accumulated over a round trip is an integral multiple of (*N*) of *2π*. The resonance condition is given as [92]

$$\varphi_s - \varphi_d = 2\pi N \tag{3.1}$$

where $\varphi_s$ and is the $\varphi_d$ are the differential phase of solitonic and dispersive waves and are given as

$$\varphi_s = \beta_s L = \beta_0 + \beta_1 \Delta\omega - \frac{1}{2}\beta_2 \tau_0^2$$

$$\varphi_d = \beta_d L = \beta_0 + \beta_1 \Delta\omega + \tfrac{1}{2}\beta_2 \Delta\omega^2 + \tfrac{1}{6}\beta_3 \Delta\omega^3 + \cdots \tag{3.2}$$

where $\tau_0$ is the soliton length, $\beta_2$ and $\beta_3$ are the quadratic and third order dispersion per unit length of the fiber, and $\Delta\omega \equiv \omega - \omega_0$ is the frequency offset of the soliton from center angular frequency $\omega_0$. Solving Eq. (3.1) along with Eq. (3.2) the expression for the net cavity dispersion can be obtained [92]

$$\beta_2 L = -\frac{N\lambda_0^2}{\pi c^2}\left[\left(\frac{\Delta\lambda_N}{\lambda_0}\right)^2 + \frac{ln^2\left(1+\sqrt{2}\right)}{\pi^2}\left(\frac{\lambda_0}{c\Delta\tau}\right)^2\right]^{-1} \tag{3.3}$$

where $\Delta\tau$ is the pulse duration temporal FWHM, $\lambda_0$ is the center wavelength, $c$ is the speed of light, and $\Delta\lambda_N$ is the separation of the $N_{th}$ order sideband from the center wavelength. By measuring the wavelength separation $\Delta\lambda_N$ the net cavity dispersion can be computed using Eq. (3.3) and hence the GVD of the Tm/Ho co-doped fiber can be estimated since the GVD of SMF is known.

In the experiment, the net cavity dispersion can be calculated by measuring the slope of the plot between the square of the wavelength offset versus the sideband order [92] using expression $DL = \frac{2\lambda_0}{cm}$, where $m$ is the slope. So by getting the better value of $m$, a better estimation of net cavity dispersion can be obtained. This requires multiple Kelly sidebands in the mode-locked spectrum. But in Tm/Ho mode-locked laser just one sideband is observed which limits the estimation of the cavity dispersion and hence the GVD of the Tm/Ho co-doped fiber.

When the laser is operated in the solitonic regime the pulse shape is maintained inside the laser cavity due to combined action of anomalous GVD and Kerr nonlinearity. Since the nonlinear phase shift per round trip is determined by the pulse energy and is limited by the sideband generation of a periodically perturbed soliton, this sideband generation puts the upper limit on the pulse energy. In order to increase the laser's pulse energy, the intracavity group-velocity dispersion compensation is required.

## 3.5 Intracavity Dispersion Compensation

The shortest output pulses can be produced by reducing the net cavity dispersion. This can be achieved either by shortening the lengths of SMF and Tm/Ho co-doped fibers in the

cavity, or by adding other fibers that have normal GVD near 2 μm. The latter is typically difficult to achieve since most of the silica fibers exhibit anomalous GVD at 2 μm due to material dispersion of the fiber which is always negative at wavelengths longer than 1.25 μm. However, a couple of possible fibers that might have normal GVD at 2 μm were tried and as discussed in next couple of sections.

### *3.5.1 Highly Nonlinear Fiber*

First, a highly nonlinear fiber (HNLF) [93] was tried and expected to exhibit normal GVD at 2 μm. HNLF has a similar index profile as a telecom dispersion compensating fiber [94] as shown in Figure 3.9.

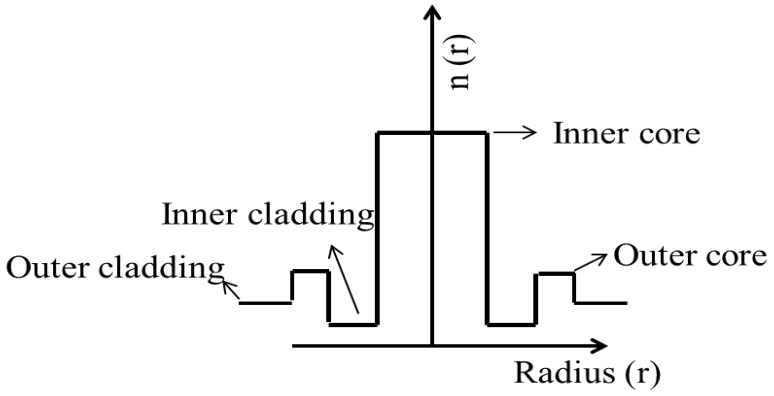


**Figure 3.9 Geometric structure of the highly nonlinear fiber (HNLF) with variation of its refractive index as a function of radius.**

This kind of index profile allows for multiple zero GVD points that would exhibit normal GVD at longer wavelengths as shown in Figure 3.10. As seen from the Figure 3.10, the GVD of HNLF is normal at 2 μm but the magnitude is very small compared with SMF.

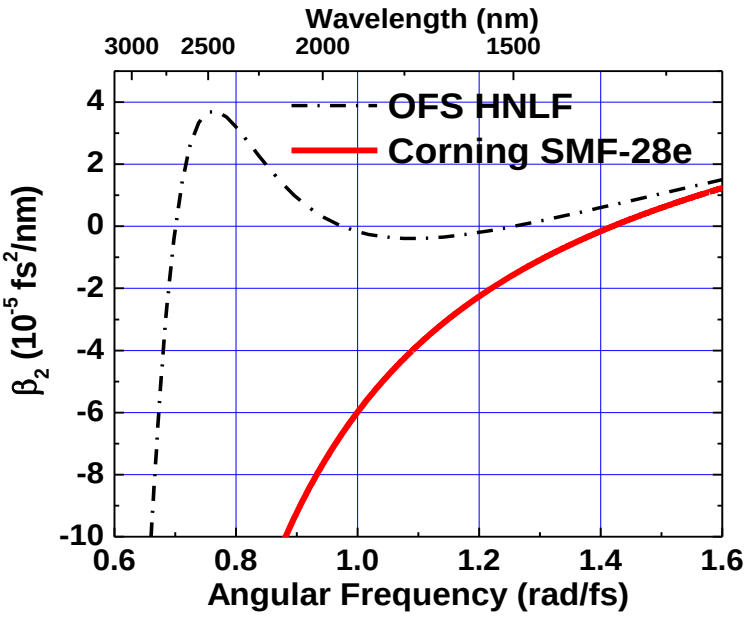


**Figure 3.10 Computed group velocity dispersion (GVD) of OFS HNLF compared to Corning SMF-28. The HNLF GVD was provided to us from OFS, while the GVD of the SMF was computed using the manufacturer's core size, the Sellmeier coefficients [95], and the weakly guiding approximation [75].**

If a larger wavelength separation of the 1st order Kelly sideband ($\Delta\lambda_1$) was observed as HNLF was added, Eq. (3.3) states that the magnitude of the net cavity dispersion would be smaller (negative) and thus the HNLF would have normal GVD at 1.96 μm. Since the actual GVD of the HNLF was unknown, I relied on a computed GVD value of $\beta_2 = +0.13\times10^{-5}$ fs$^2$/nm at 1.96 μm for a similar HNLF. For this calculated value, the changes in $\Delta\lambda_1$ would be too small (< 1 nm) to observe with our spectrometer for meter lengths of added HNLF.

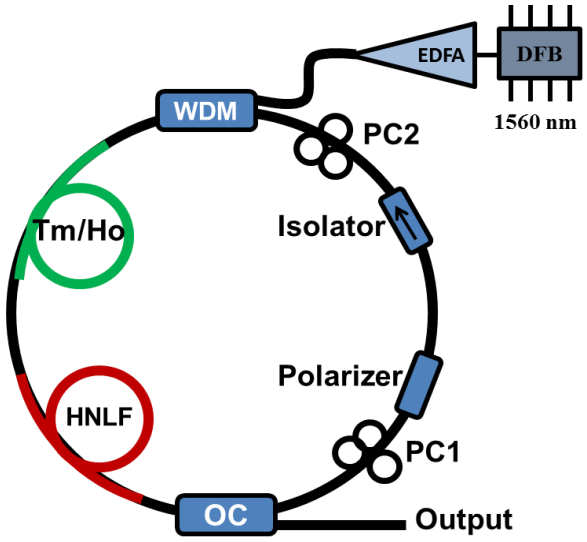


**Figure 3.11 Schematic of the intracavity dispersion compensation of Tm/Ho co-doped fiber laser ring cavity using highly nonlinear fiber (HNLF). DFB, distributed feedback laser; EDFA, erbium doped fiber amplifier: WDM, wavelength division multiplexer; OC, output coupler; PC, polarization controller.**

To test the intracavity dispersion compensation and verify the GVD value computed value of HNLF different lengths of HNLF are added in the laser cavity after Tm/Ho co-doped fiber as shown in Figure 3.11. To minimize the splice losses in the cavity a small section of SMF is spliced between Tm/Ho co-doped fiber and HNLF. The laser is mode-locked for each length of HNLF and the separation of first order Kelly sideband from the center wavelength is measured. The mode-locked spectrum is measured for 1 m, 5.1 m and 5.7 m of HNLF. The mode-locked spectrum with 5.1 m of HNLF and without HNLF in the cavity along are shown in Figure 3.12. No significant outward shifts of Kelly sidebands were observed with 5.1 m of HNLF, indicating that it has a very small GVD, thus confirming the magnitude of the HNLF's dispersion.

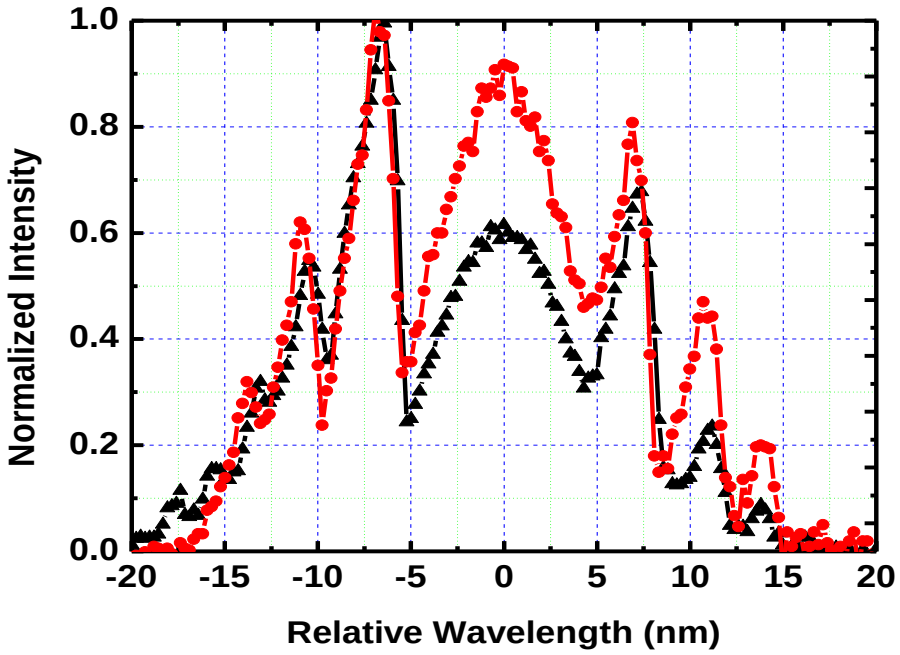


**Figure 3.12 Mode-locked spectrum of Tm/Ho co-doped fiber laser with (red circle) and without (black triangle) highly nonlinear fiber (HNLF) in the laser cavity. For better comparison of spectral bandwidth it is plotted with respect to relative wavelength.**

### *3.5.2 Erbium Doped Fiber*

Previously, Wang *et al.* demonstrated intracavity compensation using normal GVD erbium-doped fiber [96], so a length of erbium-doped fiber was added for intracavity dispersion compensation. Same as in the case of HNLF, different lengths of erbium-doped fiber are used inside the laser cavity and the spacing of the first order Kelly sideband from the center wavelength is measured. The experimental set up is the same as in Figure 3.11 where the HNLF is replaced by erbium-doped fiber. Here, again a small section of SMF is spliced between Tm/Ho co-doped and erbium-doped fibers. Three different erbium-doped fibers, Er30 (highly doped erbium fiber designed for c- and L- band amplifiers and ASE sources), Er80 (large mode area

erbium doped fiber suitable for medium power amplifiers and lasers), and HP980 (high performance erbium doped fiber used for high power 980 nm pumping) are used. For all of these three fibers, no significant outward shift of the Kelly sideband is observed indicating that erbium-doped fiber might not have normal dispersion to compensate the anomalous dispersion of SMF and Tm/Ho co-doped fiber. The mode-lock spectrum for one of the erbium-doped fibers Er30 is shown in Figure 3.13. When the erbium-doped fiber is used in the cavity the mode-locking is not stable and the center wavelength also shifts around. This might due to more loss created by the erbium fiber at lasing wavelengths.

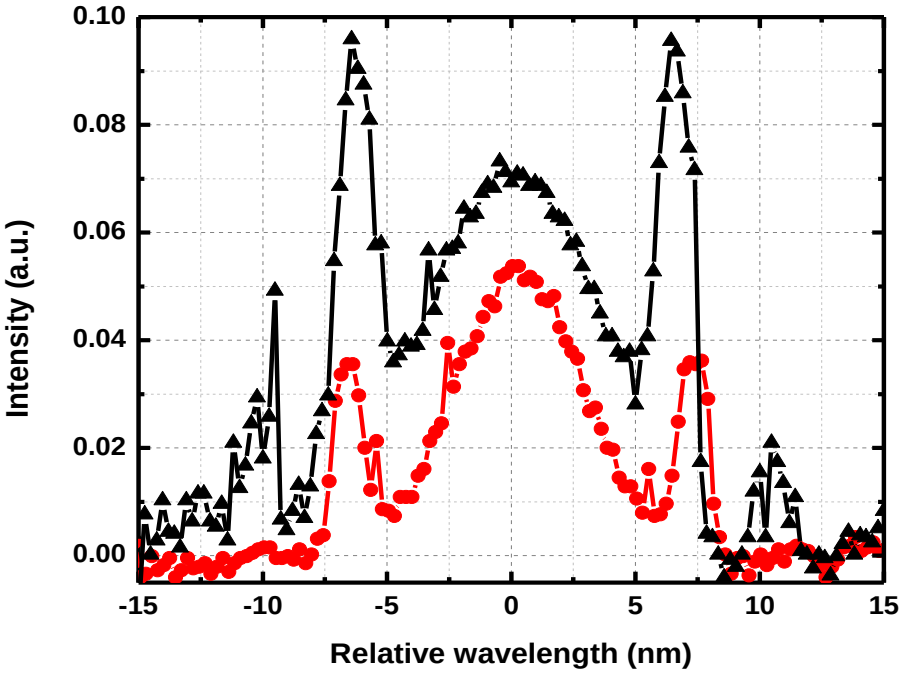


**Figure 3.13 Mode-locked spectrum of Tm/Ho co-doped fiber laser with (red circle) and without (black triangle) erbium-doped fiber in the laser cavity. For better comparison of spectral bandwidth it is plotted with respect to relative wavelength.**

According to Eq. (3.3) when the longer lengths of fibers having anomalous GVD added in the laser cavity the Kelly sideband should move towards the center wavelength. To verify this, lengths of SMF are added in the laser cavity. The laser is mode-locked and the spacing of first Kelly sideband from the center wavelength is measured for each added length of SMF. As it expected the inward shift of the Kelley sideband is observed when more SMF is added in the cavity as shown in Figure 3.14.

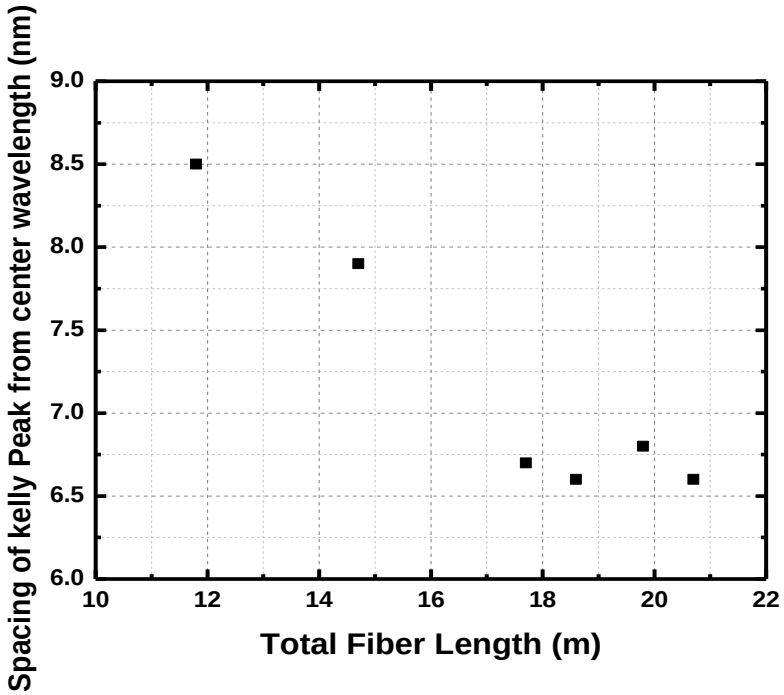


**Figure 3.14 The spacing of first order Kelly peak from the center wavelength as a function of total fiber length in the cavity. Total length of fiber is obtained as the sum of individual fibers used.**

### *3.5.3 Vascade Fiber*

Since both highly nonlinear and erbium-doped fibers could not compensate the anomalous dispersion of the cavity, I looked through other possible fibers which might have normal dispersion at longer wavelength. Among them Vascade fiber is tried. It is a dispersion

compensating fiber specially designed for use in submarine optical transmission cables. The index profile of the Corning Vascade fiber is similar to the HNLF. Although there is no information of the GVD of this fiber at longer wavelengths; it was tried relying on its geometry so that it might have normal GVD. But unfortunately this fiber also could not able to compensate the anomalous dispersion of Tm/Ho co-doped and SMF because no outward shift of Kelly sideband as well as increase in spectral width of the laser output are observed.

## 3.6 Tm/Ho Fiber Cut-Back Measurement

The dispersion of all the dispersion compensating fibers is too small to compensate the anomalous dispersion of Tm/Ho co-doped fiber and SMF while maintaining a repetition frequency of the laser larger than 10 MHz. In order to minimize the net cavity dispersion, I decided to reduce the lengths of Tm/Ho co-doped fiber and SMF from the cavity while maintaining the mode-locking stability. First, the length of Tm/Ho co-doped fiber is reduced from the cavity keeping the length of the SMF same and the laser is mode-locked for each cut-back. As the length of Tm/Ho co-doped fiber is reduced, the spectral bandwidth of the laser increased by a small amount. For each cut back, the spectral bandwidth and the spacing of Kelly sideband from the center wavelength were measured. The variation of spectral bandwidth with respect to the Tm/Ho co-doped fiber length is plotted in Figure 3.15.

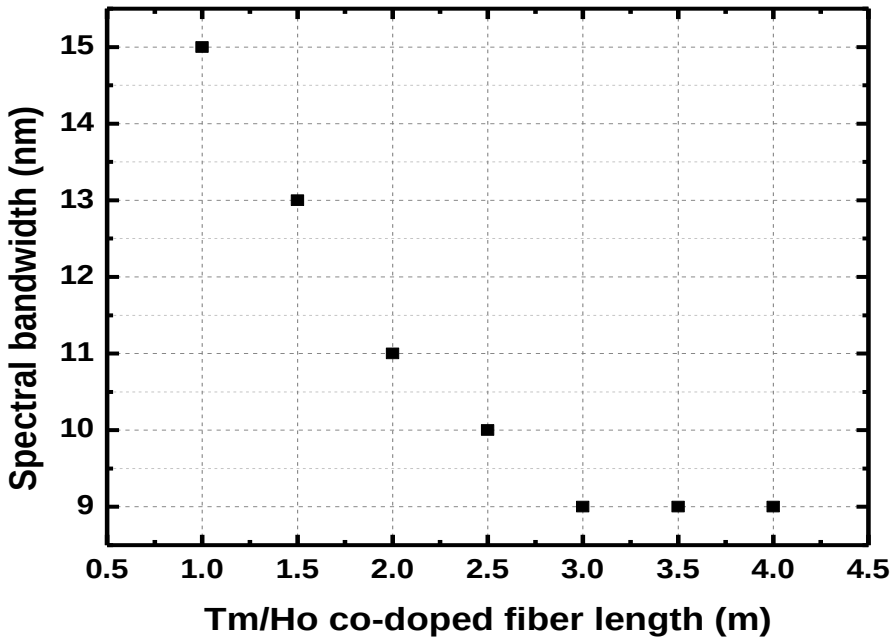


**Figure 3.15 Variation of spectral bandwidth of the mode-locked laser with the length of Tm/Ho co-doped fiber. The lengths of SMF and pump power are kept constant for each cut-back.**

It is observed that the spectral bandwidth increased as the length of Tm/Ho co-doped fiber reduced from the cavity. During this measurement it is observed that the spacing of Kelly sideband from the center wavelength increased as the fiber length decreased. For 4 m of Tm/Ho co-doped fiber the spacing is 8 nm but it becomes 11 nm when the fiber length is 1 m for same length of SMF in the cavity. The increase in spectral bandwidth and decrease in spacing of the Kelly sideband while shortening the length of Tm/Ho fiber from the cavity indicate that the Tm/Ho co-doped fiber has anomalous dispersion at 2 μm. The mode locked spectrum for both cases plotted together are shown in Figure 3.16.

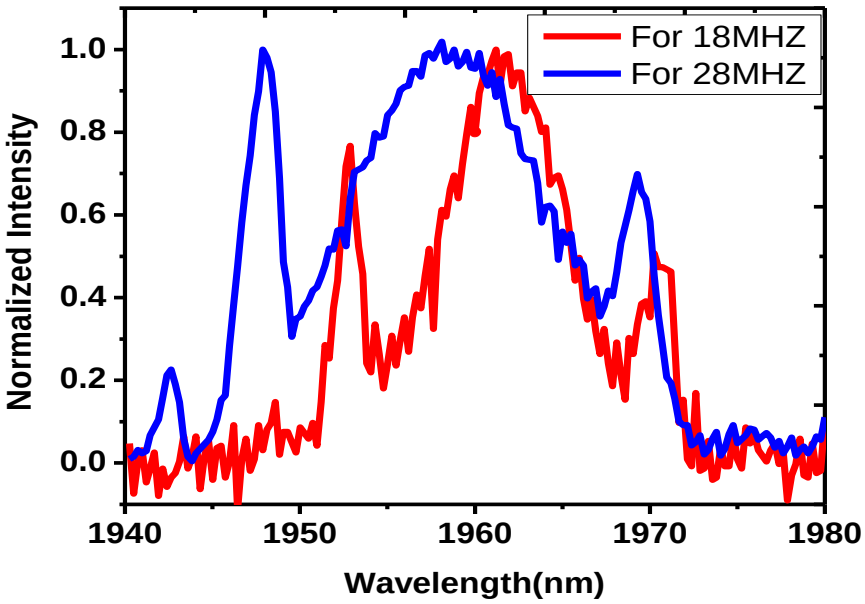


**Figure 3.16 Mode-locked output spectrum for 4 m (red line) and 1 m (blue line) of Tm/Ho co doped fiber with 6 m of SMF28 when pumping at 1.56 µm. The spectral widths are 9 nm and 15 nm respectively at FWHM.**

The optimized cavity length is 7 m with 1 m of Tm/Ho co-doped fiber. Initially, mode-locking was obtained at pump powers higher than ~ 200 mW when the two polarization controllers PC1 and PC2 were carefully adjusted. Later, this configuration exhibited self-starting operation where mode locking was obtained by only increasing the pump power above the threshold without any change in the intracavity polarization. The laser remained mode locked for hours at a time, limited only by the temporal variation of the pump laser polarization. In fact, self-starting mode locking has been possible without a change in intracavity polarization over many months of operation. Figure 3.17 shows the (a) output spectrum and (b) the ESA spectrum of the mode locked Tm/Ho co-doped fiber laser in this configuration. The output power measured after the output coupler is ~ 25 mW, with repetition frequency of 28.4 MHz and

spectral bandwidth of 15 nm FWHM. The 28.4 MHz repetition frequency signal was observable using a 15 MHz detector producing a 50 dB signal to noise ratio (300 kHz resolution bandwidth) peak on an electrical spectrum analyzer. The measured repetition frequency was in agreement with the total length of fiber in the laser cavity.

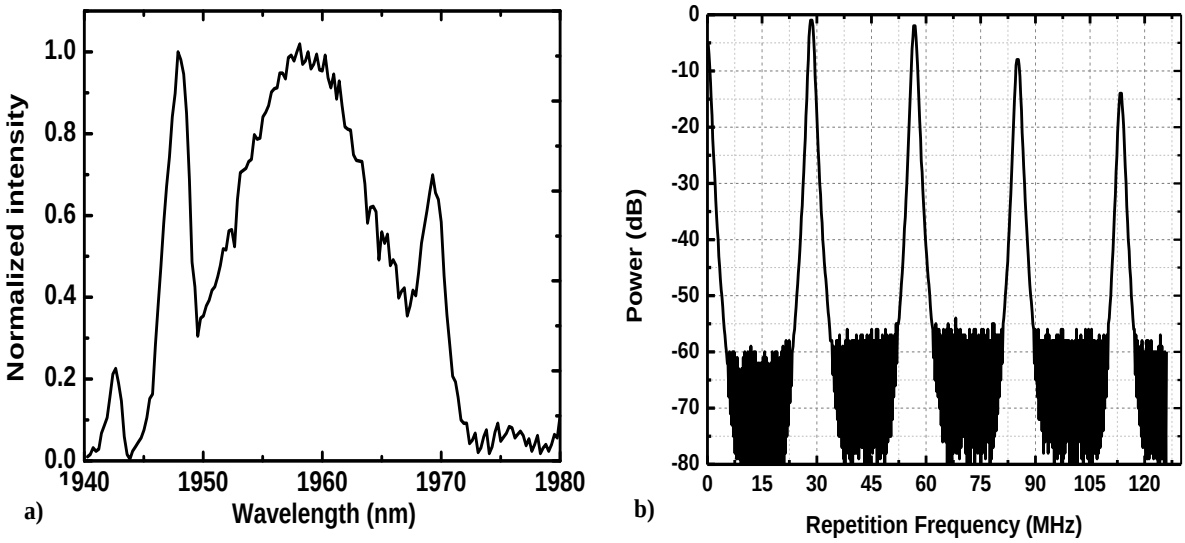


**Figure 3.17 a) Mode-locked output spectrum b) electrical spectrum analyzer (ESA) spectrum for 1 m of Tm/Ho co-doped fiber and 6 m of SMF28 when pumping at 1.56 µm. The spectral width is 15 nm FWHM [90].**

Further optimization would require obtaining knowledge of both the magnitude and sign of the GVD for both the SMF and Tm/Ho co-doped fiber. While the GVD value for the SMF (which was calculated using the proper Sellmeier coefficients [95], the fiber core size, and the weakly guiding approximation [75]) only have an order of magnitude approximation from the literature. Equation (4.3) could be used to compute the GVD of the Tm/Ho co-doped fiber, but this requires a measurement of the pulse duration. If one assumes the transform limited pulse duration for a spectral bandwidth of 15 nm (269 fs) and uses the measured sideband spacing, the

net cavity dispersion is $\beta_2 L = 1.87\times10^{-5}$ fs$^2$ at the center wavelength of 1.96 μm. Given the value of $\beta_2$ for SMF and the experimental fiber lengths, a positive value of GVD for the Tm/Ho co-doped fiber is computed. However, it is observed during cut-back measurement that the sideband wavelength separation increased as the length of Tm/Ho co-doped fiber is decreased, indicating that the Tm/Ho co-doped fiber has anomalous GVD [as from Eq. (3.3)]. Therefore, the observed spectra are inconsistent with a transform-limited pulse. Although I cannot measure the Tm/Ho co-doped fiber GVD, I can instead estimate the pulse duration from this measurement. Assuming that the magnitude of the Tm/Ho co-doped GVD is $10^{-5}$ fs$^2$/nm, which is on the order of a similar fiber reported in [97], the estimated pulse duration is ~800 fs. To verify this pulse duration, an interferometric autocorrelation (IAC) measurement on the laser output [98] is performed, as described below.

## 3.7 Pulse Characterization

The optimum operation of the mode-locked laser can be verified by measuring the temporal profile of an ultrashort pulse. The ultrashort pulse can be measured using either an electronic or optical device. The standard opto-electronic devices include fast photodiode, and streak cameras based on linear techniques, can measure ps pulse durations but cannot successfully measure the sub-femtosecond time scale directly, since the time response of these devices is only on the order of ps. A simple and widely used method to measure the duration of ultrashort pulses employ optical interferometry and gating via nonlinear effects in a crystal or semiconductor diode. Optical interferometry is based on the optical correlation function given by

$$G(\tau) = \int_{-\infty}^{\infty} F_1(t)F_2(t-\tau)d\tau \tag{3.4}$$

where $F_1(t)$ and $F_2(t)$ are two independent functions of time, and τ is the delay between them. When both $F_1(\tau)$ and $F_2(t)$ are the same function then it is referred to as a second order correlation

$$A^{(2)}(\tau) = \int_{-\infty}^{\infty} F(t)F(t-\tau)d\tau \tag{3.5}$$

Experimentally, the second order correlation is obtained either by second harmonic generation (SHG) or two photon absorption (TPA) at the output of the interferometer. $A^{(2)}(\tau)$ is symmetric with respect to time delay τ, it is always positive, and has maximum value at zero delay, τ = 0 [99]. Due to symmetric properties of the second order autocorrelation, any asymmetry in the pulse will be lost.

The actual pulse duration of the laser output can be estimated from the autocorrelation trace by using conversion factors as shown in Table 3.1 [98], where $\tau_p$ is the full width half maximum (FWHM) pulse duration, and $\tau_a$ is the FWHM of the autocorrelation trace.

**Table 3-1 Temporal conversion factors for second order autocorrelation function for Gaussian and hyperbolic secant pulses. Actual pulse duration can be found by dividing the autocorrelation width by the conversion factor for each case.**

| Pulse Type | Intensity | Conversion factor ($\tau_p$ / $\tau_a$) |
|---|---|---|
| Gaussian | $e^{-t^2}$ | 1.414 |
| Hyperbolic secant | $sech^2 t$ | 1.543 |

In this experiment, a second-order collinear autocorrelation also known as fringe resolved autocorrelation (FRAC) or interferometric autocorrelation [100] is used. A schematic diagram of

interferometric autocorrelation is shown in Figure 3.18 and the actual experimental set up in the lab is shown in Figure 3.19. It is based on a Michelson interferometer and the signal detection is accomplished using TPA in an InGaAs detector. The output of the Tm/Ho co-doped fiber laser is collimated using a lens of 11 mm focal length. The light is then split in half using a 50/50 beam splitter; one of the beams reaches a fixed mirror M1 which is placed on a linear translation stage and reflected back to the beam splitter. The other beam is reflected back to the beam splitter from movable mirror M2 glued on a speaker. The reflected beams from both arms are then combined by the same beam splitter and finally focus onto a detector using 4 mm focal length lens.

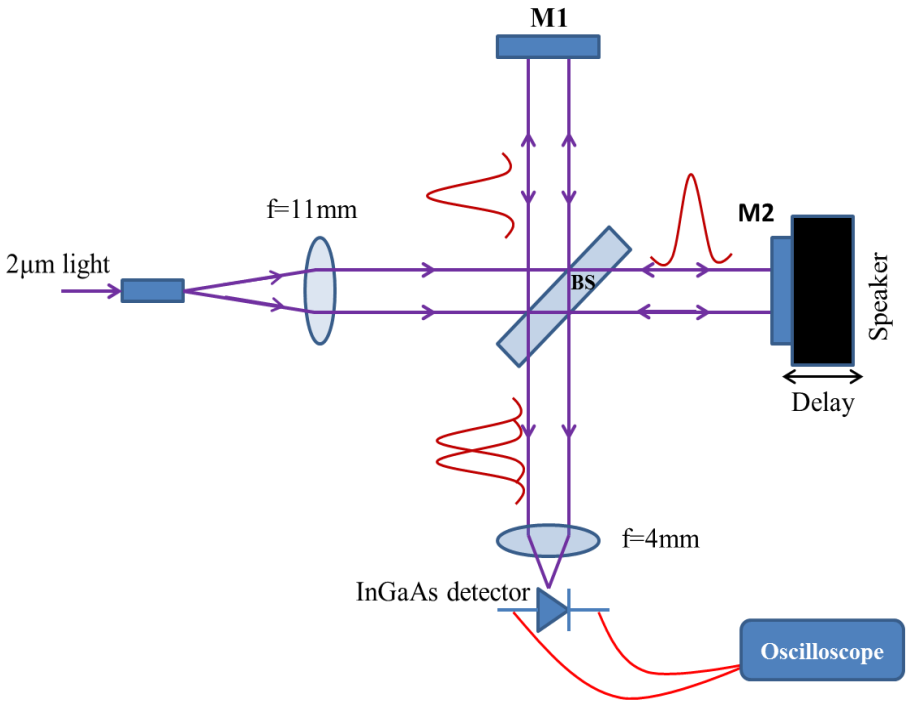


**Figure 3.18 Schematic of the collinear interferometric autocorrelation based on Michelson interferometer. BS, beam splitter; M, mirror. The input beam is split into two equal parts by the 50/50 beam splitter. The reflected beam from two mirrors M1 and M2 combine together by the same beam splitter.**

I used 1.5/2 μm WDM and germanium (Ge) filter to ensure no residual pump (1.56 μm) was incident on the InGaAs detector. To monitor the interferometric autocorrelation trace, the output

of the detector is connected to an oscilloscope. This technique has two major consequences; first interference fringes will appear across the pulse as a function of delay, and second, there will be background output even when the two pulses are not overlapping. The background detection is an important limitation of this type of autocorrelation because the low lying features such as pedestal and wings may be swamped and not be detected [101].

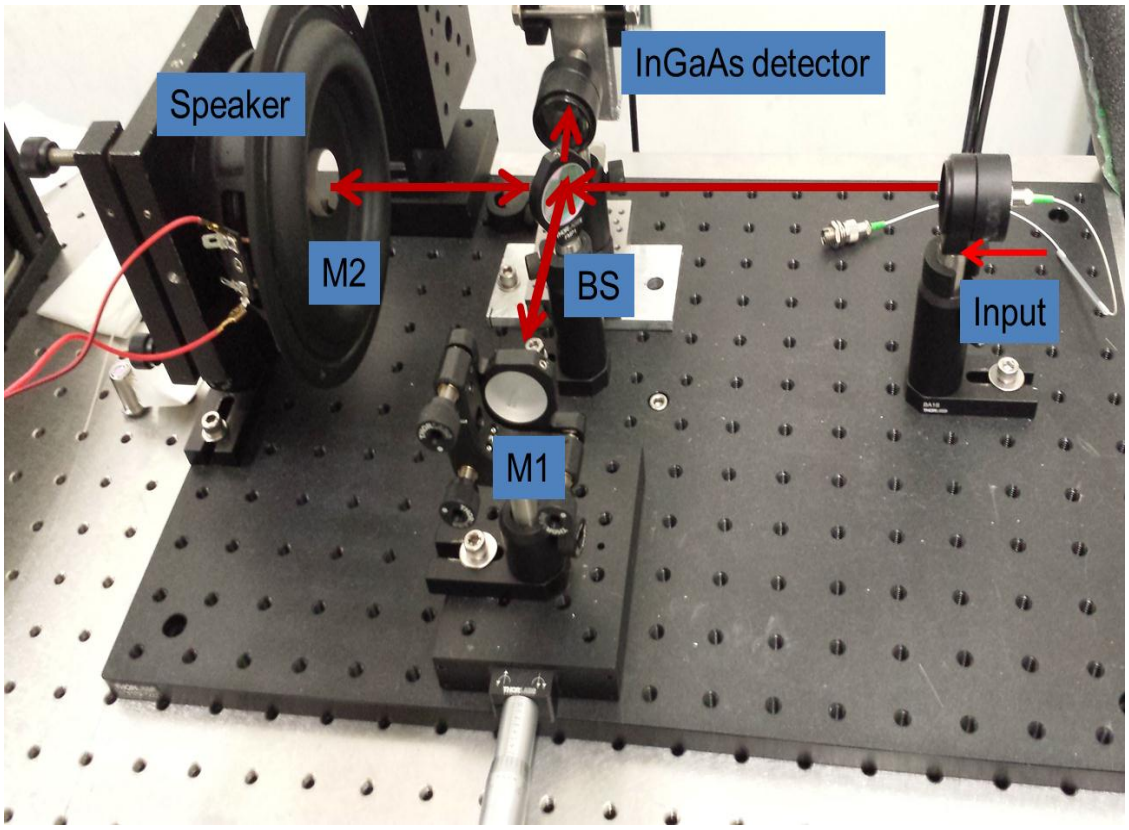


**Figure 3.19 Experimental setup of the collinear interferometric autocorrelation based on Michelson interferometer. BS, beam splitter; M, mirror. 50/50 beam splitter is used to divide the light in two equal amounts. Mirror M1 is fixed and mirror M2 is attached to the speaker to provide the variable delay in one of the arm. The reflected beams from M1 and M2 are combined on the BS and focused into InGaAs detector using a 4 mm focal length lens.**

For the given electric field the interferometric autocorrelation is given by

$$IA^{(2)}(\tau) = \int_{-\infty}^{\infty} |[E(t) + E(t-\tau)]^2|^2 dt \tag{3.6}$$

with $I(t) = |E(t)|^2$. Eq. (3.3) can be expanded to

$$IA^{(2)}(\tau) = \int_{-\infty}^{\infty} [I^2(t) + I^2(t-\tau)]dt + 4\int_{-\infty}^{\infty} I(t)I(t-\tau)dt +$$

$$+2\int_{-\infty}^{\infty} [I(t) + I(t-\tau)]\, E(t)E^*(t-\tau)dt + c.c.$$

$$+\int_{-\infty}^{\infty} [E^2(t) + E^{*2}(t-\tau)]dt + c.c. \tag{3.7}$$

where the first term on right hand side is a constant, the second term is the intensity autocorrelation giving the outer shape of the pulse, the third term is the interferogram of *E(t)* which oscillates at $\omega$, and the fourth term is the interferogram of the $E^2(t)$ which oscillates at $2\omega$. For the ideal 50/50 beam splitter the interferometric autocorrelation has peak to background ratio of 8:1 which is higher than the conventional intensity autocorrelation (3:1). For 2 μm light with pulse duration 1000 fs the computed interferometric autocorrelation trace for transform limited and chirped pulses [Appendix D] are as shown in Figure 4.20, for hyperbolic secant pulse shape. In order to get the chirped pulse 1000 fs transform limited pulse is propagated through the length of SMF.

The interferometric autocorrelation is very sensitive to the extract pulse shape because the fourth power of the electric field amplitude is involved in the measurement of intensity of the second harmonic field amplitude. Hence, any vibrations introduced by the delay stage should be minimized, and also all the opto-mechanical components should be fixed firmly.

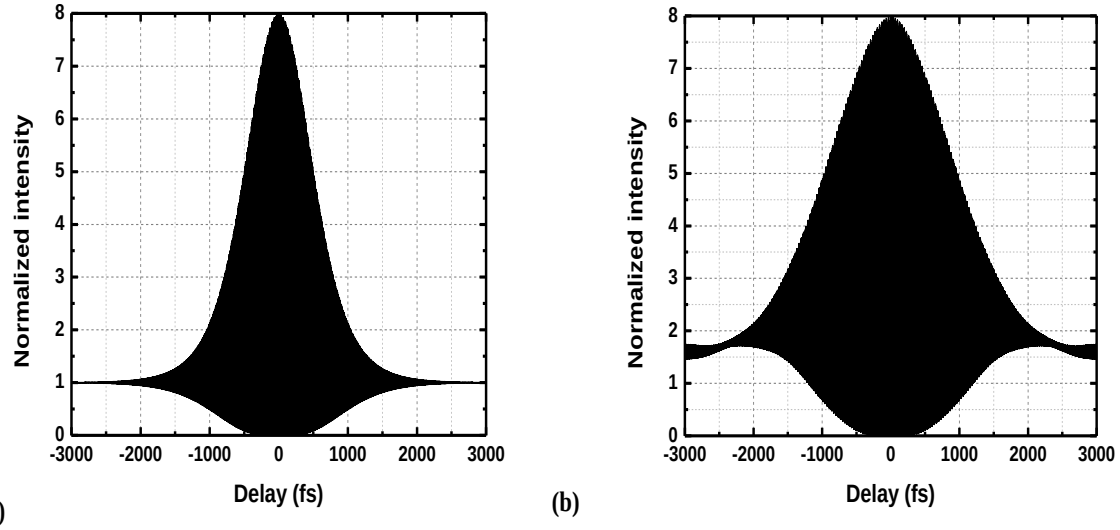


**Figure 3.20 IAC trace for hyperbolic secant (a) transform limited and (b) chirped pulse for 1000 fs pulse width at 2 μm. The chirped pulse is obtained by propagating 1000 fs transform limited pulse through a length of SMF.**

### *3.7.1 Delay Calibration*

In order to determine the actual pulse duration, one needs to calibrate the delay introduce by the movable stage in the time scale of the pulse duration. When the mirror M2 is fixed the path length between two arms is same but once the speaker starts to move, it creates an extra path length. This extra path length corresponds to the delay between two the arms and is given by

$$\tau = \frac{2\,\Delta l}{c} \tag{3.8}$$

where $c$ is the speed of light, and $\Delta l$ is the linear displacement provided by the speaker. In practice it is hard to measure this linear displacement experimentally. But, what I can measure is

the driving voltage applied to the speaker. So, I calculated the delay in terms of the voltage applied to the speaker. The calibrated delay in terms of applied voltage is 7 ps/V.

### *3.7.2 Two Photon Current Measurement*

Since the signal measurement in interferometric autocorrelation is based on the two photon measurement the lowest two photon current needs to calculate that the detector can see. The two photon measurement is the nonlinear process so the nonlinear responsivity of the InGaAs detector is used to calculate the threshold. Nonlinear responsivity of the detector is $3.4\times10^{-5}$ nA/mW$^2$ as given by [102]

$$R_{NL} = \frac{I_{TPA}}{P_0 P_{avg}} \tag{3.9}$$

where $I_{TPA}$ is the two photon current, and $P_0$ and $P_{avg}$ are the peak and average power of the laser output. Using the laser parameters and the nonlinear responsivity of the detector, the lowest two photon current that the detector can see is 170 nA. The minimum power that is needed to generate 170 nA current is 0.23 μW. To verify that the measured current in the detector is due to two photon absorption, the output current is measured after the neutral density (ND) filter. The measured output current with respect to input power is plotted and shown in Figure 3.21. As expected, the response of the detector should be nonlinear with respect to the input power that is going into the detector after the ND.

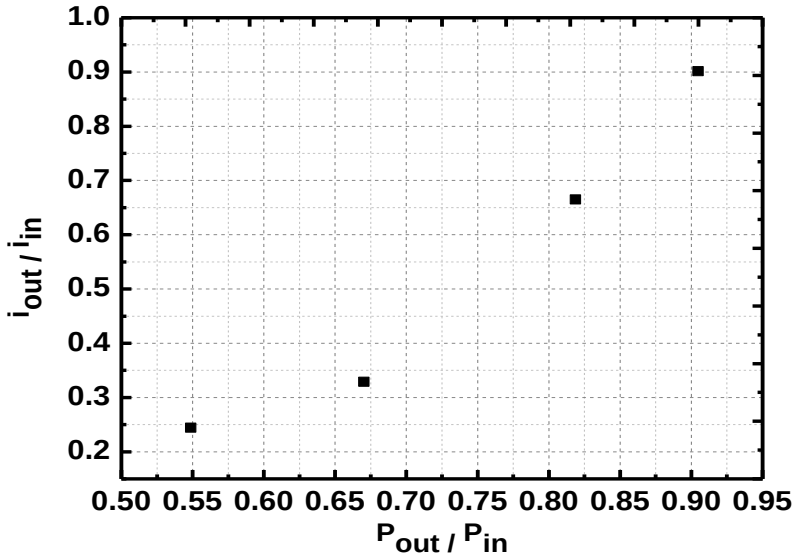


**Figure 3.21 Two photon current of InGaAs detector for incident 2 μm light. The output two photon current is measured when neutral density (ND) filter is introduced in front of the detector.**

### *3.7.3 Pulse Width Measurement*

After carefully aligning the laser beam from both the arms and focusing tightly onto the detector the interferometric autocorrelation (IAC) trace is obtained. It exhibits the proper 8 to 1 ratio between peak and background as shown in Figure 3.22 along with the computed IAC envelope using analytical expressions for a hyperbolic secant temporal electric field [98]. The IAC full width half maximum (FWHM) is 1833 fs and this measurement is consistent with the sideband spectral measurements. The temporal conversion factor of a pulse- to-IAC width for a hyperbolic secant temporal electric field is 0.53, which gives a pulse duration of 966 fs.

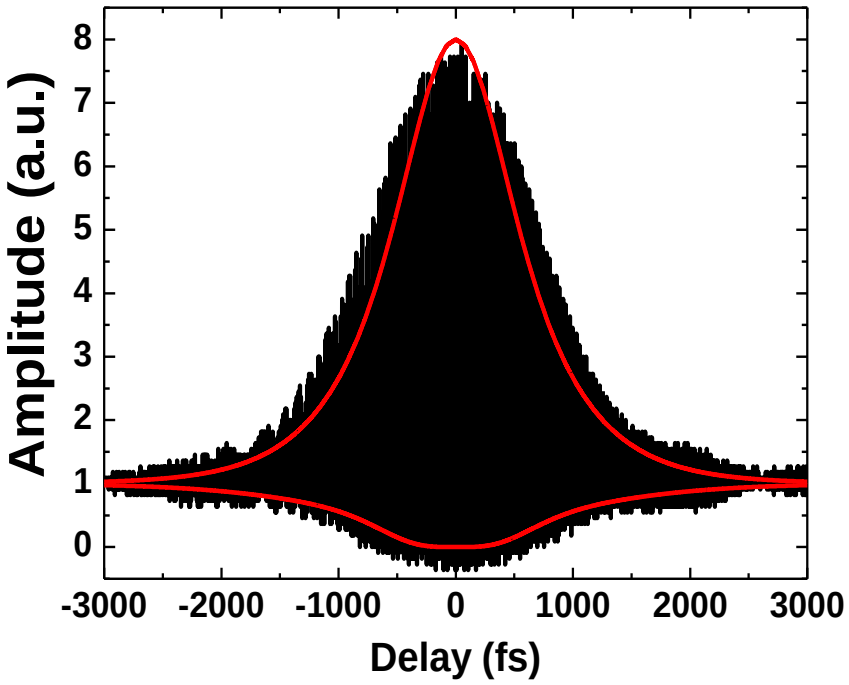


**Figure 3.22 Interferometric autocorrelation trace of the laser output. The autocorrelation FWHM was 1833 fs corresponding to pulse duration of 966 fs. The computed IAC envelope for a 966 fs pulse that exhibits self-phase modulation is plotted for comparison [90].**

Information about the pulse's phase distortion can be deduced from the IAC trace as well. The phase distortion is primarily due to self-phase modulation (SPM) and not GVD since the IAC measurement exhibits fringes across the entire trace [98]. SPM preserves the pulse coherence and thus fringes can be seen across the entire IAC trace, which is not the case for a pulse that exhibits only second order phase distortion.

The spectral measurement at the time of the IAC measurement revealed that the spectral bandwidth reduced from 15 nm to 8 nm over the course of six months. The spectrum corresponds to the above IAC trace as shown in Figure 3.23. The cause of bandwidth reduction is

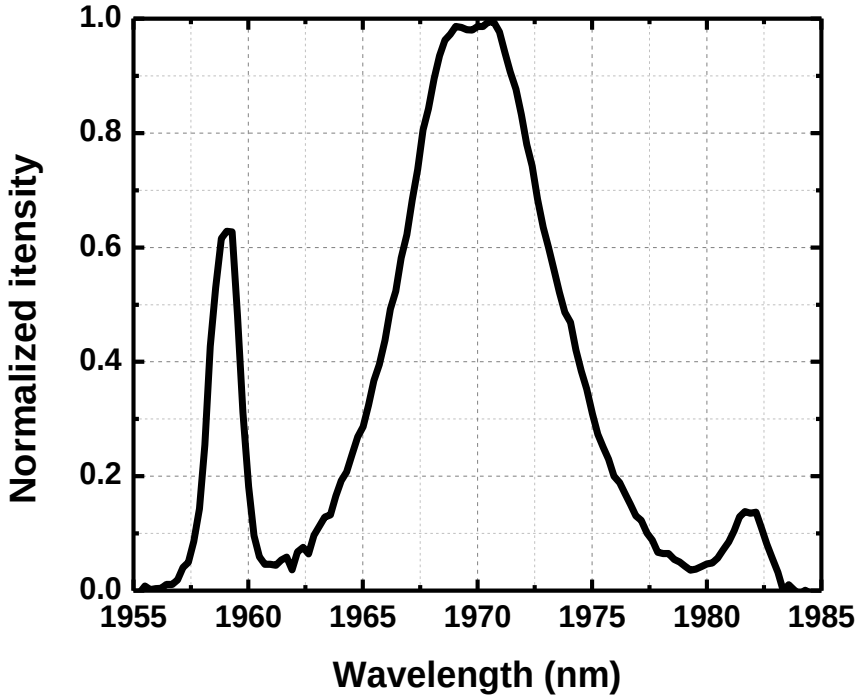


**Figure 3.23 The mode-locked spectrum of Tm/Ho co-doped fiber laser at the time of autocorrealtion measurement [90]. The full width half maximum (FWHM) is 8 nm.**

unclear: the bandwidth could not be increased by changing the intracavity polarization. The optical components, specifically polarization sensitive isolator (c-band) used in the cavity were not designed for 2 μm. It is believed that the insertion loss of the isolator may have increased over the six months, caused possibly by inadvertently passing more than maximum recommended power (300 mW) through it during the initial mode-locking attempts. Increasing the insertion loss will create a larger cavity loss, so the gain will be saturated less when lasing occurs. Due to the wavelength-dependent absorption and emission cross section, this will change the center wavelength. A reduction of intracavity power will also reduce the total nonlinear phase shift and thus the spectral width.

## 3.8 Mode-Locking at Two Different Center Wavelengths

The laser is able to mode-lock at one of two center wavelengths by carefully adjusting the intracavity polarization during the process of mode-locking. The output spectra at two different center wavelengths ~80 nm apart are shown in Figure 3.24.

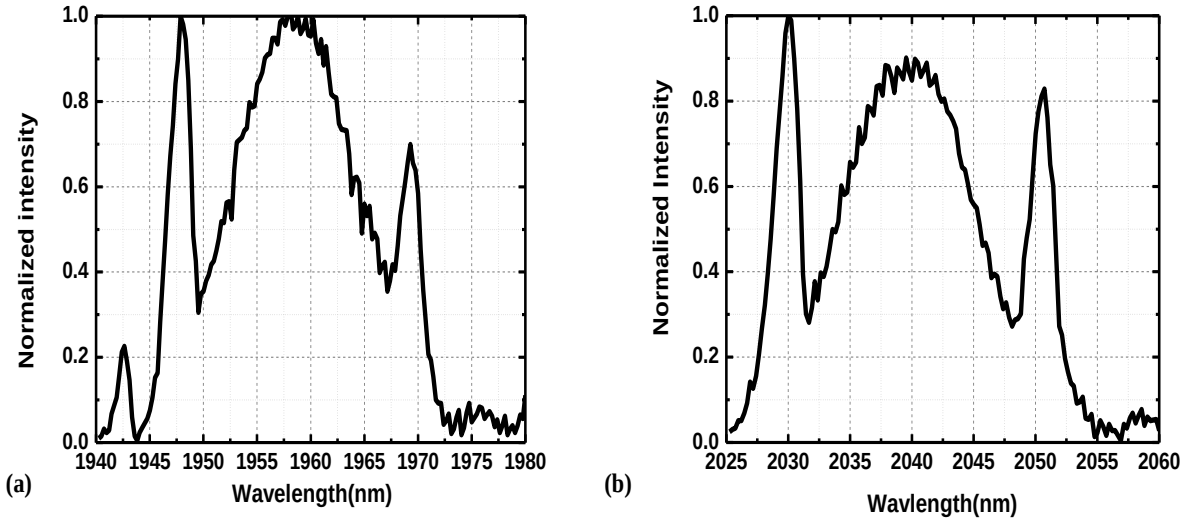


**Figure 3.24 Mode-locked spectrum for 1 m of Tm/Ho co-doped fiber when pump power is ~300 mW with center wavelengths at a) 1.96 μm and b) 2.04 μm. Each spectrum was obtained under separate mode-locking conditions [90].**

The left spectrum is centered at 1.96 μm with a FWHM bandwidth of ~15 nm and the output power measured is ~25 mW. Mode-locking can be stopped by external perturbation, decreasing the pump power or changing the position of polarization controllers. Once the mode-locking has been terminated, it can be initiated again with the same pump power but at a different position of the polarization controllers and the laser can be mode-locked at a different

center wavelength. Figure 3.24 (b) shows the mode-locked spectrum at a center wavelength of 2.40 μm with a bandwidth of 13 nm and the output power is almost the same.

The ability to lase on one of the two center wavelengths is a result Tm/Ho co-doping. For Tm/Ho fiber lengths of ~1 m, it has been observed that the ASE exhibits a peak near 2 μm but a shoulder near 1.9 μm [11]. The emission at 1.97 μm is due to the $Tm^{3+}$ emission while the 2.04 μm is due to $Ho^{3+}$. In another study [103], the fluorescent from a 6:1 ratio Tm/Ho fiber was measured as a function of fiber length. Fiber lengths smaller than 0.5 m exhibited more fluorescence at ~1.97 μm compared ~2.04 μm, while a fiber of ~1 m exhibited similar levels of fluorescence at these two wavelengths. Longer fiber have reduced emission at the shorter wavelength due to the energy transfer from $Tm^{3+}$ to $Ho^{3+}$, and due to re-absorption of the $Tm^{3+}$ emission [103]. To optimize the ability to mode-lock at these center wavelengths, the fiber length must be chosen to permit some energy transfer but not at the cost of depleting the $Tm^{3+}$ emission.

## 3.9 Summary

An all fiber Tm/Ho co-doped mode-locked laser operating in the solitonic regime is demonstrated and that can lase at one of two center wavelengths by adjusting the polarization controllers and pump power. The laser is self-starting by increasing the pump power above the threshold without any change in the polarization of the cavity. The pulse width of the laser is measured using interferometric autocorrelation. The intracavity dispersion compensation is studied using various fibers such as highly nonlinear fiber, erbium doped fiber and Vascade

fiber. A large spectral bandwidth could not be obtained due to the lack a large normal GVD fiber in to compensate anomalous dispersion of other fibers.

Since the short pulse and high peak power laser is required for applications, I will introduce other kind of normal GVD fiber to compensate the intracavity dispersion in next chapter and the laser will operate in the stretched-pulse.

Note: This research in Chapter 3 has been published in Ref. [90].

# Chapter 4 - Stretched-Pulse Operation and Study of Laser Dynamics

## 4.1 Introduction

In Chapter 3, I discussed the mode-locked Tm/Ho co-doped fiber laser operating in the solitonic regime where the net cavity group velocity dispersion (GVD), defined as the sum of each fiber's GVD times length, is always negative. The formation of dispersion managed solitons in the cavity, which occurs when the net cavity GVD is negative, limits the output pulse duration and hence peak power and pulse energy due to the formation of spectral sidebands (Kelly sidebands) and saturation of the nonlinear polarization rotation [16]. To increase the spectral bandwidth of the mode-locked laser the intracavity dispersion need to be managed. The net cavity GVD of the fiber laser cavity can be controlled by introducing the sections of normal and anomalous dispersion (GVD or $\beta_2$) in the cavity. When the net cavity GVD is small but positive solitons do not form but the intracavity pulse periodically stretches and compresses for each round trip, allowing for the formation of shorter pulses as shown in Figure 5.1. This mode-locking regime is called the stretched-pulse regime. Here, the average peak power in the laser cavity is lowered significantly as the pulse width changes by an order of magnitude and hence the net nonlinear shift per round trip is small, and the saturation effect is avoided. Similar to the erbium doped fiber lasers, Tm/Ho co-doped fiber lasers can be mode-locked in the stretched-pulse regime which produces a wider spectral bandwidth than operating in the solitonic regime [20].

Achieving a positive net cavity GVD is challenging for Tm/Ho co-doped fiber lasers since it is hard to find a fiber has normal GVD at 2 μm to compensate the anomalous GVD of the gain fiber and the Corning SMF-28 single mode fiber (SMF) in the laser cavity. Bulk fused silica has anomalous GVD at 2 μm, so a fiber would need a very large and positive waveguide dispersion to exhibit normal GVD at 2 μm. As discussed in Chapter 3, I used couple of fibers such as HNLF, Er-doped fiber and Vascade fiber to compensate the anomalous dispersion but these fibers did not exhibit enough normal GVD for effective dispersion compensation.

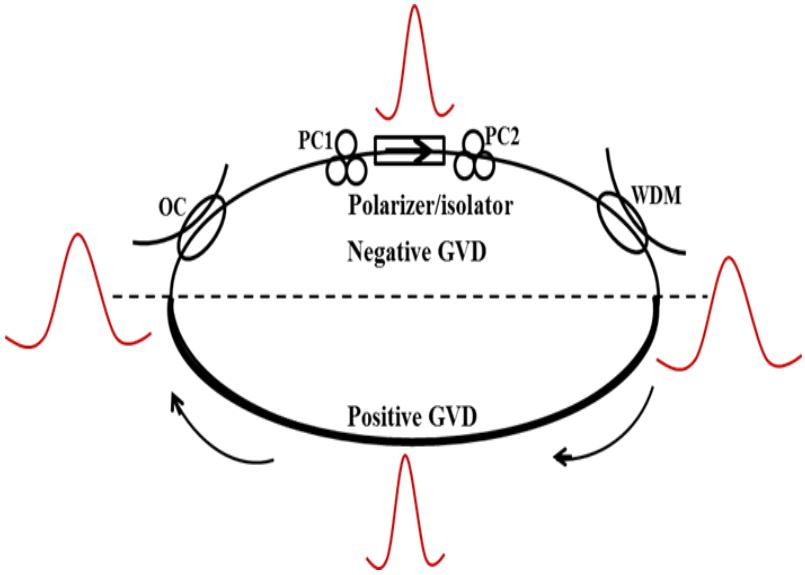


**Figure 4.1 Schematic of the all fiber stretched-pulse operation; WDM, wavelength division multiplexer; OC, output coupler; PC, polarization controller [104].**

Recently, a number of attempts at dispersion compensation have been used both in free-space and fiber based compensation methods. Haxsen *et al.* demonstrated stretched-pulse operation from a Tm-doped fiber laser using an intracavity pulse stretcher composed of a free space section with a telescope and grating pairs [105]. Wang *et al.* demonstrated intracavity compression using a normal GVD erbium-doped fiber [96] and Gumenyuk *et al.* demonstrated a dissipative dispersion- managed soliton fiber laser employing chirped fiber Bragg grating [106].

In these works, the laser cavity has a free space section. But, to keep the laser in all fiber formats with high repetition rate, it is necessary to have a fiber which has normal GVD at 2 μm. As discussed in Chapter 2, the total dispersion of the fiber is given by the sum of material and waveguide dispersion. So the net GVD of the fiber can be made normal if the waveguide dispersion is higher than the material dispersion, where material dispersion of the fused silica fiber is always negative at 2 μm. The waveguide dispersion can be tailored by changing the geometry of the fiber such as core size and numerical aperture (NA). Recently, ultrashort pulses were generated from mode-locked thulium fiber laser using high NA fiber as normal dispersion fiber inside the laser cavity [107, 108]

In this chapter, I will discuss the dispersion compensation of the Tm/Ho co-doped fiber laser both internally and externally. First, I will discuss the external pulse compression using hollow core photonic bandgap (HC-PBG) fiber. In next few sections, I will discuss the intracavity dispersion compensation using narrow core and high NA fiber to operate the laser in the stretched-pulse regime. Finally, I will discuss the dynamics of the laser while going from stretched-pulse to the solitonic regime.

## 4.2 External Pulse Compression

One way of getting shorter pulses from the mode-locked fiber laser is external pulse compression using a fiber with an opposite sign of the GVD than the net cavity GVD. In the Tm/Ho co-doped fiber laser, the net cavity GVD is always negative. In order to compensate this net negative cavity GVD a hollow core photonic bandgap fiber HC-2000 manufactured by NKT photonics is used outside the laser cavity. This particular HC-PBG fiber is designed for 2 μm

wavelength where light is guided in hollow core, surrounded by a microstructure cladding of air holes and silica. The manufacture's specification of this fiber is shown in Table 4.1.

**Table 4-1 Physical and optical properties of HC-2000 PBG fiber provided by the manufacturer, NKT photonics [109].**

| Physical properties | |
|---|---|
| Core diameter | 15 ± 1 µm |
| Cladding pitch | 4.8 ± 0.1 µm |
| Diameter of PCF region | 90 ± 5 µm |
| Cladding diameter | 155 ± 5 µm |
| Coating diameter | 275 ± 30 µm |
| Coating material | Single layer acrylate |

| Optical properties | |
|---|---|
| Design wavelength | 2000 nm |
| Attenuation @ 2000 nm | < 20 dB/km |
| Typical GVD @ 2000 nm | -20 ps/nm/km |
| Operating wavelength(1) | 1965-2125 nm |
| Estimated MFD @ 2000 nm(2) | 11 µm |

The GVD of HC-2000 provided by the manufacturer is as shown in Figure 4.2. This fiber has zero group velocity dispersion is at wavelength 2.01 µm; below this wavelength it has normal GVD and above this wavelength it has anomalous GVD. In Chapter 3, it is shown that the laser can be mode-locked at two separate wavelengths, one around 1.96 µm and other around 2.04 µm by adjusting the polarization controllers and pump power. So when the laser is mode-locked below 2 µm wavelength, the normal GVD of HC-2000 can compensate the anomalous net GVD of the cavity and pulse compression can be achieved.

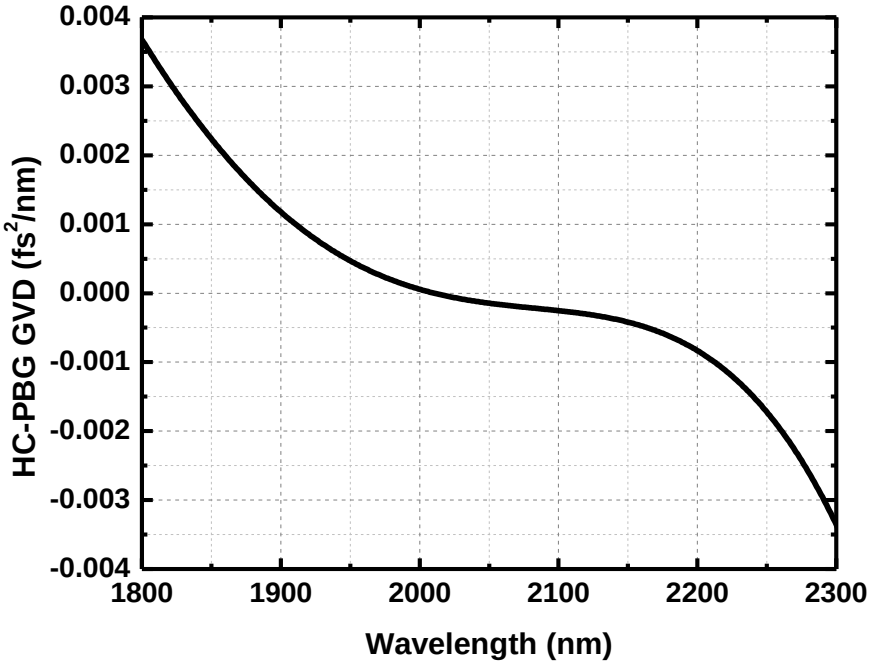


**Figure 4.2 Group velocity dispersion (GVD) of HC-2000 PBG provided by the fiber's manufacturer NKT photonics [109]. The fiber has zero group velocity dispersion near at 2.01 μm.**

### *5.2.1 Experimental Setup*

The experimental set up for the external pulse compression of a mode-locked Tm/Ho co-doped fiber laser using HC-2000 PBG fiber is as shown in Figure 4.3. Mode-locking of the Tm/Ho co-doped fiber laser is obtained via nonlinear polarization rotation when it is pumped by 1.56 μm laser same as in Ref. [90]. The mode-locked spectrum has a spectral bandwidth of 10 nm with a repetition rate of 53 MHz.

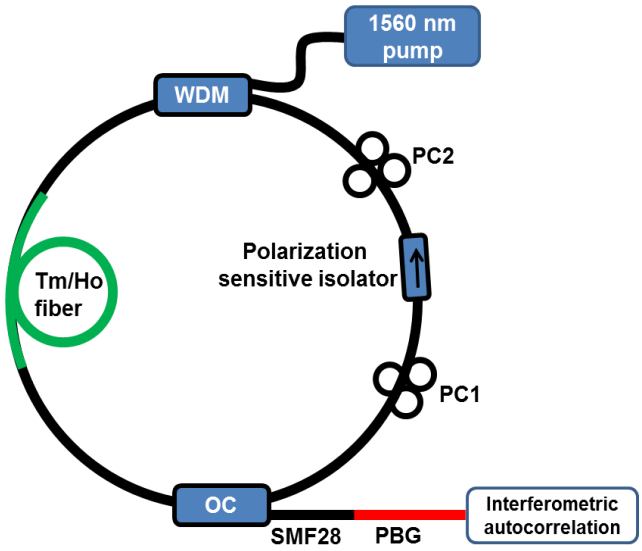


**Figure 4.3 Tm/Ho co-doped fiber laser and external pulse compression using HC-2000 photonic bandgap (PBG) fiber. WDM, wavelength division multiplexer; OC, output coupler; PC, polarization controller.**

At the output of the laser, HC-2000 is spliced with SMF using Vytran PM splicer where the splice loss is 2 dB. The other end of HC-2000 is placed in 5-axis stage and output light is coupled into the interferometer. The pulse width is measured by interferometric autocorrelation (IAC) as described in Section 3.7 of Chapter 3.

### *4.2.2 Pule Width Measurement*

Since the laser can be mode-locked at two different center wavelengths by changing the polarization controllers and the pump power, the pulse duration was measured at 1.99 μm and 2.02 μm. From the dispersion curve, it is seen that the sign of dispersion at these two wavelengths are opposite. At 1.99 μm the GVD is normal and at 2.02 μm the GVD is anomalous. In Figure 4.4 the pulse duration measured at 2.02 μm before and after HC-2000 is shown. Although inadequate interferometer alignment prevented us from obtaining the proper 8-to-1

ratio between the peak and long-delay background, this data could be used to estimate the pulse duration. The pulse duration after the laser cavity is 1.13 ps and 1.30 ps after the HC-2000 PBG. At 2.02 μm, the GVD of both the SMF and HC-2000 fiber is negative of magnitude $-8.64\times10^{-5}$ $fs^2$/nm and $-4.57\times10^{-5}$ $fs^2$/nm respectively. The pulse gets wider and chirped more after the HC-2000 fiber. The IAC measurement is consistent with the sign of the GVD and manufacturer's dispersion value.

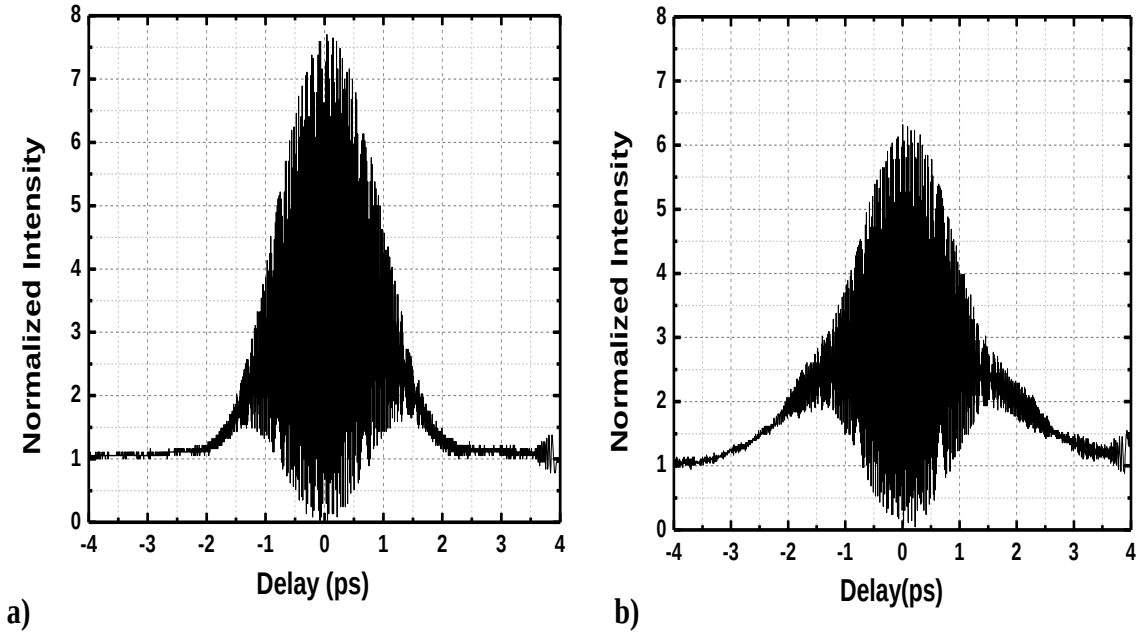


**Figure 4.4 Interferometric autocorrelation traces for Tm/Ho co-doped laser mode-locked at 2.02 μm. a) IAC measurement after laser cavity with 1.2 m of SMF28, and b) IAC measurement after 1.6 m of SMF and 0.45 m of HC-2000 PBG.**

The pulse duration before and after the HC-2000 fiber is measured when the laser is mode-locked at 1.99 μm where the GVD of the HC-2000 fiber is normal. The IAC pulse measurement is as shown in Figure 4.5. The pulse duration is 1.32 ps before the HC-2000 fiber and 1.09 ps after the HC-2000. For better comparison of pulse duration at two positions, both are

plotted with same ratio between peak to background. At this wavelength the GVD of the HC-2000 fiber is $+11.7\times10^{-5}$ $fs^2$/nm compared to $-8.05\times10^{-5}$ $fs^2$/nm for SMF28. The pulse compression is observed when the laser is mode-locked at wavelength where the GVD of the HC-2000 fiber is normal. But, the compressed pulse still wider than the transform limited value ~ 470 fs. This might due to inability to compensate the net negative cavity GVD by the normal GVD of given length of HC-2000 fiber and also the total third order dispersion of SMF is not compensated by the HC-2000 fiber.

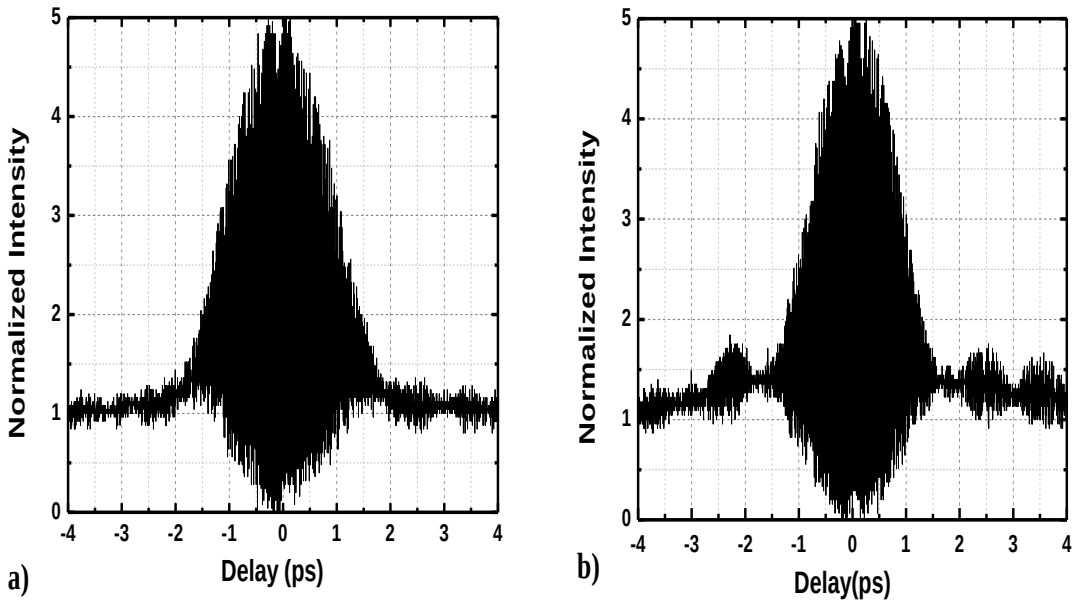


**Figure 4.5 Interferometric autocorrelation traces for Tm/Ho co-doped laser mode-locked at 1.99 µm. a) IAC measurement after laser cavity with 1.2 m of SMF28, and b) IAC measurement after 1.6 m of SMF and 0.45 m of HC-2000 PBG.**

Since the external dispersion compensation was not able to compress the pulse significantly to get transform limited value, other possible methods were explored to create a shorter pulses. Basically, I would like to use intracavity dispersion compensation to increase the spectral bandwidth and consequently to get shorter pulse.

## 4.3 Ultra High Numerical Aperture Fiber

Depressed cladding or W-profile fibers exhibit multiple zero group velocity dispersion points that produce normal GVD at long wavelengths [94]. Telecom dispersion compensating fibers and highly nonlinear fibers fall in this category. The previous chapter showed how highly nonlinear fiber exhibited too small normal GVD to compensate the large anomalous GVD of SMF [110]. A family of ultra-high numerical aperture (UHNA) fibers manufactured by Nufern as a candidate of normal GVD fiber at 2 μm is explored. These UHNA fibers are standard silica fibers with narrow and nearly pure $GeO_2$ core, so there is large difference in the refractive index between core and cladding. According to manufacturer, these UHNA fibers are designed as bridge fibers between high NA waveguide and low NA optical fibers, so my application is outside the fiber's design specification [111]. Their application is to couple the light from regular SMF to planar waveguides, fluoride and other non-silica fibers. They also used them as fiber tails for high NA sources.

### *4.3.1 Computation of GVD of UHNA Fibers*

Although the NA and core radius of the UHNA fibers was known, specific information about the index profile of UHNA fibers is proprietary. Furthermore, the dispersion of these UHNA fibers was not specified by the manufacturer. But as specified in Ref. [112], the index profile of these fibers is similar to step index fiber but with proprietary methods of enhancing the NA. The GVD of these UHNA fibers computed from the fiber core size and the NA using the analytic equations developed for step index fibers [75]. To calculate the material dispersion of the UHNA fiber I considered the germanium (Ge)-doped fused silica in the core. The refractive

index of such fiber is given by Eq. (2.4) with Sellmeier coefficients $A_1$=0.6867, $A_2$=0.4348, $A_3$=0.8966, $B_1$=0.07268, $B_2$=0.1151, and $B_3$=10.0 [113]. The effective refractive index of the fiber with both material and waveguide dispersion is given by

$$n(\omega) = n_0(\omega)\sqrt{1 + 2\,\Delta n\, b(\omega)} \tag{4.1}$$

where $n_0(\omega)$ is the material refractive index given by Eq. (2.4), $\Delta n = \frac{NA^2}{2n_0(\omega)}$, and $b(\omega) = 1 - \left(\frac{1+\sqrt{2}}{1+\sqrt[4]{4+v(\omega)^2}}\right)^2$ with $v(\omega) = \frac{r\,\omega}{c}\, n_0(\omega)\sqrt{2\,\Delta n}$ , c is the speed of light, $r$ is the core radius of fiber and $\omega$ is the angular frequency. The group velocity dispersion is given by the second derivative of $n(\omega)$ with respect to $\omega$ as

$$\beta_2 = \frac{d^2 n(\omega)}{d\omega^2} \tag{4.2}$$

The GVD of various UHNA fibers was computed using the information provided by Nufern using Eq. (4.2) (Appendix C). For different UHNA fibers named as UHNA1, UHNA3, UHNA4 and UHNA7 were used whose specification are shown in Table 4.2.

**Table 4-2 Specification of families of high numerical aperture fibers provided by manufacturer Nufern along with SMF28.**

| Fibers | Core radius (μm) | Numerical aperture (NA) |
|---|---|---|
| SMF28 | 4.5 | 0.14 |
| UHNA1 | 1.25 | 0.28 |
| UHNA3 | 0.9 | 0.35 |
| UHNA4 | 1.1 | 0.35 |
| UHNA7 | 1.2 | 0.41 |

The GVD of the UHNA fibers were computed using equations (4.1) and (4.2) for given radius and numerical aperture of each fibers. The computed GVD of the UHNA fibers along with SMF is shown in Figure 4.6

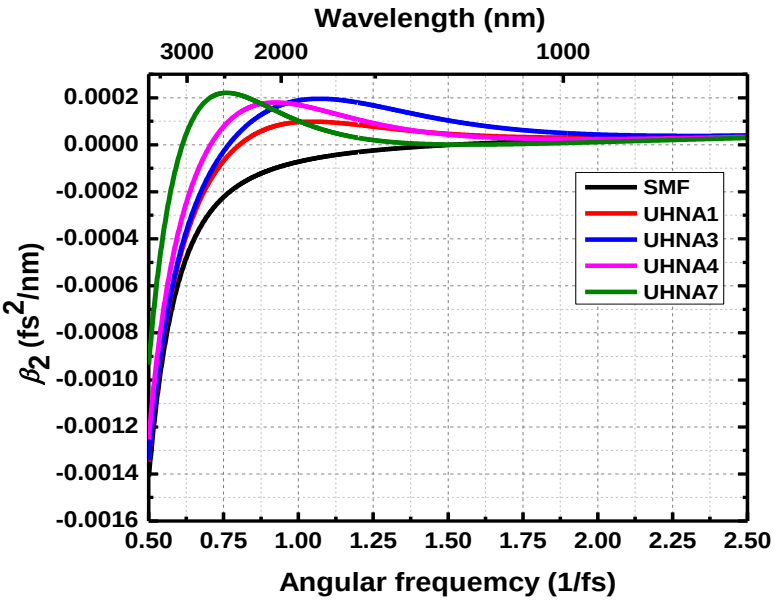


**Figure 4.6 Computed group velocity dispersion (GVD) of UHNA fibers (red-UHNA1, blue-UHNA3, pink-UHNA4, and green-UHNA7) and SMF28 (black) as function of angular frequency when including both material and waveguide dispersion.**

Figure 4.7 shows the GVD of different fibers at wavelength 2 μm. The core radius of UHNA fibers is smaller than the SMF but the numerical aperture is higher. Also the numerical aperture of UHNA fiber is increasing in ascending order. It is seen that GVD of SMF (r=4.5 μm and NA=0.14) at 2 μm is anomalous with magnitude of $-9.15\times10^{-5}$ fs$^2$/nm but when the fiber's core radius is decreased and NA increased, the sign GVD is changed and it becomes normal in the same order of magnitude as SMF. The magnitude of GVD of UHNA1, UHNA3, UHNA4 and UHNA7 are $8.6\times10^{-5}$ fs$^2$/nm, $16.93\times10^{-5}$ fs$^2$/nm, $17.9\times10^{-5}$ fs$^2$/nm and $13.79\times10^{-5}$ fs$^2$/nm respectively. From Figure 4.7, it is seen that when numerical aperture is increased further the GVD starts to decrease.

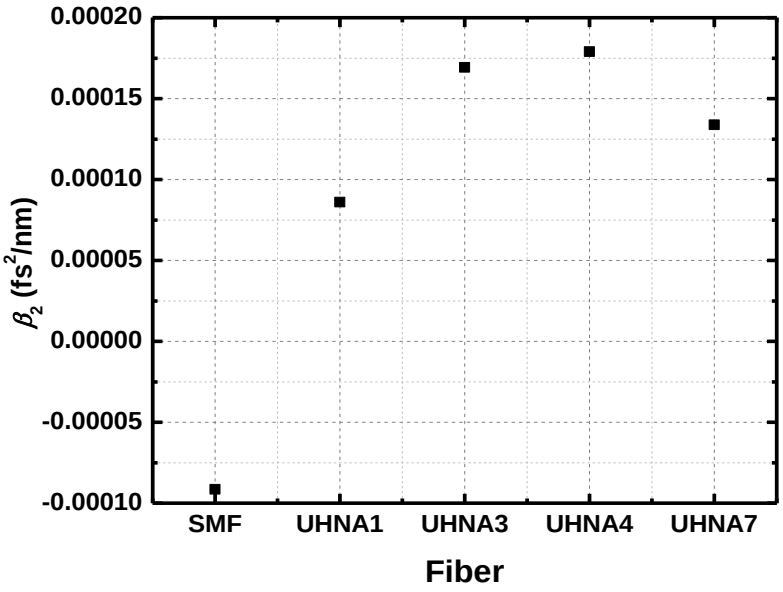


**Figure 4.7 Variation of computed group velocity dispersion of various fibers when including both material and waveguide dispersion at wavelength 2 μm.**

### *4.3.2 Estimation of GVD of UHNA Fibers*

The above calculation shows that some UHNA fibers exhibit normal GVD at 2 μm on the same order of the anomalous GVD of SMF. Hence, UHNA fibers could be used to compensate the anomalous dispersion provided by the gain fiber and SMF in the laser cavity. To verify both the sign and magnitude of computed GVD of UHNA fibers, the GVD of the UHNA fibers was estimated experimentally by external pulse compression measurement of Tm/Ho co-doped fiber laser operating in the solitonic mode. Without any normal GVD fibers in the laser cavity, it was expected that the output pulses to be negatively chirped because 1.0 m length of SMF is used after the output coupler of the laser cavity. Indeed, chirped pulses of 1.25 ps in duration were observed in the IAC measurement. These negatively chirped pulses were injected into a length of

UHNA fibers and output pulse duration was measured using IAC. Among the UHNA fibers, I used UHNA1, UHNA4 and UHNA7 for external pulse compression.

#### *4.3.2.1 Splicing Between UHNA Fiber and SMF*

According to manufacturer, the UHNA fibers were designed as bridge fiber between high NA waveguide and low NA optical fiber. The high-NA fibers here are used as dispersion compensating fibers inside the laser cavity. So, it is very important that the splice loss between UHNA fibers and SMF should be small since the stability of mode-locked fiber laser is very sensitive to the cavity loss as it modulates the pulse energy inside the cavity [114]. According to the manufacturer, the compositions of UHNA fibers are tailored to thermally expand the core during splicing and thereby achieving lower loss. To measure the splice loss between UHNA fibers and SMF, UHNA fiber and SMF are spliced using an arc fusion splicer with a program specially designed for splicing between HNLF and SMF. The SMF is spliced on both ends of the UHNA fiber and the power is measured before and after SMF as shown in Figure 4.8. For convenience, 1560 nm light is used for the loss measurements.

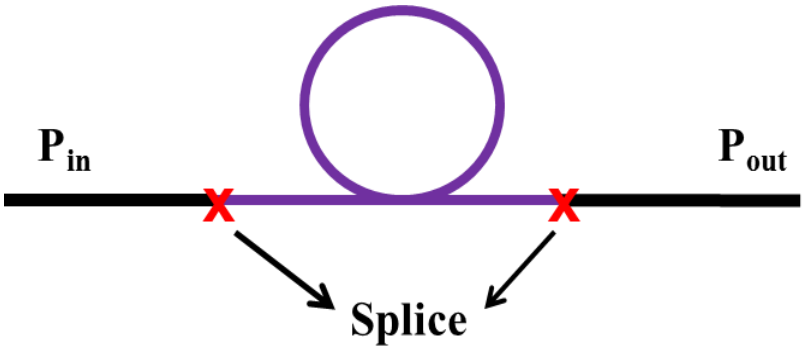


**Figure 4.8 Schematic of measuring the splice loss between UHNA fiber and SMF. To estimate the splice loss both input and output power are measured at wavelength 1560 nm.**

From the power measurement at 1560 nm, the loss per splice between UHNA fiber and SMF is determined. I used three UHNA fibers; UHNA1, UHNA4 and UHNA7. For UHNA1 fiber the splice loss is 0.44 dB per splice. For UHNA4 fiber the splice loss is 0.27 dB per splice and for UHNA7 fiber the splice loss is 0.8 dB/splice. Depending on core size and numerical aperture of the fibers, the splice loss is small.

#### *4.3.2.2 Experimental Setup*

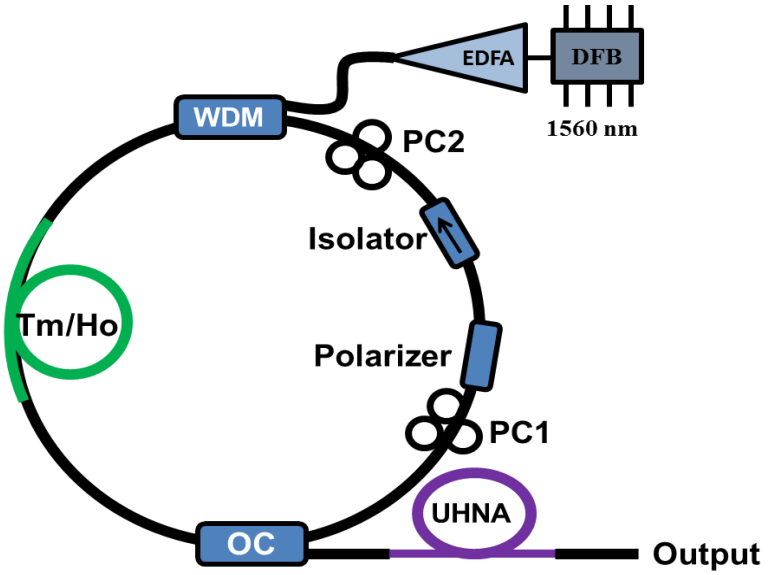


**Figure 4.9 Schematic of estimation of group velocity dispersion of ultrahigh numerical aperture fiber by external pulse compression measurement. WDM, wavelength division multiplexer; OC, output couple; PC, polarization controller; DFB, distributed feedback laser; EDFA, erbium doped fiber amplifier; UHNA, ultrahigh numerical aperture.**

The experimental set up of the estimation of the group velocity dispersion of UHNA fibers by external pulse compression is shown in Figure 4.9. The UHNA fiber is spliced at the output of a mode-locked Tm/Ho co-doped fiber laser operating in the solitonic regime. The laser is mode-locked via nonlinear polarization rotation, same as described in Ref. [90]. But here the

polarization sensitive isolator was replaced by a separate polarizer and isolator. The isolator is designed to work at 2 µm wavelength but the polarizer is still specified for 1.5 µm. The pulse width is measured before and after UHNA fiber using interferometric autocorrelation.

#### *4.3.2.3 UHNA1 Fiber*

First, 3 m of UHNA1 fiber is used at the output of the laser cavity to measure the pulse width before and after it. There is a small section of SMF (~ 30 cm) after the UHNA1 fiber before the autocorrelator. The IAC traces are shown in Figure 4.10, a) after the laser cavity, and b) after the 3 m of UHNA1 fiber. No significant change in the pulse is observed after the UHNA1 fiber. This indicates that the UHNA1 fiber has very small normal GVD at 2 µm which is cancel out by the anomalous GVD of SMF after it. So, this fiber may not be suitable to put inside the laser cavity to compensate the large anomalous GVD of SMF and the laser is mode-locked in the stretched pulse regime.

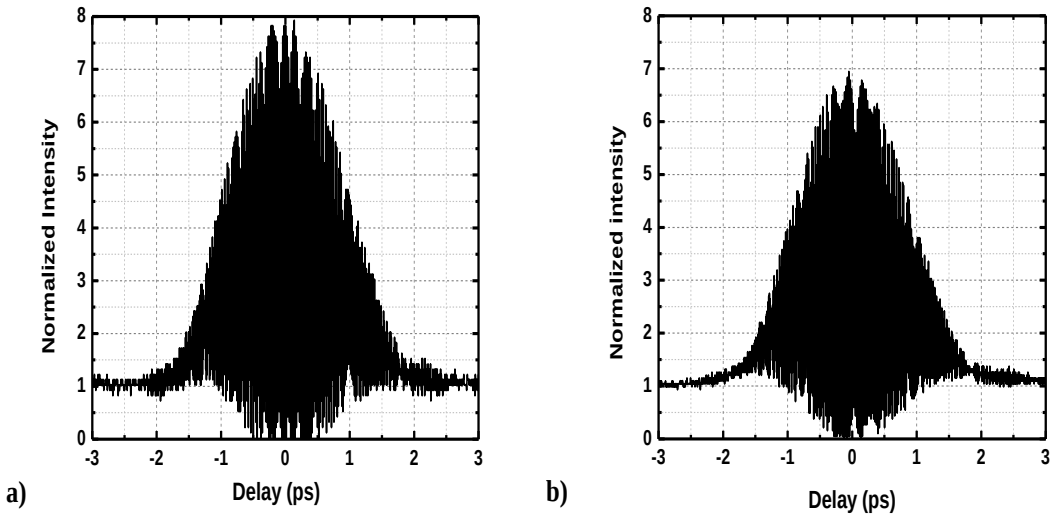


**Figure 4.10 Interferometric autocorrelation trace a) after the laser cavity operating in solitonic regime, b) after 3 m of UHNA1 fiber.**

#### *4.3.2.4 UHNA4 Fiber*

Same as in UHNA1 fiber, the pulse width at the output of the laser before the UHNA4 fiber and then after the 3 m of UHNA4 fiber is measured. The IAC traces are shown in Figure 4.11, a) after the laser cavity and b) after 3 m of UHNA4 fiber. The pulse duration after the laser cavity is 1.25 ps and negatively chirped as shown in Figure 4.11 (a). After propagation through 3 m of UHNA4 fiber the pulse becomes more chirped and wider with duration of 1.37 ps as shown in Figure 4.11 (b). This indicates that the UHNA4 fiber either has anomalous dispersion or large normal dispersion.

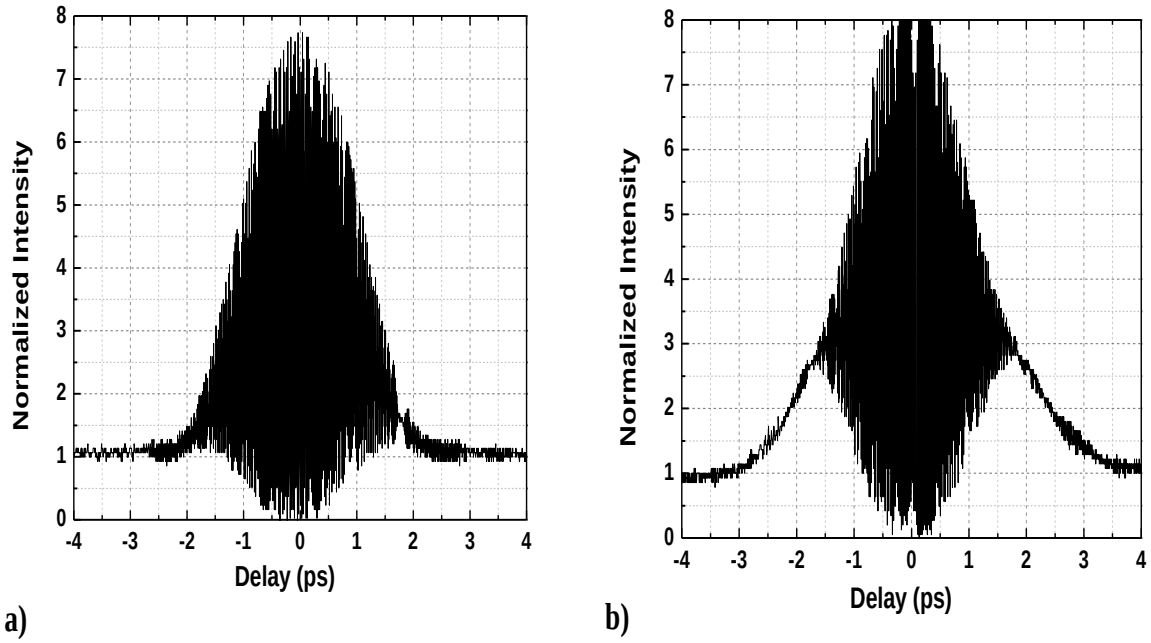


**Figure 4.11 Interferometric autocorrelation trace a) after the laser cavity operating in the solitonic regime, and b) after 3 m of UHNA4 fiber.**

To determine the sign of the GVD, 2.5 m of SMF was added after the 3 m of UHNA4 fiber. As seen in Figure 4.12 (a), the pulse is no longer chirped and the pulse duration is reduced

to 0.91 ps. This implies that the UHNA4 fiber has the opposite sign of GVD as the SMF. To estimate the magnitude of the GVD, finally, 5.5 m of SMF were added. As seen in Figure 4.12 (b), the pulse duration and chirp are similar to what was observed only after the UHNA4 fiber (Figure 4.11 (b)). From these measurements, the GVD of UHNA4 is estimated and has the same order of magnitude but opposite sign of the GVD of SMF at 2 μm. Specifically a GVD of $\beta_2 \approx +9.1\times10^{-5}$ fs$^2$/nm was estimated for UHNA4 which is a factor of two off from the calculated value. This measurement provided enough confidence that the UHNA4 fiber has normal group velocity dispersion on the order of $10^{-5}$ fs$^2$/nm at 2 μm.

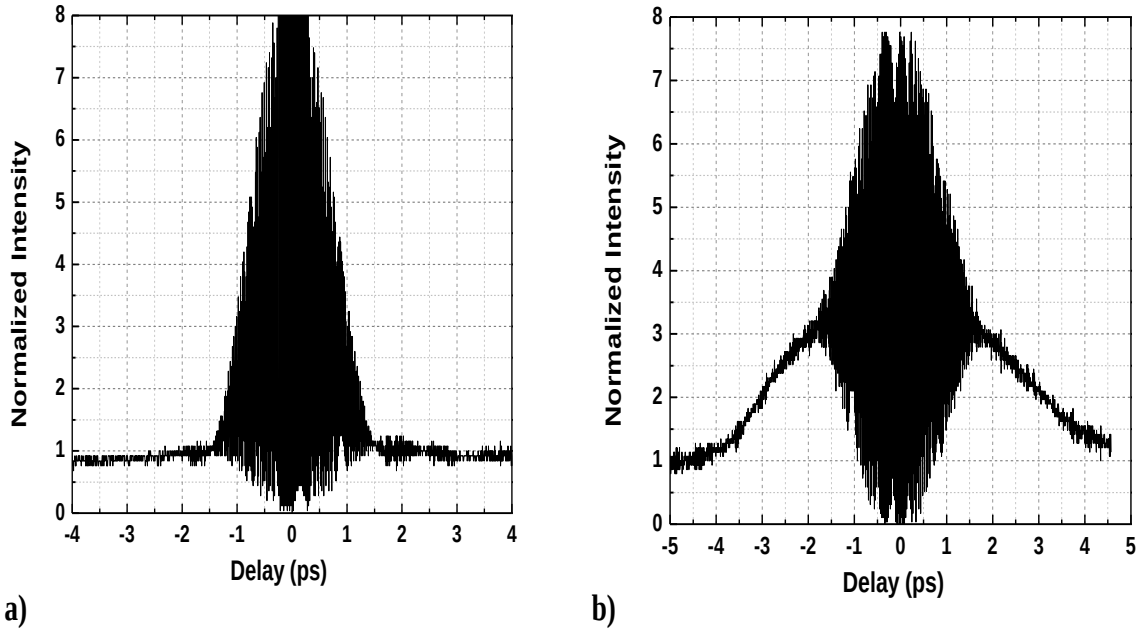


**Figure 4.12 Interferometric autocorrelation trace a) after 3 m of UHNA4 fiber and 2.5 m of SMF, and b) after 3 m of UHNA4 fiber and 5.5 m of SMF.**

#### *4.3.2.5 UHNA7 Fiber*

According to the manufacturer, UHNA7 fiber is designed to work near 2 μm and hence I tried to estimate the GVD of this fiber. Similar to the previous measurement, the pulse width before and after 3 m of UHNA7 fiber is measured. The measured IAC traces are shown in Figure 4.13, a) after the laser cavity and b) after 3 m of UHNA7 fiber. The pulse after the UHNA7 fiber gets compressed and chirped more but it has some structure at the wings and the ratio of peak to background is decreased. The reason for the asymmetry and the structure at the wings is unclear but it may be due to high NA of this fiber or the nonlinearity in the speaker's travel.

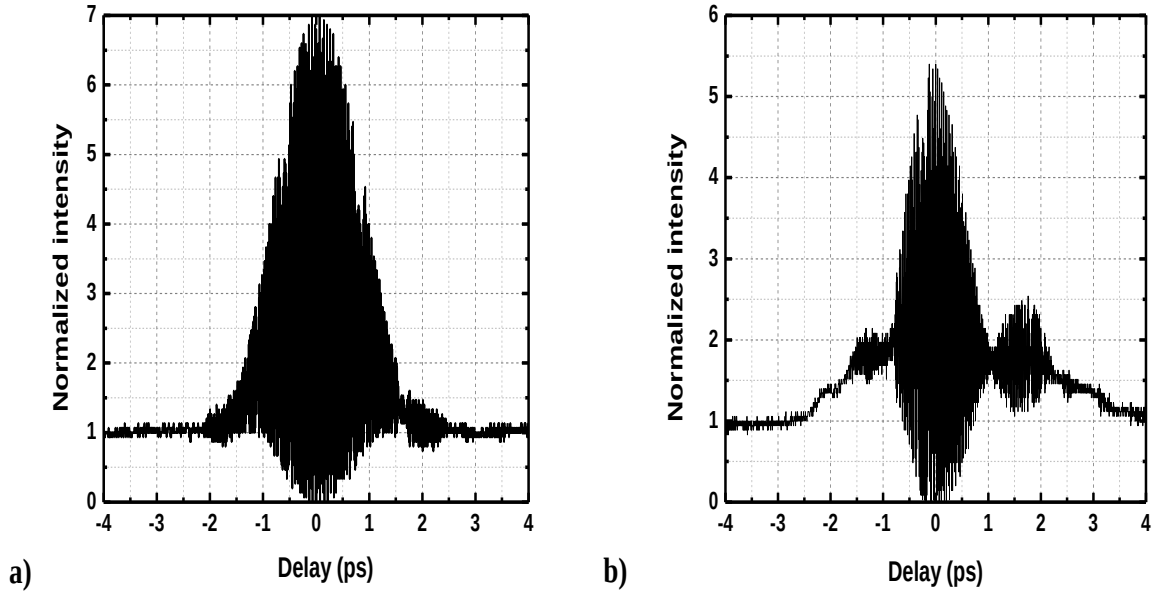


**Figure 4.13 Interferometric autocorrelation trace a) after the laser cavity operating in thw solitonic regime, and b) after the UHNA1 fiber.**

From the above measurement it can be seen that UHNA7 fiber has normal GVD at 2 μm but also has some other effect, like self-phase modulation when pulse propagating through it, which prevents us from getting 8-to-1 IAC ratio. To make sure that the pulse gets self-phase modulated the spectrum after 3 m of UHNA7 fiber is measured. It is seen that the spectrum was broader than after the laser cavity with Kelly peaks at the same position as shown in Figure 4.14

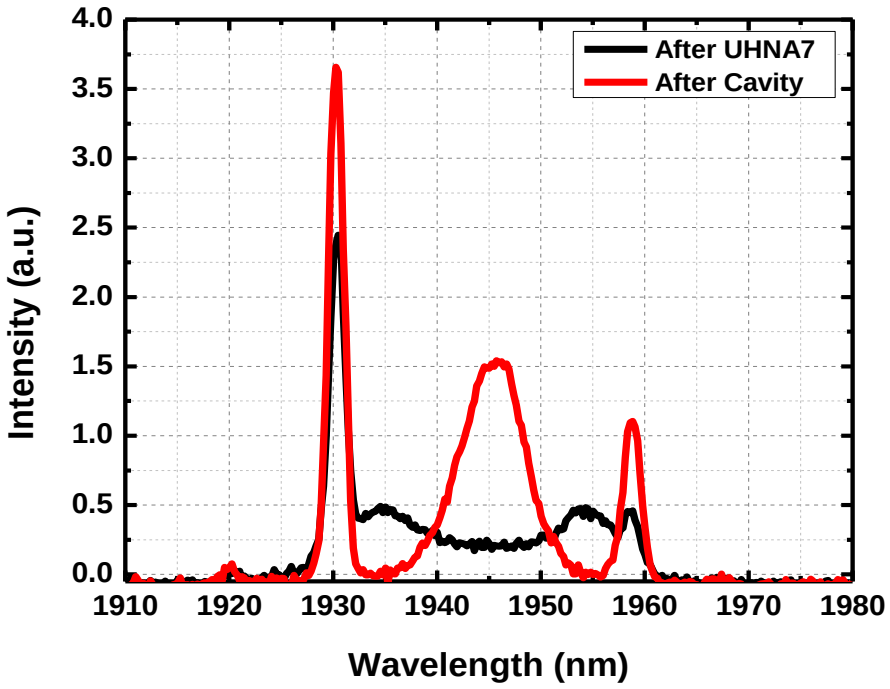


**Figure 4.14 Spectrum after the laser cavity operating in solitonic regime (red), after the 3 m of UHNA7 fiber (black).**

After estimating the group velocity dispersion of various UHNA fibers, I was confident on the sign of the GVD of UHNA4 fiber so the UHNA4 fiber was inserted in the laser cavity to attempt mode-locking via nonlinear polarization rotation.

## 4.4 Stretched Pulse Operation

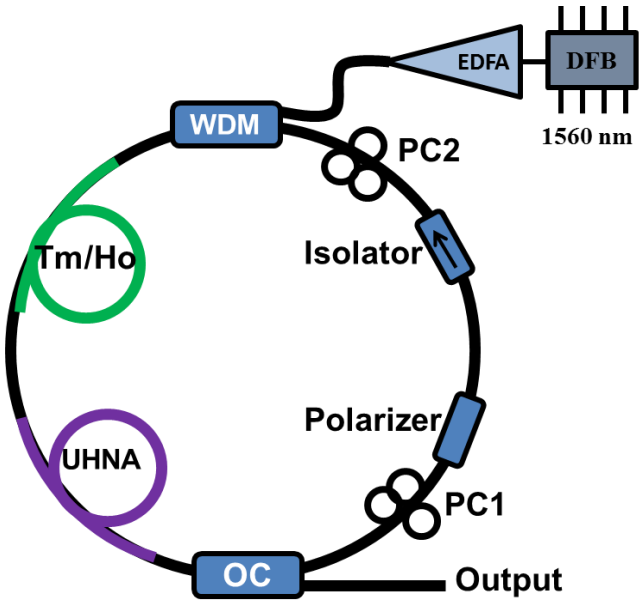


**Figure 4.15 Stretched-pule Tm/Ho co-doped fiber laser with UHNA4 fiber as a normal dispersion fiber: WDM, wavelength division multiplexer; OC, output couple; PC, polarization controller; DFB, distributed feedback laser; EDFA, erbium doped fiber amplifier.**

As discussed previous, when normal GVD fiber is added inside the cavity in such way that the net cavity dispersion is positive, the laser can be mode-locked in the stretched-pulse regime. Since the UHNA fibers have normal GVD at 2 μm, the anomalous GVD of SMF and Tm/Ho co-doped can be compensated and the laser can be mode-locked in the stretched pulse regime. I started with the original experimental setup where c-band in-line polarizer and isolator designed to work at 2 μm are used. The experimental setup for the stretched pulse Tm/Ho co-doped fiber laser is illustrated in Figure 4.15. An amplified 1560 nm pump light is coupled into the cavity using 1560/2000 nm wavelength division multiplexer (WDM). The total length of the Tm/Ho co-doped gain fiber is 0.85 m. The high-NA fiber is used for dispersion

compensation. When there was no high-NA fiber in the cavity the laser was mode-locked in solitonic mode with spectral bandwidth 9 nm [90]. The laser is mode-locked via nonlinear polarization rotation by adjusting the two polarization controllers PC1 and PC2 when the pump power is about 300 mW. The spectrum and pulse duration of the laser output are measured after 0.9 m of SMF by a spectrometer and an interferometric autocorrelator (IAC).

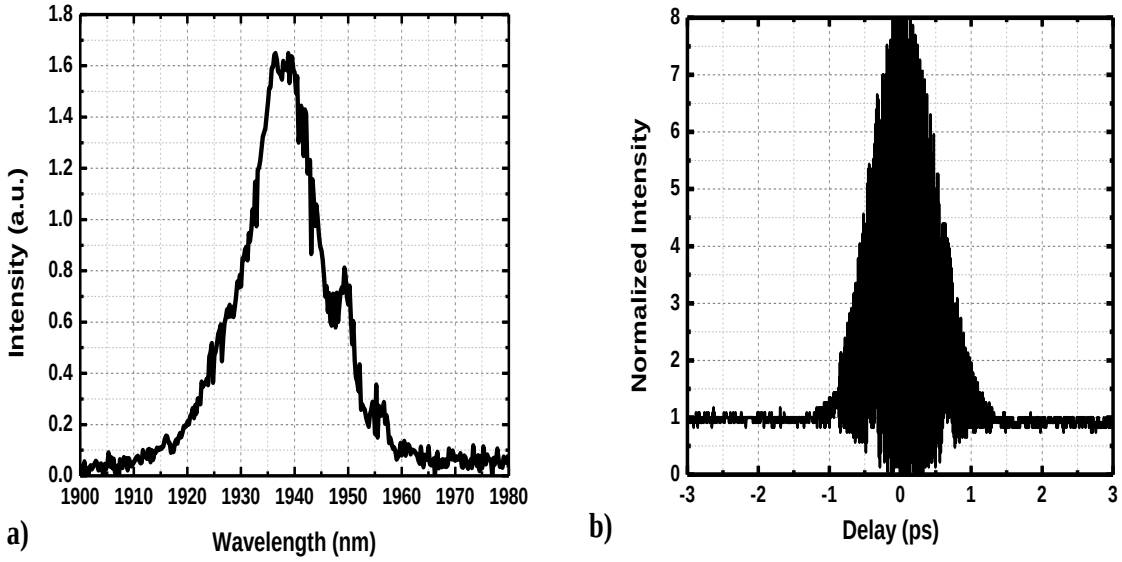


**Figure 4.16 a) Laser spectrum, and b) interferometric autocorrelation trace of mode-locked stretched-pulsed operation with 1.85 m of UHNA4 fiber.**

A small section of SMF is spliced between Tm/Ho co-doped fiber and UHNA4 fiber in order to reduce the total loss in the cavity. 3 m of UHNA4 fiber was initially in the laser cavity. After series of cut backs the laser is mode-locked when the fiber length became 1.85 m and the pump power is about 300 mW. The output spectrum and the pulse duration of the mode-locked laser are shown in Figure 4.16. The center wavelength of the mode-locked spectrum is at 1940 nm with spectral bandwidth of 15 nm at full width half maximum, Figure 4.16 (a). The

interferometric autocorrelation trace is shown in Figure 4.16 (b) and the IAC width is 1.48 ps measured after 0.9 m of SMF. The pulse duration corresponding to this IAC width is 0.77 ps assuming the hyperbolic secant pulse shape. The pulse duration is smaller than solitonic pulse (1.17 ps). The repetition rate of the laser is 34 MHz.

The increase in the spectral bandwidth and the decrease in the pulse duration when UHNA4 fiber is added to the cavity suggest that the UHNA4 has normal dispersion at 1.94 μm. The wider spectrum and absence of Kelly sidebands indicates that the laser is operating in the stretched pulse regime.

As I discussed in Chapter 2, the Tm/Ho fiber has wide gain bandwidth which can support very short pulses. Furthermore, lasers operating in the stretched-pulse regime have significantly larger spectral bandwidth because there are no solitonic effects to restrict the bandwidth. However, the observed spectral bandwidth is not as large as expected since large bandwidth is observed in an erbium-doped fiber laser when operating in the stretched pulse regime [104]. Attempts to increase the bandwidth were done by adjusting the fiber lengths, polarization controller, and pump power. The question is what are the possible factors that are limiting the spectral bandwidth? Since the in-line polarizer used in the laser cavity is specially designed for c-band, I thought this limited to achieve the spectral bandwidth. So, the c-band in line polarizer is replaced by one which is designed for 2 μm in Figure 4.15 and mode-locked the laser via nonlinear polarization rotation. The laser is mode-lock at different lengths of UHNA4 fiber (2.8 m or shorter) in the laser cavity. When the laser is mode-locked with 2.35 m of UHNA4 fiber the maximum spectral bandwidth of 31 nm is observed as shown in Figure 4.17, which is factor of 2 higher than before. The center wavelength of this mode-locked spectrum is at 1970 nm. I will discuss the variation of spectral bandwidth with respect to length of UHNA4

fiber in next section. Same as before the absence of Kelly sidebands and wide spectral bandwidth indicate that the laser is operated in the stretched-pulse regime. The laser did not self-start as in the solitonic operation but it was easily mode-locked by adjusting the polarization controllers and the pump power.

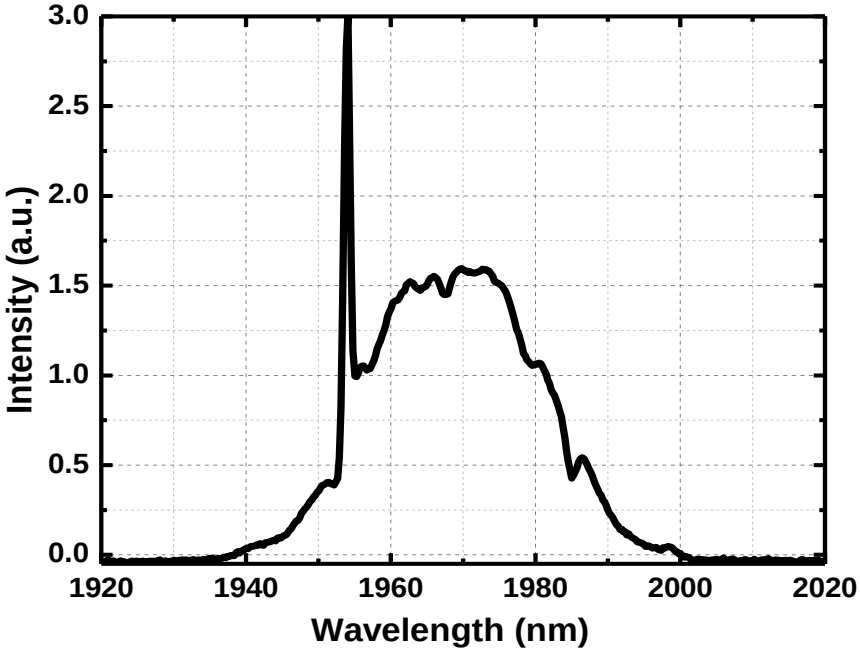


**Figure 4.17 Mode-locked spectrum of Tm/Ho co-doped fiber laser with 2.35 m of UHNA4 fiber operating in stretched-pulsed regime. The center wavelength is at 197 nm.**

The mode-locked laser produced a steady 35 MHz pulse train observed on an electrical spectrum analyzer and oscilloscope. The interferometric autocorrelation trace measured for this operation is as shown in Figure 4.18. It has the proper 8-to-1 ratio between the peak and long-delay background. The IAC full width half maximum is 0.76 ps. To measure the actual pulse duration a Gaussian pulse shape was assumed and computed the ratio of pulse width to

IAC width using analytical expression from Ref. [98]. The ratio is 0.59 and which gives the pulse duration of 0.45 ps.

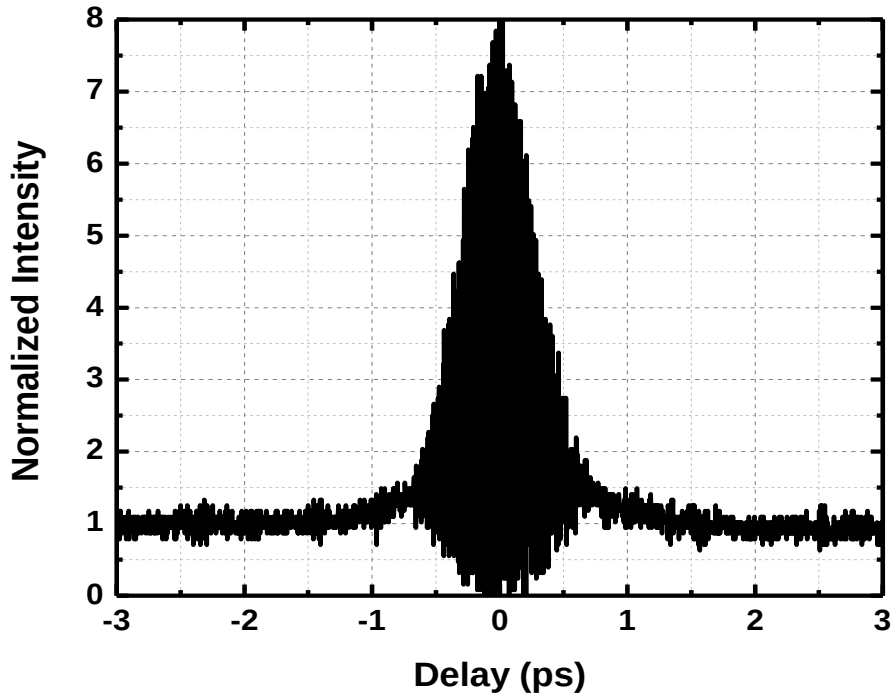


**Figure 4.18 The interferometric autocorrelation trace for stretched-pulse operation with 31 nm spectral bandwidth measured after 0.9 m of SMF.**

The comparison of spectrum and pulse duration of the stretched-pulse and the solitonic operations are shown in Figure 4.19. The stretched-pulse spectrum is three times wider than the solitonic spectrum where Kelly sidebands are no longer present Figure 4.19 (a). Also, the pulse duration is significantly shorter as compared with solitonic operation. The pulse duration of solitonic operation is 1.24 ps where conversion factor of 0.527 is used assuming hyperbolic secant pulse shape Figure 4.19 (b).

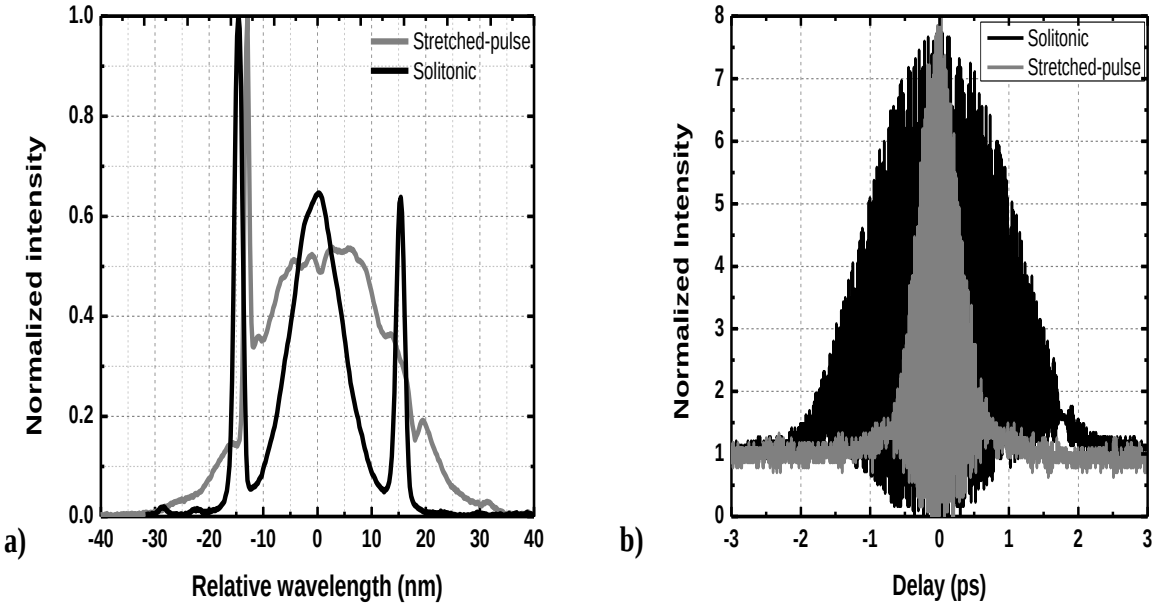


**Figure 4.19 (a) Output spectra of the laser in stretched-pulse (gray) and solitonic (black) operation for a UHNA4 length of 2.2 m. The center wavelengths were 1960 nm and 1940 nm in solitonic and stretched-pulse regimes respectively. (b) The IAC trace for stretched-pulse (gray) and solitonic (black) operation for a UHNA4 length of 2.35 m.**

## 4.5 Laser Dynamics: From Stretched-Pulse to Solitonic Regime

To study the laser dynamics of a Tm/Ho fiber laser while going from the stretched-pulse to solitonic operation, the laser was mode-locked for various lengths of UHNA4 fiber so that the net cavity group velocity dispersion varies from positive to negative. In order to do that, a series of UHNA4 fiber cut-back measurement is performed keeping other fibers length same. So the net cavity GVD will be different in each UHNA4 fiber cut-back. Both spectral and IAC traces were taken for each length of the UHNA4 fiber. The variation of both spectral bandwidth and the pulse duration is plotted with respect to the UHNA4 fiber length and shown in Figure 4.20.

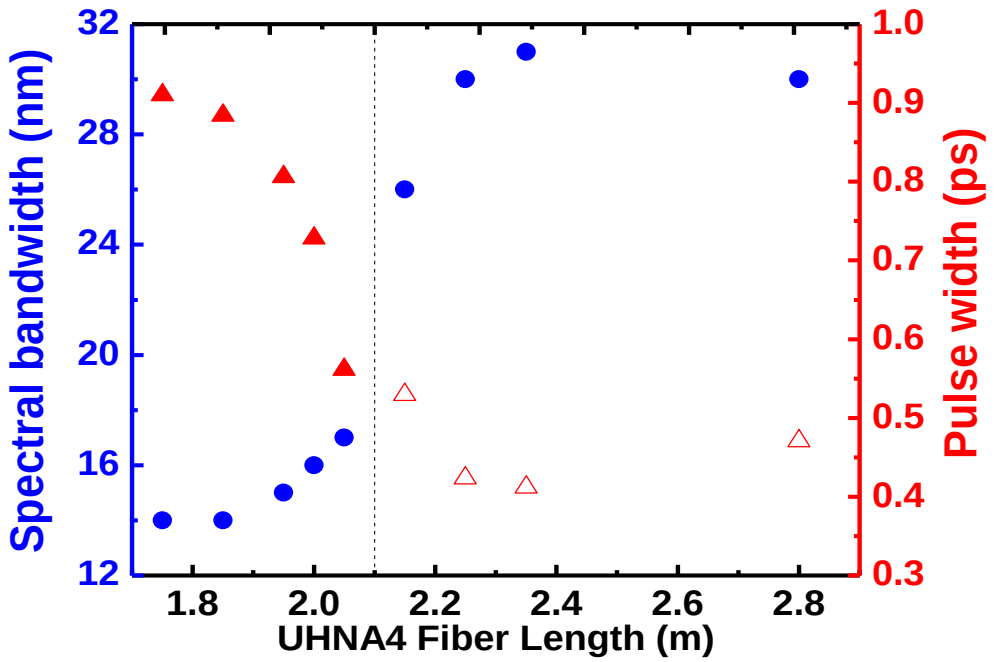


**Figure 4.20 Output spectral bandwidth (blue circles) and pulse widths (red triangles) for different lengths of UHNA4 fiber inside the cavity. Pulse width was determined assuming Gaussian (open triangles) and sech$^2$ (filled triangles) pulse shapes.**

From the spectral measurement, it is seen that the laser is operated in the stretched-pulse regime for the UHNA4 fiber lengths from 2.80 to 2.15 m, with nearly constant bandwidth of 30 nm. This observation is consistent with measured spectral bandwidths as a function of net cavity GVD for stretched-pulse operation of the erbium-doped fiber laser [115]. As the fiber length is further decreased, the spectral bandwidth decreased dramatically to 17 nm at 2.05 m of UHNA4 fiber. Also Kelly sidebands were also observed indicating that the laser is now operating in the solitonic regime as shown in Figure 4.21. The pulse duration follows exactly opposite relation compared to the spectral bandwidth with the fiber lengths. The pulse width is narrower when the laser is operating in the stretched-pulse regime and increases significantly

when it goes to the solitonic regime as shown in red triangles in Figure 4.20. The pulse width was determined assuming Gaussian shape (open triangles) in stretched-pulse regime and hyperbolic secant shape (closed triangles) in solitonic regime.

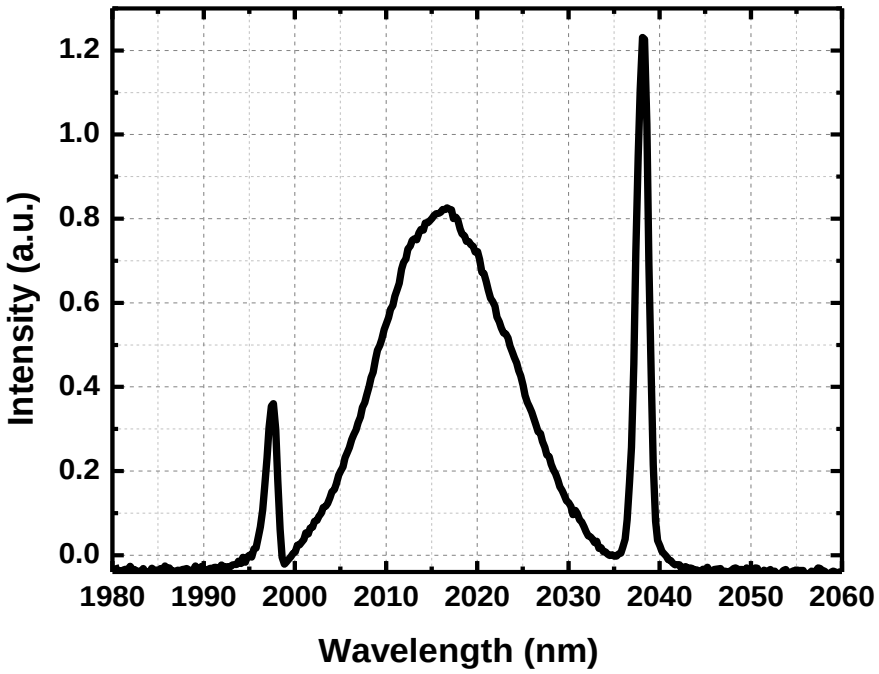


**Figure 4.21 Mode-locked spectrum of Tm/Ho co-doped fiber laser with 2.05 m of UHNA4 fiber.**

The laser operates in stretched-pulse regime when the fiber length is longer than 2.15 m indicating that the net cavity GVD is positive. But, when the fiber length is shorter than 2.05 m, the laser is mode-locked in the solitonic regime indicating that the net cavity GVD is negative. So, we estimate that at 2.1 m of fiber length the net cavity GVD is zero. At this length of UHNA4 fiber, the laser is very unstable and the spectrum contains an unexpected dip at the center wavelength as shown in Figure 4.22. The instability occurs because the pulses become so short that their effective gain becomes less than that for continuous wave (CW) [73]. The size

and existence of this unstable region are a function of the intracavity SPM and amount of nonlinear polarization rotation. But the laser is stable in both solitonic and stretched-pulsed regime.

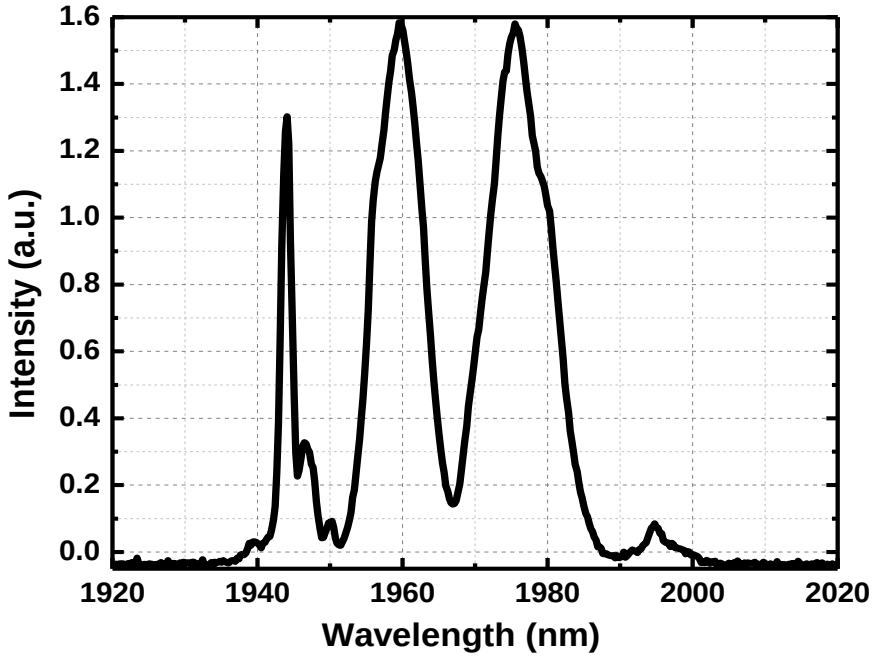


**Figure 4.22 Mode-locked spectrum of Tm/Ho co-doped fiber laser with 2.1 m of UHNA4 fiber.**

Considering the net cavity dispersion is zero when UHNA4 fiber is 2.1 m, I can better estimate the group velocity dispersion. The net cavity dispersion is given by

$$(\beta_2 L)_{net} = (\beta_2 L)_{SMF} + (\beta_2 L)_{Tm/Ho} + (\beta_2 L)_{UHNA4} \quad (4.3)$$

At this configuration the length of Tm/Ho co-doped fiber is 0.85 m and the SMF is 2.9 m. With the group velocity dispersion of SMF and Tm/Ho co-doped fiber -0.085 $ps^2$/nm and -0.01 $ps^2$/nm respectively, the GVD of UHNA4 fiber is calculated using Eq. (4.3) and is

+0.12 $ps^2$/nm. This is consistent with the estimated value from external pulse compression measurement and the computational value.

## 4.6 Summary

An all fiber stretched-pulsed Tm/Ho co-doped fiber laser is demonstrated employing ultra-high numerical aperture fiber (UHNA) inside the laser cavity for GVD compensation. The laser is mode-locked via nonlinear polarization rotation. The GVD of UHNA fibers is computed numerically and estimated experimentally. The stretched-pulse laser has spectral width of 31 nm and pulse duration of 450 fs. The laser dynamics of Tm/Ho co-doped fiber laser is studied for the transition between stretched-pulse and solitonic regime by changing the net cavity dispersion. The measured pulse duration is still not short enough and close to the transform limited value. So, better control of higher order dispersion is necessary to produce shorter pulses.

In next chapter, I will discuss about the conclusion of this thesis along with the future work to achieve the shorter pulse and mid-infrared supercontinuum generation in ZBLAN fiber using this laser as a pump source.

# Chapter 5 - Conclusion and Outlook

## 5.1 Principle Research Contributions

In this research, I have focused on generation of ultrashort pulses from a mode-locked thulium/holmium co-doped fiber laser and have studied the laser dynamics in the different mode-lock regimes. The laser was mode-locked using nonlinear polarization rotation in all fiber formats. The laser was able to mode-lock in both solitonic and stretched-pulse regime by adjusting the net cavity dispersion. For intracavity dispersion management, different possible normal GVD fibers were used such as HNLF, erbium-doped fiber, Vascade fiber, photonic bandgap fiber and UHNA fibers. Among them only UHNA fiber has large enough normal GVD to compensate the anomalous GVD of SMF and gain fiber. Without any normal dispersion fiber inside the laser cavity, the laser is mode-locked in the solitonic regime with spectral bandwidth of 15 nm at FWHM and the corresponding pulse duration of 966 fs. The spectral bandwidth and the pulse duration are limited in the solitonic regime due to the presence of the sidebands. The center wavelength of the mode-locked spectrum changes and can be mode-locked at two separate wavelengths depending on the position of the polarization controllers. The pulse duration is measured by interferometric autocorrelation where the signal is measured by two-photon absorption in an InGaAs detector.

One way of getting shorter pulses form the mode-locked laser is external dispersion compensation where the spectral bandwidth of the laser output is the same but the pulse is compressed temporally, called the external pulse compression. For external pulse compression, I used hollow core photonic bandgap fiber at the output of the laser. The pulse gets compressed

but it difficult to obtain the 8 to 1 signal to noise ratio in autocorrelation trace due to high splice loss between SMF and PBG.

Another method for achieving shorter pulse durations is intracavity dispersion compensation where the spectral bandwidth is increased so the laser can support short and high peak power pulses. So to increase the spectral bandwidth and hence generate a shorter pulse, first intracavity GVD is compensated using UHNA fiber. The GVD of the UHNA fibers were computed using Sellmeier equation considering step index fiber with weakly guide approximation and then estimated experimentally from external pulse compression method. The computed and estimated GVD value of one of the UHNA fibers (UHNA4) agreed in the order of magnitude. The computed value is $18\times10^{-5}$ $fs^2/nm$ and the estimated value is $12\times10^{-5}$ $fs^2/nm$. With UHNA4 fiber in the laser cavity, the laser can be mode-locked in the stretched-pulse regime so that the spectral bandwidth increases and the pulse duration decrease by factor of two as compared with the solitonic regime. The spectral bandwidth is 31 nm and the pulse duration is 470 fs in the stretched-pulse regime. By changing the length of UHNA4 fiber the net cavity GVD can be changed and hence the laser can be mode-locked in both solitonic and stretched-pulse regimes. The laser dynamics is studied while going from one regime to the other. The Tm/Ho co-doped fiber laser followed the exact pattern that was observed in an erbium doped fiber laser. But the spectral bandwidth is not as large as expected and observed in the other fiber laser system such as Er- and Yb- fiber lasers.

## 5.2 Outlook and Future Direction

### *5.2.1 Generation of Short Duration, High Peak Power Pulses*

Further increase of spectral bandwidth of the laser output can be achieved by better control of higher order dispersion of the fiber, specifically third order dispersion (TOD) while operating in the stretched-pulse regime. While demonstrating the stretched-pulse laser in Chapter 5 only the anomalous GVD of the SMF and the gain fiber is compensated by the normal dispersion of the UHNA4 fiber. But the TOD of UHNA4 fiber is not negative enough to compensate the normal TOD of the SMF as seen from Figure 5.1. But the TOD of the UHNA7 fiber is large and negative as well has normal GVD than that of the SMF and hence using this fiber as dispersion compensating fiber should allow to control over both GVD and TOD of the cavity, thereby generating large bandwidth spectrum and hence shorter pulses.

Recently C. Zhang *et al.* demonstrated both theoretically and experimentally that the ultra-broadband optical spectrum can be generated from a stretched-pulse erbium fiber laser using zero-dispersion fiber (ZDF) inside the laser cavity [116]. They used 70 m of OFS 980 nm fiber as ZDF whose GVD is -0.0013 $ps^2/m$ which is 17 times smaller than SMF at 1550 nm and were able to generate 172 nm spectral bandwidth with 36 fs transform limited pulse. The laser was mode-locked via nonlinear polarization rotation. Similar techniques can be used in thulium/holmium co-doped fiber laser since zero-dispersion fiber near 2 μm could be available such as highly nonlinear fiber.

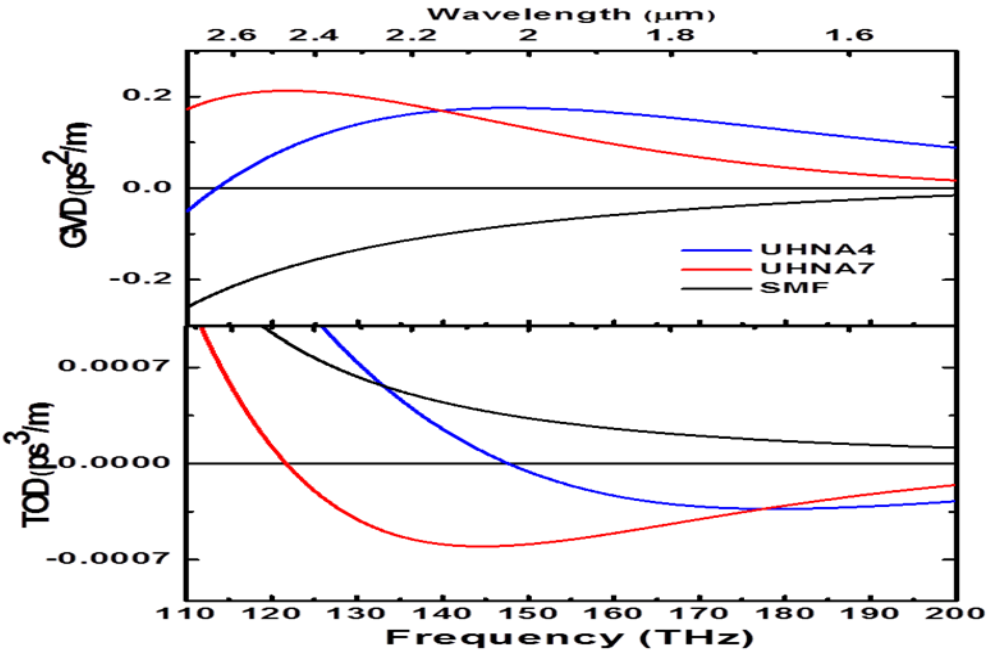


**Figure 5.1 Computed second order (upper) and third order (lower) dispersion as a function of frequency for SMF, UHNA4, and UHNA7 fibers. The dispersion was computed analytically assuming a step-index profile and using the manufacture's numerical aperture (NA) and core radius. At 2 μm UHNA4 and UHNA7 fibers have normal GVD and anomalous TOD that are opposite of SMF.**

### *5.2.2 Mid-infrared Supercontinuum Generation*

In the future, high peak power pulses generated from mode-locked Tm/Ho co-doped fiber laser can be used to pump the ZBLAN fiber in order to generate supercontinuum in the mid-infrared region. The ZBLAN fiber is a good candidate for mid-infrared supercontinuum generation since it has very good transmission (loss = ~0.1 dB/m) in this region and high nonlinear refractive index compared with fused silica fiber. In Figure 5.2, the schematic of MIR supercontinuum is shown along with numerically simulated MIR supercontinuum after 10 m of

ZBLAN fiber. For numerical simulation, the nonlinear Schrodinger equation given in Eq. 5.1 is solved numerically

$$i\frac{\partial A}{\partial z} + \frac{i\alpha}{2}A - \frac{\beta_2}{2}\frac{\partial^2 A}{\partial t^2} + \gamma(\omega)|A|^2 A = 0 \tag{5.1}$$

where $A$ is pulse amplitude, $\alpha$ is the loss through the fiber, $\beta_2$ is the GVD of the fiber, and γ is the nonlinear parameter of the fiber given by

$$\gamma(\omega) = \frac{n_2(\omega)\omega}{c\pi r^2} \tag{5.2}$$

where $n_2$ is the nonlinear refractive index, $c$ is the speed of light, ω is the carrier frequency and $r$ is the mode field radius of the fiber.

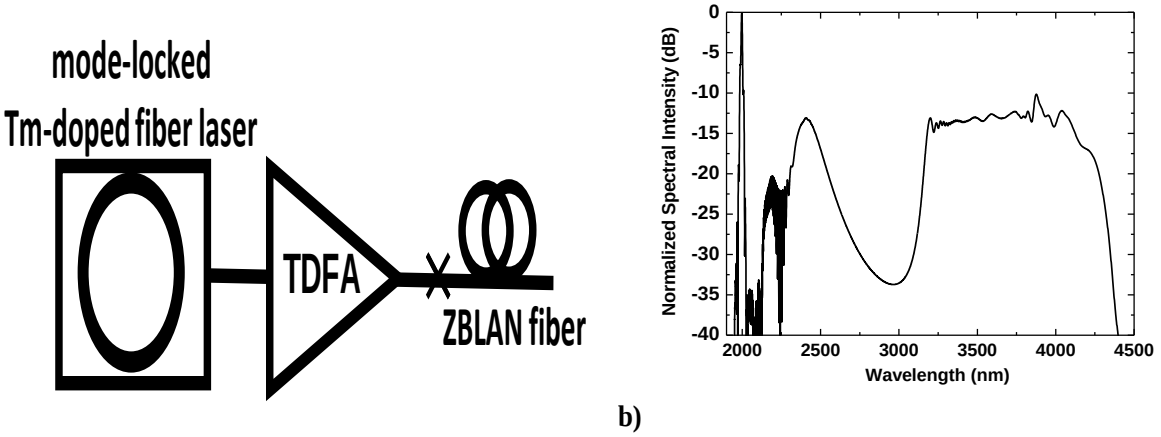


**Figure 5.2 a) Schematic of mid-infrared supercontinuum generation from ZBLAN fiber while pumping by an amplified pulse generated from mode-locked 2 µm laser. B) The simulated supercontinuum generation from 10 m of ZBLAN fiber pumping with 500 fs 2 µm pulse with peak power 2 kW.**

Equation (5.1) is solved numerically with the following laser parameter 500 fs pulse duration and peak power of 2 kW at 2 µm. The MIR supercontinuum after 10 m of ZBLAN fiber

with core radius of 9 µm, loss 0.05 dB/m at 2 µm, nonlinear refractive index of $2.1\times10^{-20}$ $m^2/W$. The GVD of the fiber is taken based on Ref [117]. The simulated MIR supercontinuum is shown in Figure 5.2 (b) and it is clearly seen that the supercontinuum can be extended all the way up to 4.5 µm.

A preliminary experiment was attempted to generate a MIR supercontinuum in a ZBLAN fiber. Here pulses from mode-locked Tm/Ho co-doped fiber laser are coupled into 6 m of ZBLAN fiber as shown in Figure 5.3 (a). The laser was mode-locked in the solitonic regime with long pulse ~966 fs and peak power about 1 kW at 1.96 µm. From Figure 5.3 (b) only about 200 nm of spectral broadening is observed after 6 m of ZBLAN fiber. This is mainly due to two reasons: one is low peak power at the input of the ZBLAN fiber and the other is coupling loss between SMF and ZBLAN fiber. So it is necessary to have high peak power pulses at 2 µm to get MIR supercontinuum and can be obtained as discussed in above section.

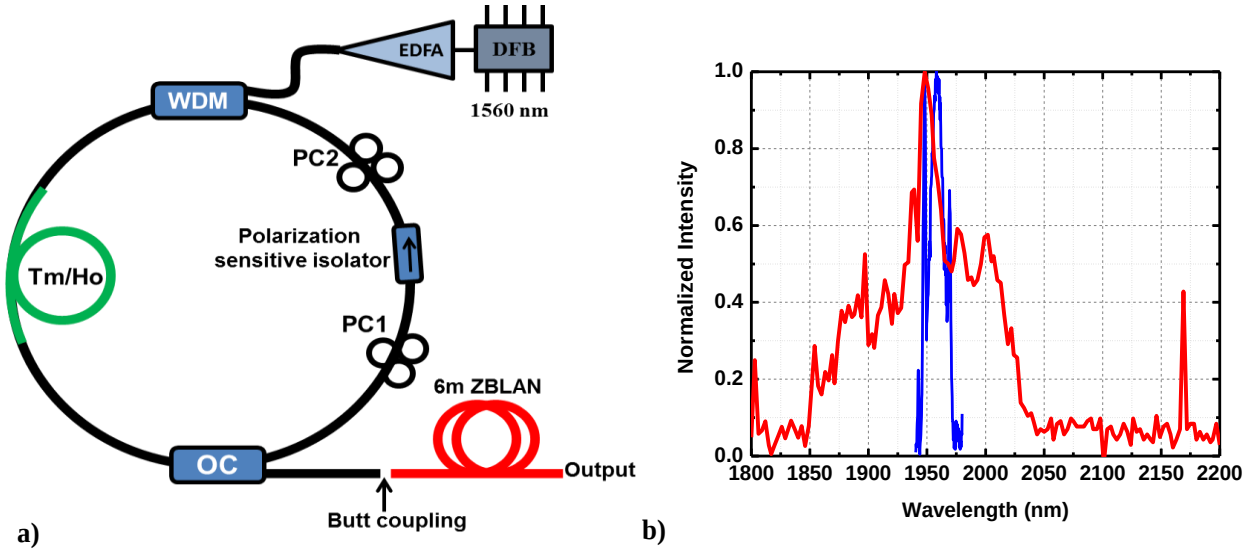


**Figure 5.3 a) Experimental setup for mid-infrared supercontinuum generation from ZBLAN fiber, DFB; distributed feedback laser, EDFA; erbium doped fiber amplifier, WDM; wavelength division multiplexer, OC; output coupler. Output of the mode-locked**

**laser is butt coupled into the 6 m of ZBLAN fiber. B) Measured output spectrum after 6 m of ZBLAN fiber (red curve) measured from spectrometer with input spectrum (blue curve).**

### *5.2.3 Generating a Frequency Comb at 2 μm and Longer Wavelengths*

The pulse train generated by the mode-locked laser consists of a discrete, regularly spaced series of sharp lines in the frequency domain, known as a frequency comb. Frequency combs have revolutionized the precise measurements of frequency and time after their introduction in late 1990s. The frequency combs in the visible and near-infrared domains have enabled the development of new ultraprecise optical atomic clocks and are now becoming enabling tools for an increasing number of applications, ranging from the calibration of astronomical spectrograph to molecular spectroscopy. Hence the extension of frequency combs into the mid-infrared region will bring a new set of tools for precision spectroscopy since a large number of molecules undergo strong characteristic vibrational transitions in this region as shown in Figure 5.4. Another future direction is making a stabilized frequency comb near 2 μm [62, 118] using mode-locked Tm/Ho co-doped fiber lasers demonstrated in Chapter 4 or at longer wavelengths [64] via supercontinuum generation in highly nonlinear fibers such as ZBLAN fiber. To realize such a frequency comb first it is necessary to amplify the output of the Tm/Ho laser. So next step is to build a thulium or thulium/holmium fiber amplifier and used the same approach that discussed in Ref [83] to make a stabilized frequency comb near 1.5 μm using erbium doped mode-locked fiber laser.

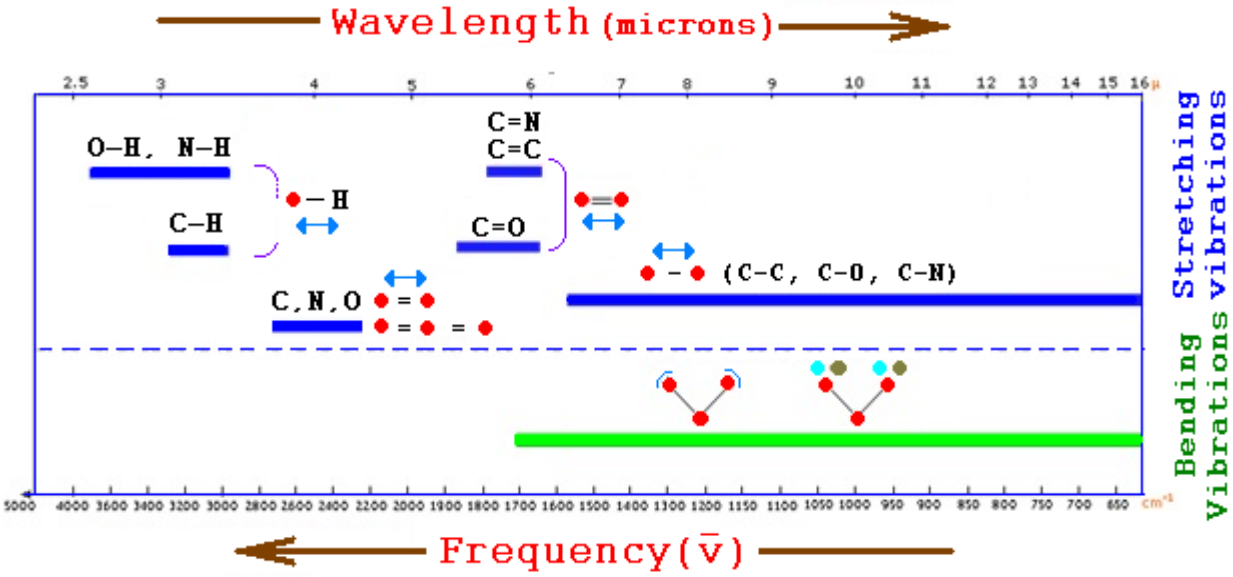


**Figure 5.4 Ro-vibrational absorption of many molecules in the mid-infrared wavelength region. The fingerprint region of the most of the molecules lies in the mid-infrared. This graph is reproduced from Ref [119].**

# References


[1] C. J. Koester and E. Snitzer, "Amplification in a fiber laser," *Appl. Opt.*, vol. 3, 1964.

[2] D. S. Funk, J. W. Xarlson, and J. G. Eden, "Room-temperature fluorozincronate fiber laser in the violet (412 nm)," *Opt. Lett.* , vol. 20, 1995.

[3] J. Y. Allain, M. Monerie, and H. Poignant, "Room temperature CW tunable green upconversion holmium fiber laser," *Electron. Lett.*, vol. 26, 1990.

[4] J. Y. Allain, M. Monerie, and H. Poignant, "Tunable green upconversion erbium fiber laser," *Electron. Lett.*, vol. 28, 1992.

[5] D. S. Funk, J. W. Xarlson, and J. G. Eden, "Ultraviolet (381 nm) room temperature laser in neodymium-doped fluorozicronate fiber," *Electron. Lett.*, vol. 30, 1994.

[6] H. M. Pask, R. J. Carman, D. C. Hanna, A. C. Tropper, C. J. Mackechnine, P. R. Barber, *et al.*, "Ytterbium-doped silica fiber laser: versatile sources for the 1-1.2 μm region," *IEEE J. Sel. Top. Quantum Electron.*, vol. 1, 1995.

[7] H. Po, J. D. Cao, B. M. Laliberte, R. A. Minns, R. F. Robinson, B. H. Rockney, *et al.*, "High power neoydymium-doped single transverse mode fiber laser," *Electron. Lett.*, vol. 29, 1993.

[8] R. J. Mears, L. Reekie, M. Jauncey, and D. N. Payne, "Low-noise erbium-doped fiber amplifier operating at 1.54 μm," *Electron. Lett.* , vol. 26, 1987.

[9] D. C. Hanna, I. M. Jauncey, R. M. Percival, I. R. Perry, R. G. Smart, P. J. Suni, *et al.*, "Continuous-wave oscillation of a monomode thulium-doped fiber laser," *Electron. Lett.* , vol. 24, 1988.

[10] J. Wu, S. Jiang, T. Luo, J. Geng, N. Peygharmbarian, and N. P. Barnes, "Efficient thulium-doped 2 μm grmanate fiber laser," *IEEE Photon. Technol. Lett,* vol. 18, 2006.

[11] K. Oh, T. F. Morse, A. Kilian, L. Reinhart, and P. M. Weber, "Continuous-wave oscillation of thulium-sensitized holmium-doped silica fiber laser," *Opt. Lett.,* vol. 19, 1994.

[12] S. D. Jackson, "Towards high-power mid-infrared emission from a fiber laser," *Nature photonics,* vol. 6, 2012.

[13] M. E. Fermann, M. Hofer, F. Habrel, and S. P. Craigoryan, "Femtosecond fiber laser," *Electron. Lett.,* vol. 26, 1990.

[14] M. E. Fermann, M. Hofer, F. Habrel, M. H. Ober, and A. J. Schmidt, "Additive-pulse-compression mode locking of a neodymium fiber laser," *Opt. Lett.,* vol. 16, 1991.

[15] I. N. Duling III, "All-fiber ring soliton laser mode locked with a nonlinear mirror," *Opt. Lett.,* vol. 16, 1991.

[16] L. E. Nelson, D. J. Jones, K. Tamura, H. A. Haus, and E. P. Ippen, "Ultrashort-pulse fiber ring laser," *Appl. Phys. B,* vol. 65, 1997.

[17] J. D. Kafka, T. Bear, and W. Hall, "Mode-locked erbium-doped fiber laser with soliton," *Opt. Lett.,* vol. 24, 1989.

[18] S. T. Cundiff, "Metrology: New generation of combs," *Nature,* vol. 450, 2007.

[19] K. Tamura, H. A. Haus, and E. P. Ippen, "Self starting additive pulse mode-locked erbium fiber ring laser," *Elect. Lett.,* vol. 28, 1992.

[20] K. Tamura, E. P. Ippen, H. A. Haus, and L. E. Nelson, "77-fs pulse generation from a stretched-pulse mode-locked all-fiber ring laser," *Opt. Lett.,* vol. 18, 1993.

[21] D. Ma, Y. Cai, C. Zhou, W. Zong, L. Chen, and Z. Zhang, "37.4 fs pulsegeneration in an Er:fiber laser at a 225 MHz repetition rate," *Opt. Lett.*, vol. 35, 2010.

[22] A. Chong, H. Liu, B. Nie, B. G. Bale, S. Wabnitz, W. H. Renninger, *et al.*, "Pulse generation without gain-bandwidth limitation in a laser with self-similar evolution," *Opt. Express*, vol. 20, 2012.

[23] X. Zhu and R. Jain, "Compact 2 W wavelength-tunable Er:ZBLAN mid-infrared fiber laser," *Opt. Lett.*, vol. 32, 2007.

[24] S. Tokita, M. Murakami, S. Shimizu, M. Hashida, and S. Sakabe, "Liquid-cooled 24 W mid-infrared Er:ZBLAN fiber laser," *Opt. Lett.*, vol. 34, 2009.

[25] S. D. Jackson, "Single transverse-mode 2.5-W holmium-doped fluoride fiber laser operating at 2.86 μm," *Opt. Lett.*, vol. 29, 2004.

[26] J. Scheider, C. Carbonnier, and U. B. Uneau, "Characterization of a $Ho^{3+}$-doped fluoride fiber laser with a 3.9 μm emission wavelength," *Appl. Opt.*, vol. 36, 1997.

[27] D. Hofstetter and J. Faist, "High performance quantum cascade lasers and their applications," *Top. Appl. Phys.*, vol. 89, 2003.

[28] S. A. Reid and Y. Tang, "Generation of tunable, narrow-band mid-infrared radiation through a 532-nm-pumped KTP optical parametric amplifier," *Appl. Opt.*, vol. 35, 1996.

[29] P. A. Bundi, L. A. Pomeranz, M. I. Lemons, C. A. Miller, J. R. Mosoto, and E. P. Chicklis, "Efficient mid-infrared laser using 1.9-μm-pumped Ho:YAG and $ZnGeP_2$ optical parametric oscillators," *J. Opt. Soc. Am. B*, vol. 17, 2000.

[30] E. M. Dianov and A. M. Prokhorov, "Medium-power CW Raman fiber lasers," *IEEE J. Sel. Top. Quantum Electron.*, vol. 6, 2000.

[31] D. Nodop, C. Jauregui, D. Schimpf, J. Limpert, and A. Tunnermann, "Efficient high power generation of visible and mid-infrared light by degenetrate four-wave-mixing in a large-mode-area photonic crystal fiber," *Opt. Lett.,* vol. 15, 2009.

[32] C. L. Hagen, J. W. Walewski, and S. T. Sanders, "Generation of a continuum extending to the mid-infrared by pumping ZBLAN fiber with an ultrafast 1550-nm source," *IEEE Photon. Technol. Lett,* vol. 18, 2006.

[33] M. N. Cizmeciyan, H. Cankaya, A. Kurt, and A. Sennaroglu, "Kerr-lens mode-locked femtosecond $Cr^{2+}$:ZnSe at 2420 nm," *Opt. Lett.,* vol. 34, 2009.

[34] S. M. Foreman, D. J. Jones, and J. Ye, "Flexible and rapidly configurable femtosecond pulse generation in the mid-IR," *Opt. Lett.,* vol. 28, 2003.

[35] C. Erny, K. Moutzouris, J. Biegert, D. Kuhlke, F. Adler, A. Leitenstorfer, *et al.,* "Mid-infrared difference frequency generation of ultrashort pulses tunable between 3.2 to 4.8 μm from a compact fiber source," *Opt. Lett.,* vol. 32, 2007.

[36] P. Maddaloni, P. Malara, G. Gagliardi, and P. D. Natale, "Mid-infrared fiber-based optical comb," *New J. Phys.,* vol. 8, 2006.

[37] M. A. Gubin, A. N. Kireev, A. V. Konyashchenko, P. G. Kryukov, A. S. Shelkovnikov, A. V. Yausenev, *et al.,* "Femtosecond fiber laser based methane optical clock," *Appl. Phys. B,* vol. 95, 2008.

[38] A. Gamnetta, R. Ramponi, and M. Marangoni, "Mid-infrared optical combs from a compact amplified Er-doped fiber oscillator," *Opt. Lett.,* vol. 33, 2008.

[39] A. Ruehl, A. Gambetta, I. Hartl, M. E. Fermann, K. S. Eikema, and M. Marangoni, "Widely-tunable mid-infrared frequency comb source based on difference frequency generation," *Opt. Lett.,* vol. 37, 2012.

[40] N. M. Fried, "High-power laser vaporization of the canine prostrate using a 110 W thulium fiber laser at 1.91 μm," *Las. Surg. Med.,* vol. 36, 2005.

[41] N. M. Fried and K. E. Murray, "New Technology in endurology-high power thulium fiber laser ablation of urinary tissues at 1.94 μm," *J. Endourol,* vol. 15, 2005.

[42] J. Kourambas, F. C. Delvecchio, and G. M. Preminger, "Low-power holmium lasers for the management of urinary tract calculi, structures and tumors," *J. Endourol,* vol. 15, 2001.

[43] R. J. DeYoung and N. P. Barnes, "Profiling atmospheric water vapor using a fiber laser lidar system," *Appl. Opt.,* vol. 49, 2010.

[44] D. Creeden, P. A. Ketteridge, P. A. Budni, S. D. Setzler, Y. E. Young, J. C. MaCarthy, *et al.,* "Mid-infrared ZnGeP2 parametric oscillator directly pumped by a pulsed 2 μm Tm-doped fiber laser," *Opt. Lett.,* vol. 33, 2008.

[45] L. F. Johnson, J. E. Geusic, and L. G. V. Uitert, "Coherent oscillation from $Tm^{3+}$, $Ho^{3+}$, $Yb^{3+}$, and $Er^{3+}$ ions in yttrium aluminum garnet," *Appl. Phys. Letts.,* vol. 7, 1965.

[46] S. A. Payne, L. L. Chase, L. K. Smith, W. L. Kway, and W. F. Krupke, "Infrared cross-section measurement for crystals doped with $Er^{3+}$, $Tm^{3+}$, and $Ho^{3+}$," *IEEE J. of Quantum Electron,* vol. 28, 1992.

[47] F. S. Ermeneux, Y. Sun, R. L. Cone, R. W. Equall, R. L. Hutchenson, and R. Moncorge, "Efficient CW 2 μm $Tm^{3+}$:$Y_2O_3$ laser," *Adv. Solid-state lasers,* vol. 26, 1999.

[48] K. Scholle, E. Heumann, and G. Huber, "Single mode Tm, Ho:LuAG lasers for LIDAR applications," *Laser Phys. Lett.,* vol. 1, 2004.

[49] M. Schellhorn, A. Hirt, and C. Kieleck, "Ho:YAG laser intracavity pumped by a laser diode-pumped Tm:YLF," *Opt. Lett.,* vol. 28, 2003.

[50] D. C. Hanna, R. M. Percival, R. G. Smart, and A. C. Tropper, "Efficient and tunable operation of a Tm-doped fiber laser," *Opt. comm.*, vol. 24, 1990.

[51] J. Y. Allain, M. Monerie, and H. Poignant, "Tunable CW lasing around 0.82, 1.18, 1.88, and 2.35 μm in the thulium-doped flurozincronate fiber," *Electron. Lett.*, vol. 25, 1989.

[52] L. E. Nelson, E. P. Ippen, and H. A. Haus, "Broadly tunable sub-500 fs pulses from an additive mode-locked thulim-doped fiber ring laser," *Appl. Phys. Letts.*, vol. 67, 1995.

[53] R. C. Sharp, D. E. Spock, N. Pan, and J. Elliot, "190-fs passively mode-locked thulium fiber laser with a low threshold," *Opt. Lett.*, vol. 21, 1996.

[54] K. Scholle, S. Lamrini, P. Koopmann, and P. Fuherberg. 2 μm: Laser Sources and Their Possible Application.

[55] D. Creeden, P. A. Budni, and P. A. Ketteridge, "Pulsed Tm-doped fiber laser for mid-IR frequency conversion," in *In SPIE Photonic West*, 2009.

[56] B. E. Schmidt, A. D. Shiner, M. Giguere, P. Lassonde, C. A. Trallero-Herrero, J. C. Kieffer, *et al.*, "High harmonic generation with long-wavelength few-cycle laser pulses," *J. Phys. B. At. Mol. Opt. Phys.*, vol. 45, 2012.

[57] C. R. Philips, J. Jiang, C. Langrock, M. M. Fejer, and M. E. Fermann, "Self-referenced frequency comb from a Tm-fiber via PPLN waveguide supercontinuum generation," *in the Proceedings of the Conference on Laser and Electro-optics*, vol. paper PDPA5, 2011.

[58] P. Mazzone, "Analysis of volatile organic compounds in the exhaled breath for the diagnosis of lunf cancer," *J. Thorac. Oncol.*, vol. 3, 2008.

[59] K. Namjou, C. B. Roller, T. Reich, J. Jeffers, G. McMillen, P. McCann, *et al.*, "Determination of exhaled nitric oxide distributions in a diverse sample population using tunable diode laser absorption spectroscopy," *Appl. Phys. B*, vol. 85, 2006.

[60] F. Tittel, D. Richter, and A. Fried, "Mid-infrared laser applications in spectroscopy," *Solid-State Mid-Infrared Laser Sources,* vol. 89, 2003.

[61] M. J. Thorpe and J. Ye, "cavity-enhanced direct comb spectroscopy," *Appl. Phys. B,* vol. 91, 2008.

[62] F. Adler and S. A. Diddams, "High-power, hybrid Er:fiber/Tm:fiber frequency comb source in the 2 μm wavelength region," *Opt. Lett.,* vol. 36, 2012.

[63] A. Schliesser, N. Picque, and T. H. Hansch, "Mid-infrared frquency combs," *Nature photonics,* vol. 6, 2012.

[64] F. Adler, K. C. Cossel, M. J. Thorpe, I. Hartl, M. E. Fermann, and J. Ye, "Phase-stabilized, 1.5 W frequency comb at 2.8-4.8 μm," *Opt. Lett.,* vol. 34, 2009.

[65] T. Izawa, N. Shibata, and A. Takeda, "Optical attenuation in pure and doped fused silica in the IR wavelength region," *Appl. Phys. Lett.,* vol. 31(1), 1977.

[66] E. Snitzer, "Optical maser action of $Nd^{3+}$ in a barium crown glass," *Phys. Rev. Letts.,* vol. 7, 1961.

[67] E. Snitzer, H. Po, F. Hakimi, R. Tumminelli, and B. C. AcCollum, "Erbium fiber laser amplifier at 1.55 μm with pump at 1.49 μm and Yb sensitized Er oscillator," *in Tech. Dig. Opt. Fiber Commum. Conf. Opt. Soc. Amer.,* vol. Postdeadline paper, 1988.

[68] E. Desyrivire and J. R. Simpson, "Amplification of spontaneous emission in erbium-doped single-mode fibers," *J. of Lightwave Tech.,* vol. 7, 1989.

[69] D. C. Hanna, R. M. Percival, I. R. Perry, R. G. Smart, P. J. Sunni, J. E. Townsend*, et al.*, "Continuous-wave oscillation of a monomode ytterbium-doped fiber laser," *Elect. Letts.,* vol. 24, 1988.

[70] H. Po, R. Tumminelli, L. Zenteno, F. Hakimi, N. M. Cho, and T. Haw, "Double clad high brightness ND filter fiber laser pumped by GaAlAs phased arry," *in Digest of Optical Fiber Conference,* 1989.

[71] Y. Miyajima, T. Komukai, and T. Sugawa, "1-W cw Tm-doped fluoride fiber laser at 1.47 μm," *Elect. Lett.,* vol. 29, 1993.

[72] J. Y. Allain, M. Monerie, and H. Poignant, "High-efficiency CW thulium-sesitized holmium-doped fluoride fiber operating at 2.04 μm.," *Elect. Lett.,* vol. 27, 1991.

[73] H. A. Haus, J. G. Fujimoto, and E. P. Ippen, "Structures for additive mode locking," *J. Opt. Soc. Am. B,* vol. 8, 1991.

[74] O. E. Martinez, R. L. Fork, and J. P. Gordon, "Theory of passively mode-locked lasers including self-phase modulation and group velocity dispersion," *Opt. Lett.,* vol. 9, 1984.

[75] D. Gloge, "Dispersion in weakly guiding fibers," *Appl. Opt.,* vol. 10, 1971.

[76] M. E. Fermann, A. Galvanauskas, G. Sucha, and D. Harter, "Fiber-lasers for ultrafast optics," *Applied Physics B: Lasers and Optics,* vol. 65, pp. 259-275, 1997.

[77] E. Desurvier, *Erbium-doped Fiber Amplifiers, Principle and Applications*. New York: Wiley-Interscience, 2002.

[78] I. N. Duling III, "Dispersion in rare-earth-doped fibers," *Opt. Lett.,* vol. 16, 1991.

[79] Y. R. Shen, *Handbook of Optics*. New York: Wiley, 1984.

[80] R. H. Stolen and C. Lin, "Self-phase modulation in silica optical fibers," *Phys. Rev. A,* vol. 17, 1978.

[81] A. Hasegawa and F. Tappert, "Transmission of stationary nonlinear optical pulses in dispersive dielectric fibers. I. anomalous dispersion," *Appl. Phys. Lett.,* vol. 23, 1973.

[82] S. D. Jackson and T. A. King, "CW operation of a 1.064 μm pumped Tm-Ho-doped silica fiber laser," *IEEE J. of Quantum Electron,* vol. 34, 1998.

[83] J. Lim, "All-fiber frequency comb employing a single walled carbon nanotube saturable absorber for optical frequency metrology in near infrared," PhD Thesis, Physics, Kansas State University, Manhattan, KS, 2011.

[84] I. N. Duling III, "Subpicosecond all-fiber erbium laser," *Elect. Lett.,* vol. 27, 1991.

[85] D. Y. Tang and L. M. Zhao, "Generation of 47-fs pulses directly from an erbium-doped fiber laser," *Opt. Lett.,* vol. 32, 2007.

[86] M. E. Fermann, F. Habre, M. Hofer, and H. Hochreiter, "Nonlinear amplifying loop mirror," *Opt. Lett.,* vol. 15, 1990.

[87] K. R. Tamura, "Additive pulse mode-locking erbium-doped fiber lasers," Physics, MIT, 1994.

[88] B. R. Washburn, W. C. Swann, and N. R. Newbury, "Response dynamics of the frequency comb from a femtosecond fiber laser," *Optics express,* vol. 13, 2005.

[89] R. M. Percival, M. Monerie, and H. Poignant, "Thulim sensitized holmium-doped CW fluoride fiber laser of high efficiency," *Elect. Lett.,* vol. 28, 1992.

[90] R. Kadel and B. R. Washburn, "All-fiber passivley mode-locked thuliun/holmium laser with two center wavelengths," *Appl. Opt.,* vol. 51, 2012.

[91] S. M. Kelly, "Characteristics sidebabd of periodically amplifiers average soliton," *Elect. Lett.,* vol. 28, 1992.

[92] M. L. Dennis and I. N. Duling III, "Experimentally study of sideband geneartion in femtosecond fiber laser," *IEEE J. of Quantum Electron,* vol. 30, 1994.

[93] J. W. Nicholson, M. F. Yan, P. Wisk, J. Fleming, F. DiMarcello, E. Monberg, *et al.*, "All-fiber, octave-spanning supercontinuum," *Opt. Lett.*, vol. 28, 2003.

[94] L. Gruner-Nielse, M. Wandel, P. Kristensen, C. Jorgense, L. V. Jorgensen, B. Edvold, *et al.*, "Dispersion-Compensating Fibers," *J. of Lightwave Tech.*, vol. 23, 2005.

[95] J. A. Buck, *Fundamentals of Optical Fibers*, 2nd ed.: Wiley, 2004.

[96] Q. Wang, T. Chen, and K. Chen, "Mode-locked ultrafast thulium fiber laser with all-fiber dispersion management," presented at the in Proceeding of Conference on lasers and electro-optics, San Jose, 2010.

[97] S. Kivisto, T. Hakulinen, M. Guina, and O. G. Okhotnikv, "Tunable Raman soliton source using mode-locked Tm-Ho fiber," *IEEE Photon. Technol. Lett*, vol. 19, 20007.

[98] J. C. M. Diels, J. J. Fontaine, I. C. McMichael, and F. Simoni, "Control and measurement of ultrfast pulse shapes (in amplitude and phase) with femtosecond accuracy," *Appl. Opt.*, vol. 24, 1985.

[99] F. T. S. Yu and X. Yang, *Introduction to Optical Engineering*: Cambridge Academic Press, 1997.

[100] R. Trebino, *Frequency Resolved Optical Gating:The measurement of ultrashort optical pulses*: Kluwer Academic Publishers, 2000.

[101] P. M. W. French, "The generation of ultrashort laser pulses," *Rep. Prog. Phys.* , vol. 58, 1995.

[102] D. T. Reid, W. Sibbett, J. M. Dudley, L. P. Barry, B. Thomsen, and J. D. Harvey, "Commercial semiconductor devices for two photon absorption autocorrelation of ultrashort pulses," *Appl. Opt.*, vol. 37, 1998.

[103] S. Y. Chen, T. L. Yeo, J. Leighton, T. Sun, K. T. V. Grattan, R. Lade, *et al.*, "Tm:Ho co-doped single mode optical fiber laser pumped by a 1600 nm Er fiber laser," *Opt. comm.*, vol. 281, 2008.

[104] H. A. Haus, K. Tamura, L. E. Nelson, and E. P. Ippen, "Structure-pulse additive pulse mode-locking in fiber ring laser: Theory and experiment," *IEEE J. of Quantum Electrononics,* vol. 31, 1995.

[105] F. Haxsen, D. Wandt, U. Morgner, J. Neumann, and D. Kracht, "Pulse energy of 151 nJ from thulium-doped chirped-pulse fiber amplifier," *Opt. Express,* vol. 18, 2010.

[106] R. Gumenyuk, I. Vartiainen, H. Tuovivnen, and O. G. Okhotnikov, "Dissipative dispersion-managed soliton 2 μm thulium/holmium fiber laser," *Opt. Lett.,* vol. 36, 2011.

[107] A. Wienke, F. Haxsen, D. Wandt, U. Morgner, J. Neumann, and D. Karcht, "Ultrafast, stretched-pulse thulium-doped fiber laser with a fiber-based dispersion management," *Opt. Lett.,* vol. 37, p. 3, July 1, 2012 2012.

[108] H. Liu, L. Kieu, S. Lefrancois, W. H. Renninger, A. Chong, and F. W. Wise, "Tm fiber laser mode-locked at large normal dispersion," *OSA/CLEO,* vol. CMK1, 2011.

[109] D. C. J. K. O. Hill, B. S. Kawasaki, and R. I. MacDonald "cw three-wave mixing in single-mode optical fibers," *J. Appl. Phys.,* vol. 49, pp. 5098-5106, 1978.

[110] R. Kadel and B. R. Washburn, "An all fiber mode-locked Tm/Ho fiber laser employing c-band components," in *in Frontiers in Optics (FiO)*, San Jose, 2011.

[111] G. P. Agrawal, "Fiber-Optic Communication Systems," *Wiley, New York,* vol. 3rd edition, 2002.

[112] D. L. Marks, A. L. Oldenbur, J. J. Reynolds, and S. A. Boppart, "Study of an ultrahigh-numeical-aperture fiber continuum generation sources for optical coherence tomography," *Opt. Lett.,* vol. 27, 2002.

[113] A. Mendez and T. F. Morse, *Speciality Optical Fibers Handbook*: Academic Press.

[114] N. R. Newbury and W. C. Swann, "Low-noise fiber-laser frequency comb (Invited)," *J. Opt. Soc. Am. B,* vol. 24, 2007.

[115] K. Tamura, L. E. Nelson, H. A. Haus, and E. P. Ippen, "Soliton versus nonsoliton opeartion of fiber ring lasers," *Appl. Phys. Lett.*, vol. 64, 1994.

[116] C. Zhang, L. Chai, Y. Song, M. Hu, and C. Wang, "Ultra-broadband optical spectrum generation from a strtched pulse fiber laser utilizing zero-dispersion fiber," *Chinese Oprics Express,* vol. 11, 2013.

[117] F. Gan, "Optical properties of fluoride glasses: a review," *J. Non-Cryst. Solids,* vol. 184, pp. 9-20, 1995.

[118] J. Bethge, J. Jiang, C. Mohr, M. E. Fermann, and I. Hartl, "Optically refernced Tm-fiber-laser frequency comb," in *Lasers, Sourced, and Related Photonic Technical Digest*, 2012.

[119] http://chemistry.tutorvista.com/organic-chemistry/ir-spectroscopy.html.

[120] C. Lin, W. A. Reed, A. D. Pearson, and H. T. Shang, "Phase matching in the minimum-chromatic-dispersion region of a single-mode fibers for stimulated four-photom mixing," *Opt. Lett.*, vol. 6, 1981.

[121] J. Hanstyd, P. A. Aderkson, M. Westland, J. Li, and P. O. Hedekvist, "Fiber-based optical parametric amplifiers and their applications," *IEEE Journal on Sel. Top. In QuantnumElectronics,* vol. 8, 2002.

[122] G. P. Agrawal, *Nonlinear Fiber Optics*, 4th ed.: Academic Press, 2007.

[123] M. Marhic, *Fiber Optical Parametric Amplifiers, Oscillators, and Related Devices*. NewYork: Cambridge Univ. Press, 2007.

[124] Y. Chen and A. W. Snyder, "Four-photon parametric mixing in optical fibers: effect of pump depletion," *Opt. Lett.*, vol. 14, 1989.

[125] X. Zhu and R. Jain, "10-W-level diode -pumped compact 2.78 μm ZBLAN fiber laser," *Opt. Lett.*, vol. 32, 2007.

# Appendix A - Abbreviations

| | |
|---|---|
| **AM** | **Amplitude modulation** |
| **ASE** | **Amplifies spontaneous emission** |
| **dB** | **Decibel** |
| **CNFL** | **Carbon nanotube fiber laser** |
| **CW** | **Continuous wavelength** |
| **DCF** | **Dispersion compensating fiber** |
| **DFB** | **Distributed feedback** |
| **DFG** | **Difference frequency generation** |
| **EDF** | **Erbium doped fiber** |
| **EDFA** | **Erbium doped fiber amplifier** |
| **ESA** | **Electric spectrum analyzer** |
| **Er** | **Erbium** |
| **FOPA** | **Fiber optical parametric amplifier** |
| **FWHM** | **Full width half maximum** |
| **FWM** | **Four wave mixing** |
| **F8L** | **Figure eight laser** |
| **FRAC** | **Frequency resolved autocorrelation** |
| **HNLF** | **Highly nonlinear fiber** |
| **IAC** | **Interferometric autocorrelation** |
| **IR** | **Infrared** |
| **LD** | **Laser diode** |
| **MIR** | **Mid infrared** |
| **NA** | **Numerical aperture** |
| **NALM** | **Nonlinear amplifying loop mirror** |
| **ND** | **Neutral density** |
| **NPE** | **Nonlinear polarization evolution** |
| **NPR** | **Nonlinear polarization rotation** |
| **OC** | **Output coupler** |
| **OPA** | **Optical parametric amplifier** |

| | |
|---|---|
| **OPO** | **Optical parametric oscillator** |
| **P-APM** | **Polarization additive pulse mode-licking** |
| **PBG** | **Photonic bandgap** |
| **PC** | **Polarization controller** |
| **PD** | **Photodetector** |
| **PM** | **Polarization maintaining** |
| **SAM** | **Self-amplitude modulation** |
| **SESAM** | **Semiconductor saturable absorber mirror** |
| **SHG** | **Second harmonic generation** |
| **SMF** | **Single mode fiber** |
| **SVEA** | **Slowly varying envelop approximation** |
| **SWCNT** | **Single walled carbon nanotube** |
| **SPM** | **Self phase modulation** |
| **TIR** | **Total internal reflection** |
| **TOD** | **Third order dispersion** |
| **TPA** | **Two photon absorption** |
| **UHNA** | **Ultra-high numeric aperture** |
| **WDM** | **Wavelength division multiplexer** |
| **XPM** | **Cross phase modulation** |
| **ZDW** | **Zero dispersion wavelength** |

# Appendix B - Fiber Optical Parametric Amplifier

## B.1 Introduction

The goal of this thesis is to generate the mid-infrared laser in an all fiber format. One possible route towards this goal is to use third order nonlinear effects to covert light from shorter wavelengths to longer wavelengths. A particular process that achieves this goal is called an optical parametric process via the material third order dielectric susceptibility. The third-order susceptibility $\chi^{(3)}$ contributes to the non-linear effects in the optical fibers where four distinct waves involved in parametric processes [120] as shown in Figure B.1. Materials like fused silica do not exhibit strong second order nonlinear effects since it lacks inversion symmetry. As described in Chapter 2, third-harmonic generation, four-wave mixing (FWM) and nonlinear refraction are the nonlinear processes that can happen in optical fibers. In FWM, it can be seen from energy conservation $(\omega_{p1} + \omega_{p2} = \omega_s + \omega_i)$ that the pump wavelength can be higher or lower than the signal wavelength where as in three-wave mixing the pump wavelength is always lower than the signal wavelength in order to satisfy energy conservation$(\omega_p = \omega_s + \omega_i)$.

Since the strength of the parametric process depends on the nonlinearity of the fiber, highly nonlinear fiber is used as a nonlinear medium to generate mid-infrared wavelengths via FWM for the case of pump depletion, where the pump power decreases along the length of the fiber and hence the signal and idler powers increase. Such a FWM-based device is known as a fiber-optic parametric amplifier (FOPA). In the next sections, I will discuss both the theory and experiment of FOPA's for the case of pump depletion when there is single and double pump present.

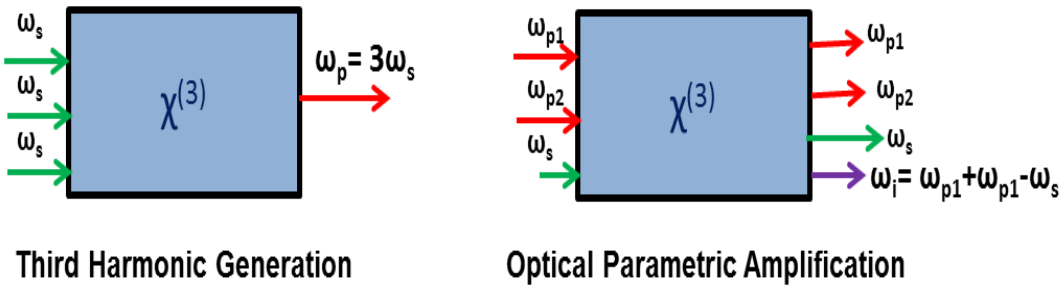


**Figure B.1 Schematic of various four-wave mixing process including third harmonic generation and optical parametric amplifier. Here $\omega_p, \omega_s,$ and $\omega_i$ are the pump, signal and idler frequencies.**

## B.2 Derivation of Fiber Optical Parametric Amplifier Equation

Optical parametric amplification in fused-silica fibers is a nonlinear process exploiting the light induced modulation of the fiber refractive index [121] where the parametric gain is often referred to as a third order parametric process since it depends on third order susceptibility $\chi^{(3)}$ of the medium. To get the wave equation for the propagation of light wave through optical medium, I begin with wave equation [122]

$$\nabla^2\vec{E} - \frac{1}{c^2}\frac{\partial^2\vec{E}}{\partial t^2} = \mu_0\frac{\partial^2\vec{P}_L}{\partial t^2} + \mu_0\frac{\partial^2\vec{P}_{NL}}{\partial t^2} \tag{B.1}$$

where $\vec{E}$ is the total electric field, $\mu_0$ is the vacuum permeability, $\vec{P}_L$ and $\vec{P}_{NL}$ are the linear and nonlinear polarizations related to the electric field as

$$\vec{P}_L = \varepsilon_0\chi^{(1)}\vec{E}$$

$$\vec{P}_{NL} = \varepsilon_0\sum_{i=1}^{3}\left[\sum_{jkl}\chi^{(3)}_{ijkl}\vec{E_j}\,\vec{E_k}\,\vec{E_l}\right] \tag{B.2}$$

where $\chi^{(1)}$ represents the linear medium i.e. the linear index of refraction, and $\chi^{(3)}$ represents the third-order nonlinear effects, which are responsible for the FOPAs and the nonlinear intensity-dependent index of refraction.

Under the slowly varying envelope approximation (SVEA), where the time variation of the electric field is slow compared with the optical carrier frequency, and when the spacing of optical frequencies of four waves involved in parametric process is relatively small i.e. $\chi^{(3)}$ is independent of frequency, Eq. (B.1) can be written as [123]

$$\frac{dA_l}{dz} = i\gamma\left[|A_l|^2 A_l + 2\sum_{j\neq l=1}^{4}\left|A_j\right|^2 A_l + 2A_m A_n A_k^* e^{i\varepsilon\Delta\beta z}\right],\ l\text{=1-4} \tag{B.3}$$

where γ in general describes the effective nonlinear phenomenon in the fiber and is given by

$$\gamma = \frac{3\mu_0\omega\chi^{(3)}}{8\bar{n}^2 A_{eff}} \tag{B.4}$$

where $\omega$ is the average value of angular frequency and $A_{eff}$ is the effective area of the same order as the area of the core .The expression for γ in Eq. (B.4) is equivalent to that given in Ref. [122]. In FOPA it is convenient to express γ in units of $W^{-1}km^{-1}$. For standard communication grade fiber (Corning SMF-28) $\gamma \approx 2\ W^{-1}km^{-1}$ and for OFS highly nonlinear fiber (HNLF) $\gamma \approx 20\ W^{-1}km^{-1}$.

Equation (B.3) is known as the propagation equation when there is a non-degenerate two pump in the OPA for the slowly varying envelope $A_k$ and the frequencies satisfy the condition $\omega_1 + \omega_2 = \omega_3 + \omega_4$ where $\omega_1$ and $\omega_2$ are the frequencies of the two pumps, $\omega_3$ is the frequency of the signal and $\omega_4$ is the frequency of the idler. $\Delta\beta = \beta_3 + \beta_4 - \beta_1 - \beta_2$, is the propagation wave vector mismatch. In the right side of Eq. (B.3) there are three terms; the first terms

corresponds to interaction of the wave with itself and leads to self-phase modulation (SPM), the second term describes the interaction between two waves and leads to cross-phase modulation (XPM) and the third term corresponds to interaction between four distinct waves i.e. non-degenerate four-wave mixing (FWM).

The integers *k, l, m,* and *n* in Eq. (B.3) are such that

for ε = 1, if *l* = 1 or 2 then *k*= 3-*l*, *m* = 3, and *n* = 4;

for ε = -1, if *l*= 3 or 4 then *k* = 7-*l*, *m* = 1, and *n* = 2.

If there is just one pump in FOPA (two pumps are degenerate) it is called one-pump FOPA. To describe one-pump FOPA the second pump is ignored and I only consider the interactions between three distinct waves then wave equation (B.3) becomes [123]

$$\frac{dA_1}{dz} = i\gamma\left[|A_1|^2A_1 + 2\sum_{j\neq 1}^{4}|A_j|^2A_1 + 2A_3A_4A_1^*e^{i\varepsilon\Delta\beta z}\right], \quad \text{(B.5)}$$

$$\frac{dA_l}{dz} = i\gamma\left[|A_l|^2A_l + 2\sum_{j\neq l=1}^{4}|A_j|^2A_l + 2(A_1)^2A_k^*e^{i\varepsilon\Delta\beta z}\right], \quad \text{(B.6)}$$

*l*=3,4, *k*=7-*l*,

with propagation mismatch $\Delta\beta = \beta_3 + \beta_4 - 2\beta_1$. In Equations (B.5) and (B.6) the first two terms on right hand side are the same as for the two-pump FOPA. The third term in Eq. (B.5) corresponds to non-degenerate FWM and in Eq. (B.6) corresponds to degenerate FWM.

### *B.2.1 Phase-Matching Condition*

The propagation wave vector mismatch for FWM is given as

$$\Delta\beta = \beta_3 + \beta_4 - \beta_1 - \beta_2 \tag{B.7}$$

with $\omega_1 + \omega_2 = \omega_3 + \omega_4$

To get sufficient conversion of input waves into third wave in nonlinear mixing processes the following condition should be satisfied

$$\Delta\beta = 0 \tag{B.8}$$

known as the phase-matching condition. When this condition is satisfied the generated wave, idler maintains a fixed phase relation with respect to the nonlinear polarization and extracts the energy from the input waves. Quantum mechanically, the phase-matching condition can be explained as, when photons from one or more waves are annihilated and new photons are created at different frequencies such that the net energy and momentum are conserved during the parametric process [122]. In FOPA, the phase-matching condition can be expressed in terms of momentum conservation as

$$\Delta K_M + \Delta K_W + \Delta K_{NL} = 0 \tag{B.9}$$

where $\Delta K_M$, $\Delta K_W$, and $\Delta K_{NL}$ are the wave-vector (or momentum) mismatch due to material dispersion, waveguide dispersion and the nonlinear effects respectively and are given as

$$\Delta K_M = [n_3\omega_3 + n_4\omega_4 - n_1\omega_1 - n_2\omega_2]/c$$

$$\Delta K_W = [\Delta b_3\omega_3 + \Delta b_4\omega_4 - \Delta b_1\omega_1 - \Delta b_2\omega_2]$$

$$\Delta K_{NL} = \gamma(P_1 + P_2) \tag{B.10}$$

Where $n$s are the index of refraction of core of the fiber, $\Delta b$s represents the difference of normalized propagation constant between core and cladding of the fiber for each wave, and $P_1$ and $P_2$ are the input pumps power. In order to satisfy the phase-matching condition (B.9) at least one of the terms in Eq. (B.10) should be negative. In single-mode fiber the phase-matching condition can be achieved in three different ways: 1) reducing the magnitude of $\Delta K_M$ and $\Delta K_{NL}$ by using small frequency shift and low pump powers since $\Delta K_W$ is very small compared with $\Delta K_M$ in single-mode fiber; 2) working near the zero group velocity dispersion wavelength so that $\Delta K_W$ nearly cancels the sum $\Delta K_M + \Delta K_{NL}$; and 3) working in the anomalous GVD regime so that $\Delta K_M$ is negative and cancels the sum $\Delta K_W + \Delta K_{NL}$. But in practice, it is very difficult to achieve the perfect phase-matching condition $\Delta\beta = 0$ due to different values of the refractive index of the material for different frequencies.

### *B.2.2 Theory for One Pump FOPA*

First consider the most general case of pump depletion where the pump power decreases along the length of the fiber; it requires a numerical solution of Eqs. (B.5) and (B.6). But under specific conditions, an analytic solution in terms of the elliptical function can be obtained [124]. Since, for every loss of one pump photon there is gain of each signal and idler photons i. e. the power of each waves either goes up or down by the same amount. If $x$ is the amount by which the power of each wave changes and the change of $x$ with fiber length is given by [123]

$$\frac{dx}{dZ} = 2\,P_1\sqrt{P_3P_4}\sin\theta \tag{B.11}$$

where $P_1$, $P_3$ and $P_4$ are the pump, signal and idler power respectively and $\theta$ is the relative phase defined as

$$\theta = \frac{\Delta\beta Z}{\gamma} + \theta_3 + \theta_4 - 2\theta_1 \tag{B.12}$$

With $P_1 = P_{10} - 2x$, $P_3 = P_{30} + x$ and $P_4 = P_{40} + x$, $P_{l0}$ is the initial power of the $l^{th}$ wave, Eq. (B.11) can be written as

$$\frac{dx}{dZ} = 2\sqrt{(P_{10} - 2x)^2(P_{30} + x)(P_{40} + x) - \frac{1}{4}\left\{K_1 + 3x^2 - \left(\frac{\Delta\beta}{\gamma} + \Delta P_0\right)x\right\}^2} = 2\sqrt{h(x)} \tag{B.13}$$

where $\Delta P_0 = 2P_{10} - P_{30} - P_{40}$, and $K_1 = 2P_{10}\sqrt{P_{30}P_{40}}\cos(\theta_{30} + \theta_{40} - 2\theta_{10})$ is the integration constant, and $\theta_{l0}$ is the initial phase of the $l^{th}$ wave.

The solution of Eq. (B.13) can be expressed in terms of Jacobian elliptic function (*sn*) and four roots of *h(x)*. In the absence of the idler at the input (i.e. $P_{40}=0$) then $x=0$ is one of the root. If $\eta_1$, $\eta_2$, $\eta_3$, and $\eta_4$are the four roots then the in power of each wave with respect to fiber length is given by

$$x(Z) = \eta_1 + (\eta_2 - \eta_1)\left\{1 - \eta sn^2\left(\frac{Z+Z_0}{Z_c}, k\right)\right\}^{-1} \tag{B.14}$$

where $Z_c = \frac{1}{|C_0|\sqrt{(\eta_3-\eta_1)(\eta_4-\eta_2)}}$

$$\eta = \frac{\eta_3-\eta_2}{\eta_3-\eta_1}$$

$$Z_0 = Z_c F\left(sin^{-1}\left[\frac{P_{40} - \eta_2}{\eta(P_{40} - \eta_1)}\right], k\right)$$

with $F(\varphi, k)$ the standard elliptical integral such that $F(0, k) = 0$ and $C_0 = \sqrt{7}/2$.

Eq. (B.14) is solved numerically to evaluate the change of pump, signal and idler power along the length of the fiber.

Since I am interested in mid-infrared (3-5 μm) generation, the idler wavelength should lie in this region. In order to choose the pump, signal and idler wavelength the phase matching condition along with energy conservation is solved i.e.

$$\Delta\beta = \beta_3 + \beta_2 - 2\beta_1 = 0 \text{ and } \omega_p = \omega_s + \omega_i \tag{B.15}$$

From the phase matching condition, it can be seen that the generated wavelengths depend on the group velocity dispersion (GVD) of the fiber used. As mentioned earlier, the parametric process depends on the fiber nonlinearity and the pump wavelength should be closer to the zero group velocity dispersion of the fiber. Since the highly nonlinear fiber has higher nonlinearity and zero group velocity wavelength can be tuned by changing the geometry of it, so we choose HNLF as a nonlinear material. The GVD of the HNLF along with SMF-28 is as shown in Figure B.2.

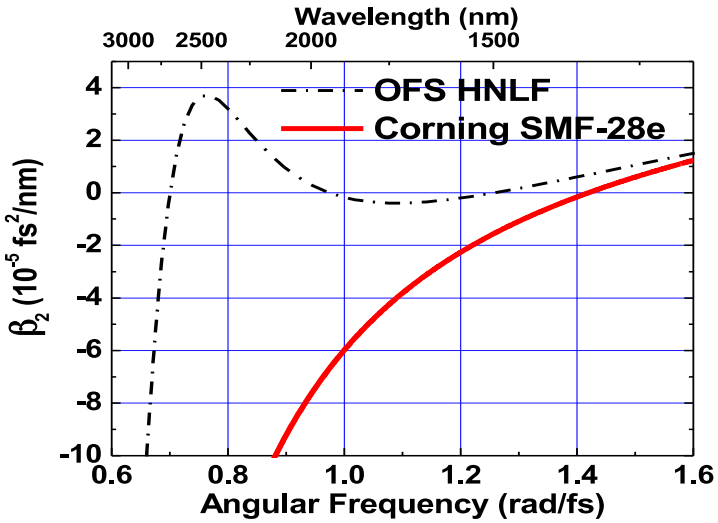


**Figure B.2 Group velocity dispersion of OFS HNLF compared to Corning SMF-28. The GVD of the HNLF was provided to us from OFS, while the GVD of the SMF was computed using the manufacture's core size, the Sellmeier coefficients, and the weakly guiding approximation.**

Eq. (B.15) is solved numerically in order to find the signal and idler wavelengths. In Figure B.3, $\Delta\beta$ as a function of frequency is plotted. When the phase matching condition $\Delta\beta = 0$ is imposed, the generated signal and idler wavelengths are 976.6 nm and 3097 nm respectively for the pump wavelength of 1485 nm.

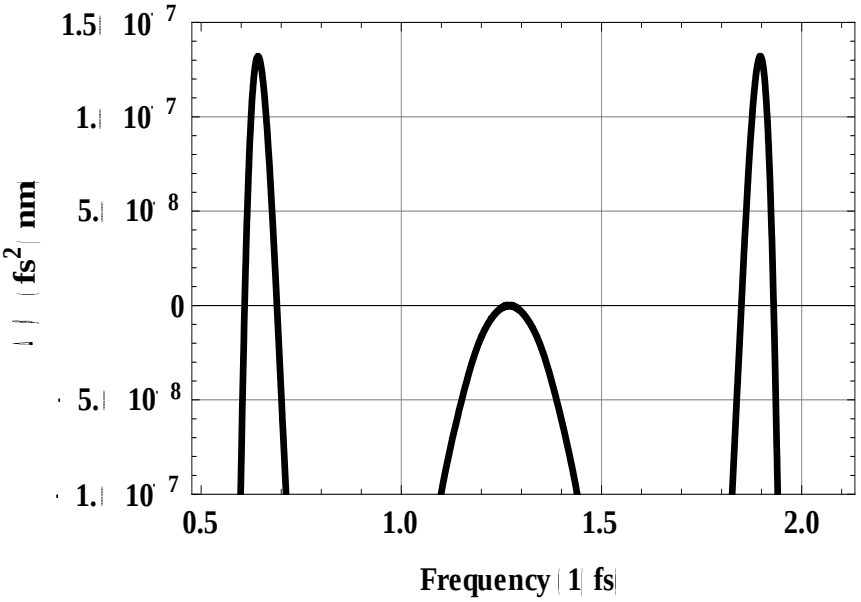


**Figure B.3 Plot of momentum mismatch with respect to frequency for highly nonlinear fiber with pump wavelength 1485 nm and power 300 mW. The signal and idler wavelengths can be evaluated at the point $\Delta\beta = 0$.**

After evaluating the signal and idler wavelengths, Eq. (B.14) is solved numerically with 300 mW of pump power and 10 mW of the signal power at the beginning of the fiber in order to get the gain in the signal and idler powers and loss in the pump power. Figure B.4 shows the plot of the gain in idler power ($P_4 = P_{40} + x$) with respect to the fiber length.

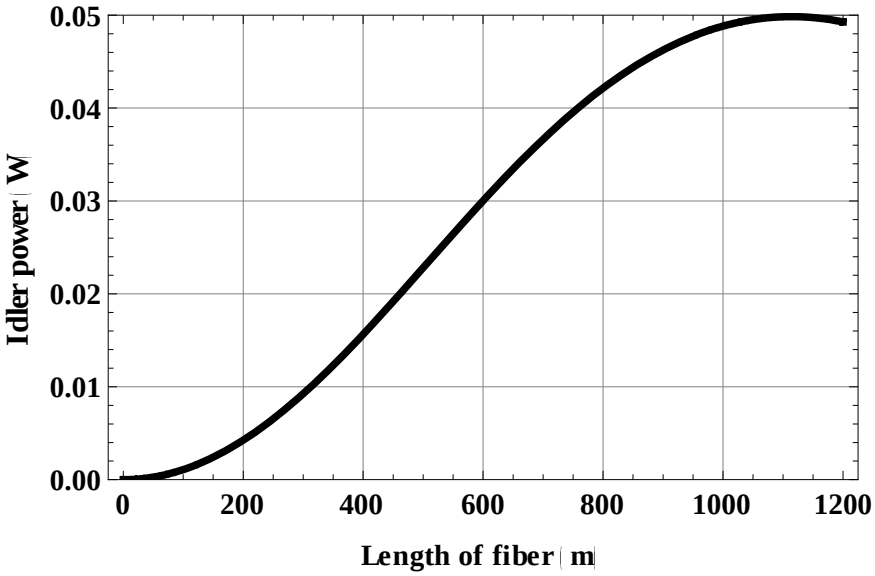


**Figure B.4 Gain in idler power with respect to fiber length for one pump FOPA. The idler wavelength is 3097 nm with pump power 300 mW and wavelength 1485 nm.**

Initially there is no idler present i.e. $P_{40} = 0$ at the input of the so idler power is zero at beginning of the fiber and starts to gain in power along the length of the fiber. It is seen from the plot that it required very long length of the fiber to get sufficient amount of idler at the output. The maximum idler power is obtained when the length of the fiber is 1100 m. After 1100 m of the fiber the idler power starts to decrease due to back conversion into the pump. The idler power at 1100 m of the fiber is 50 mW.

Similarly, the change in signal power ($P_3 = P_{30} + x$) with the fiber length is calculated same as in the case of idler wavelength. Figure B.5 shows the gain in signal power with respect to the length of HNLF.

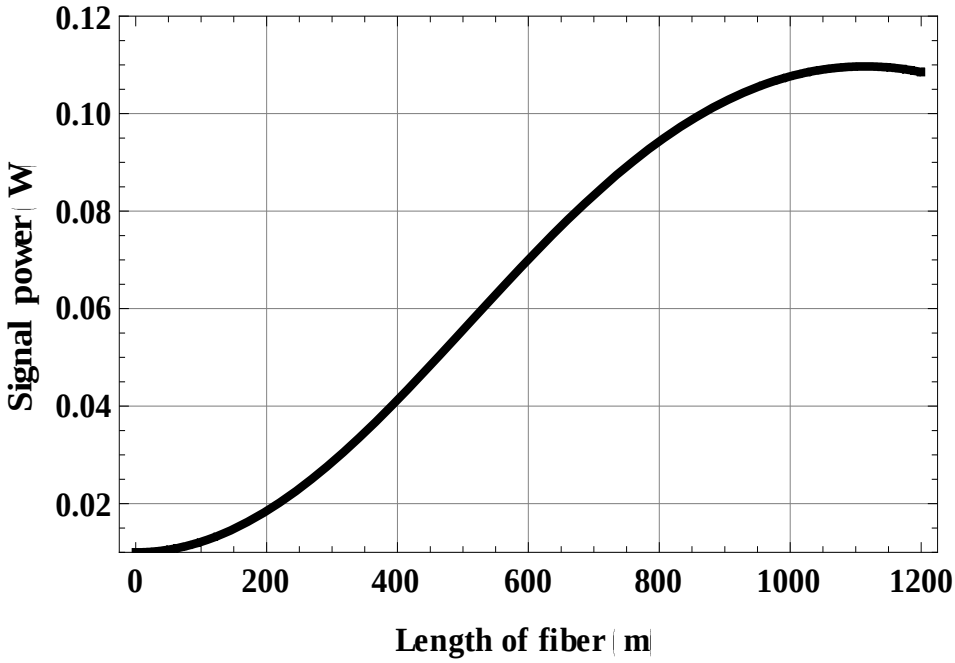


**Figure B.5 Gain in signal power with respect to fiber length for one-pump FOPA. The signal wavelength is 976.6 nm with pump power 300 mW and wavelength 1485 nm.**

As with the idler, the signal power also increases with the length of the fiber and reaches a maximum value at 1100 m of the fiber. The maximum signal power is 110 mW. The change in pump power with respect to the fiber length is as shown in Figure B.6. The pump power decreases with increasing fiber length. After 1100 m of fiber the signal and idler starts to combine back to create light at the pump wavelength. When the there is a pump deletion, the phase-mismatch changes along the length of the fiber and changes the relative phase $\theta$ from its initial value. When $\theta$ changes the sign both the signal and idler experience the deamplification [122] and convert back to the pump. So it is required to control the fiber length in order to get enough amplification of signal and idler even in the case of perfect phase-matching.

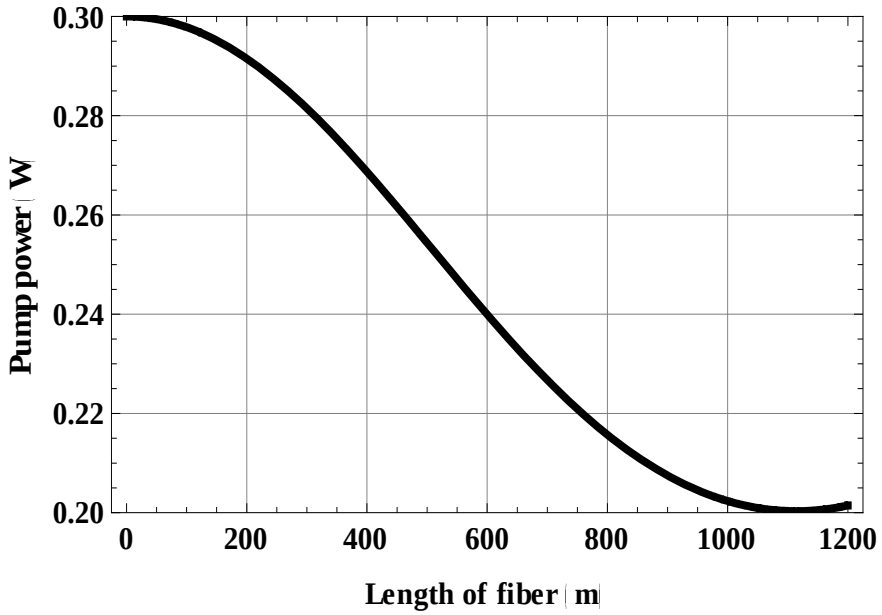


**Figure B.6 Loss in pump power (W) with respect to fiber length (m). The pump wavelength is 148 nm with pump power 300 mW and wavelength 1485 nm.**

### *B.2.3 Theory for Two Pump FOPA*

Similar to the one-pump FOPA, I derived the solution for the two pump FOPA equation for the case of pump depletion. The variation of change in loss in pump power and gain in signal and idler power is given by [123]

$$\frac{dx}{dZ} = -4\sqrt{P_1 P_2 P_3 P_4}\sin\theta \tag{B.16}$$

where the relative phase $\theta$ is given by

$$\theta = \frac{\Delta\beta Z}{\gamma} + \theta_3 + \theta_4 - \theta_1 - \theta_2 \tag{B.17}$$

with $P_1 = P_{10} - x$, $P_2 = P_{20} - x$, $P_3 = P_{30} + x$ and $P_4 = P_{40} + x$, and $P_{l0}$ is the initial power of the $l^{th}$ wave, Eq. (B.16) can be written as

$$\frac{dx}{dZ} = 2\sqrt{4(P_{10}-x)(P_{20}-x)(P_{30}+x)(P_{40}+x) - \frac{1}{4}\left[K_2 - \left(\frac{\Delta\beta}{\gamma} + \Delta P_0\right)x + 2x^2\right]^2}$$

$$= 2\sqrt{h(x)} \tag{B.18}$$

where $\Delta P_0 = P_{10} - P_{20} - P_{30} - P_{40}$, $K_1 = 4\sqrt{P_{10}P_{20}P_{30}P_{40}}\cos(\theta_{30} + \theta_{40} - \theta_{10} - \theta_{20})$ is the integration constant, and $\theta_{l0}$ is the initial phase of the $l^{th}$ wave.

The solution of Eq. (B.18) can be expressed in terms of Jacobian elliptic function (*sn*) and four roots of *h(x)*. If $\eta_1$, $\eta_2$, $\eta_3$, and $\eta_4$are the four roots then

$$x(Z) = \eta_1 + (\eta_2 - \eta_1)\left\{1 - \eta sn^2\left(\frac{Z+Z_0}{Z_c}, k\right)\right\}^{-1} \tag{B.19}$$

where $Z_c = \frac{1}{|C_0|\sqrt{(\eta_3-\eta_1)(\eta_4-\eta_2)}}$

$$\eta = \frac{\eta_3-\eta_2}{\eta_3-\eta_1}$$

$$Z_0 = Z_c F\left(sin^{-1}\left[\frac{P_{40}-\eta_2}{\eta(P_{40}-\eta_1)}\right], k\right)$$

with $F(\varphi, k)$ the standard elliptical integral such that $F(0, k) = 0$ and $C_0 = \sqrt{3}$.

To obtain loss in pump power and gain in signal and idler powers Eq. (B.19) is solved numerically and then plotted with respect to the fiber length. Same phase matching condition as in the one pump FOPA is used to calculate the signal and idler wavelengths for given pump wavelength, Figure B.3. Here, also I started with no idler at the input of the fiber and 10 mW of signal input with 300 mW of power of each pump, so the total pump power is about 600 mW.

Since $P_4 = P_{40}(0) + x$ and $P_{40}(0) = 0$, the gain in idler power is just *x*. The variation of idler power with respect to the fiber length is shown in Figure B.7. As in the one pump FOPA the idler power increases with the fiber length but due to more pump power at the input the gain is higher and requires less length of fiber in order to get same idler output. The idler power is 175 mW at 350 m of the fiber.

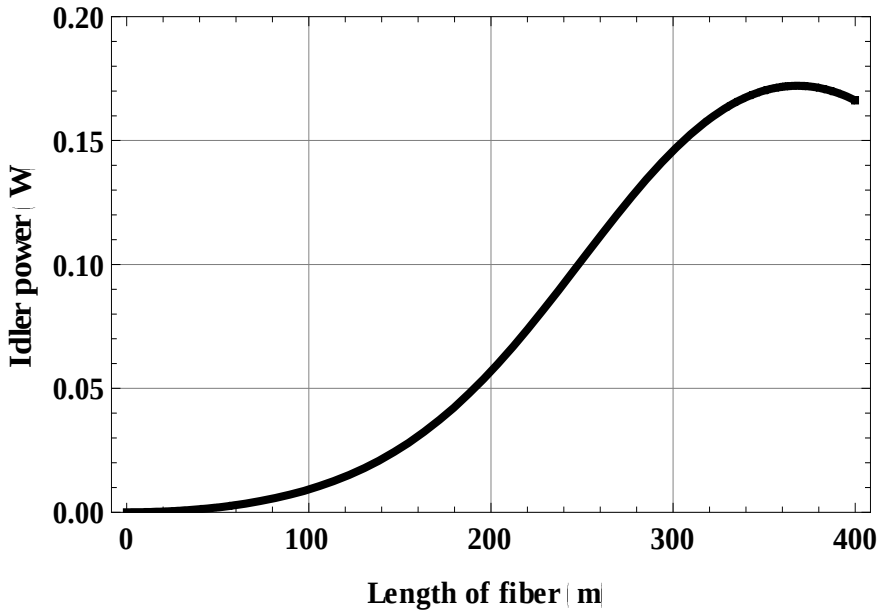


**Figure B.7 Gain in idler power with respect to fiber length for two-pump FOPA. The idler wavelength is 3097 nm with total pump power 600 mW and wavelength near 1485 nm**

The variation of the signal power with respect to the fiber length is as shown in Figure B.8. Same signal input power is used as in the case of one pump FOPA. The signal power starts from 0.01 W and becomes 0.35 W when the fiber length becomes 350 m. Due to presence of the two pump the gain in both signal and idler increases significantly.

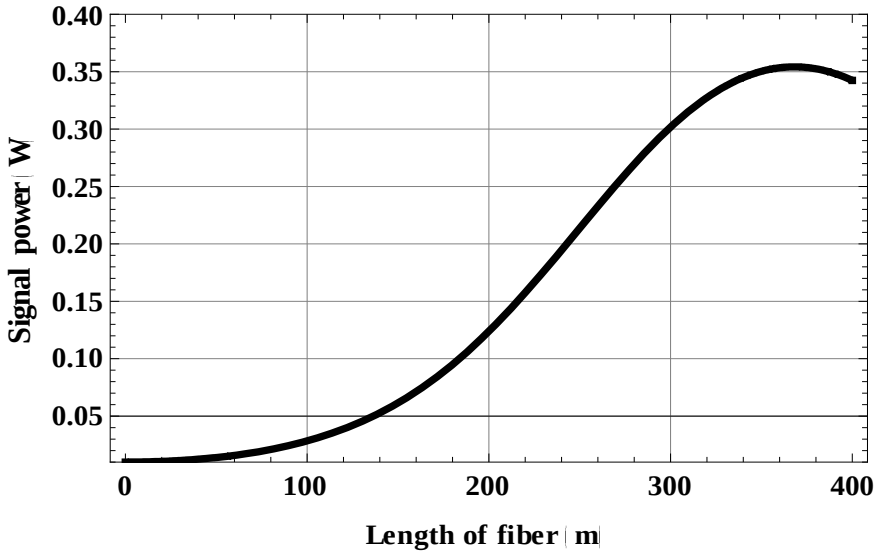


**Figure B.8 Gain in signal power with respect to fiber length for two-pump OPA. The idler wavelength is 976.6 nm with total pump power 600 mW and wavelength near 1485 nm.**

In Figure B.9, the variation of pump power with respect to fiber length is plotted. The pump power decreases as the fiber length increases and becomes 0.25 W at 350 m of the fiber.

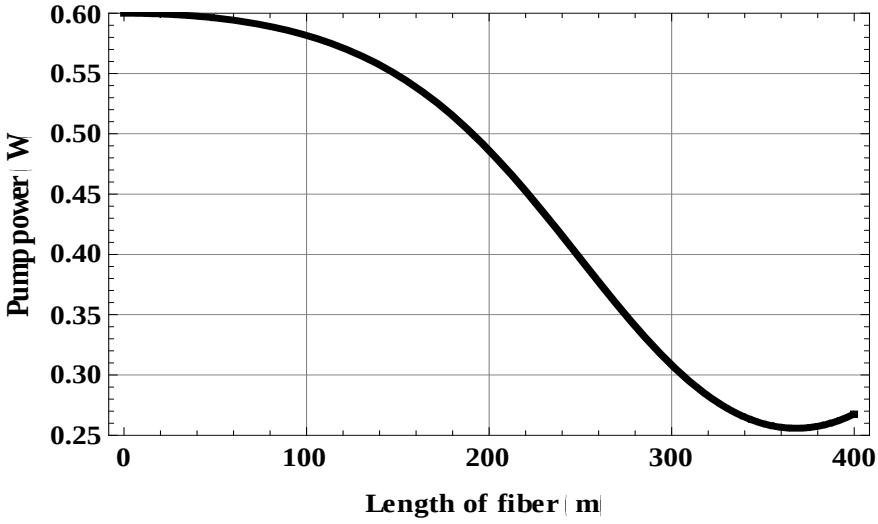


**Figure B.9 Loss in pump power with respect to fiber length for two-pump OPA. The idler wavelengths are 1485 nm with total pump power 600 mW and wavelength near 1485 nm.**

Above theoretical calculations show that significant gain in signal and idler wavelength can be achieved in both one pump and two pump FOPAs in reasonable length of the HNLF. Both one pump and two pump FOPAs are experimentally investigated with 90 m of HNLF and will be discussed in next section.

### *B.2.4 Experimental Setup*

#### B.2.4.1 One Pump FOPA

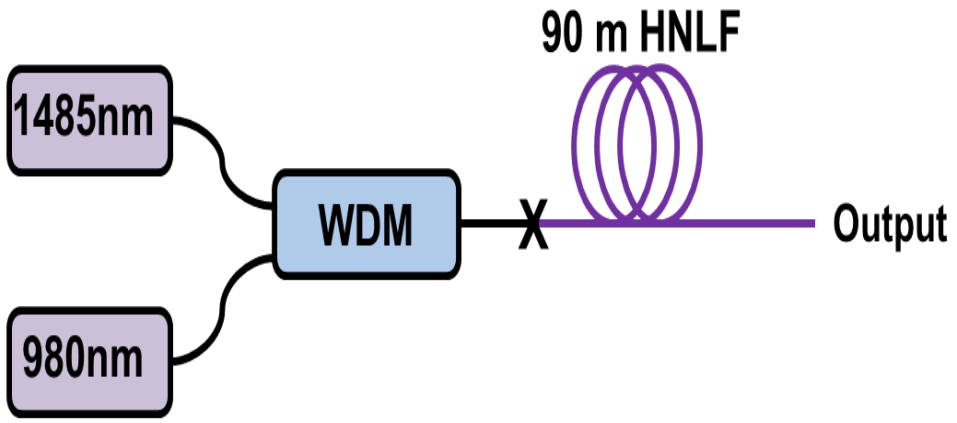


**Figure B.10 Schematic of the one pump FOPA. WDM; wavelength division multiplexer, HNLF; highly nonlinear fiber. Pump (1485 nm) and signal (980 nm) are combined using WDM and the output is measured after 90 m of HNLF.**

The experimental setup for the one pump FOPA is as shown in Figure B.10. The pump and signal wavelengths are chosen based on above theoretical calculation in order to generate the idler wavelength of our interest. The pump wavelength 1485 nm and signal wavelength 980 nm are combined using 1480/980 nm wavelength division multiplexer (WDM). For signal, 980 nm laser diode is used even in theoretical calculation the estimated signal wavelength is 976.6 nm

because 980 nm laser diode is easily available than 976.6 nm. 90 m of HNLF is used as a parametric medium for four wave mixing. One end of the HNLF is spliced with SMF and the splice loss is about 0.6 dB. The total pump power at the input end of the HNLF is always less than the power provided by the laser diode due to splice loss and the loss through the WDM. The signal and pump output after HNLF are measured by an optical spectrum analyzer (OSA) and a spectrometer is used to measure the idler wavelength.

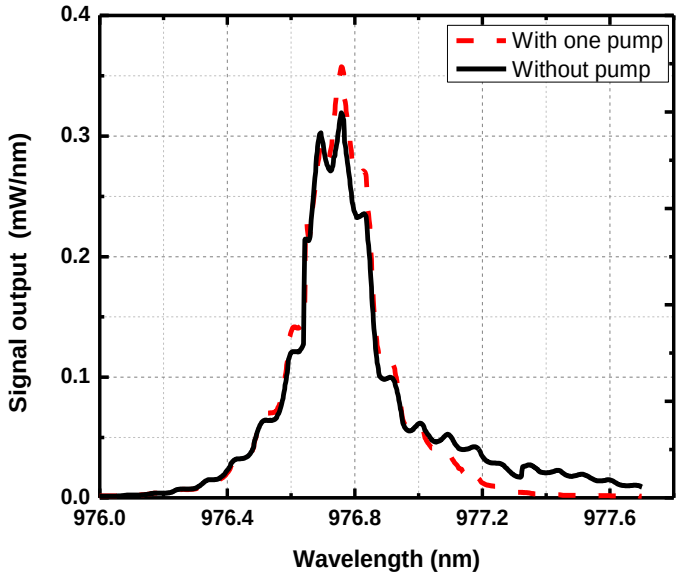


**Figure B.11 Signal spectrum before (black) and after (red) one pump optical parametric amplifier (OPA) when 250 mW of pump power at wavelength 1485 nm is used. The signal output spectrum is taken after 90 m of HNLF.**

Experimentally it is very hard to measure the power of each wave at different lengths of the fiber, so the signal, pump and idler powers are measured at the end of the fiber. The spectrum of output waves are measured first using the OSA and then power is measured. First, the spectrum of the signal is measured after the fiber when there is no pump present at the input. Then the fiber is pumped with a 1485 nm laser diode which ideally provides 300 mW and then

measured the spectrum of signal again. Due to loss through the WDM and the splice the total power at the input of the fiber is about 250 mW. The spectra for both the cases are shown in Figure B.11. The black curve represents when there is no pump at the input and red dash represents when there is one pump. Clearly, it is seen there is gain in the signal power. But the gain is not as significant compared with the theoretical calculation. This may due to the loss of signal through the fiber itself and the fact that pump is not depleted completely.

### B.2.4.2 Two Pump FOPA

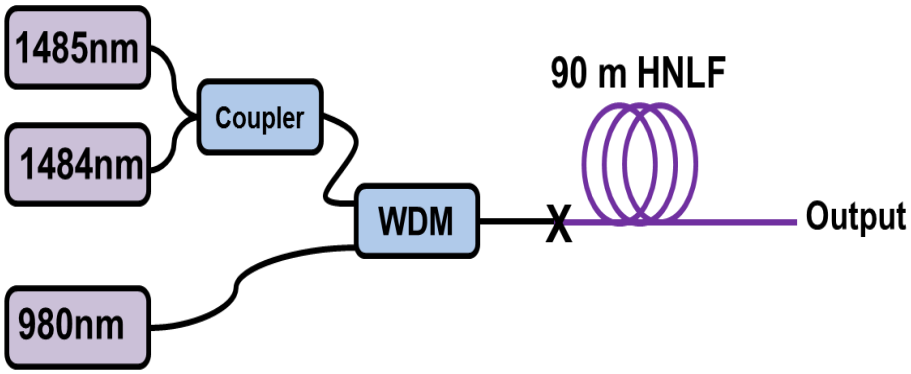


**Figure B.12 Schematic of the two-pump FOPA. WDM; wavelength division multiplexer, HNLF; highly nonlinear fiber. Two pump wavelengths are combined using polarization maintaining (PM) combiner and then combined with signal by WDM.**

The experimental setup for two-pump FOPA is as shown in Figure B.12. For two pump FOPA also the same signal and pump are used as for the one-pump FOPA but here one more pump almost at same frequency as the first pump is added. The two pump combined together using a polarization maintaining (PM) combiner. The total pump power then combined with signal using 980/1485 nm WDM and pump 90 m of the HNLF.

The spectra of the signal before and after pumping are shown in Figure B.13. It is clearly seen that the gain in signal in the two pumps FOPA is higher than the one pump FOPA which is in good agreement with the theoretical calculation. But the amount of gain doesn't match to the calculation due to the same reason as described in one pump FOPA.

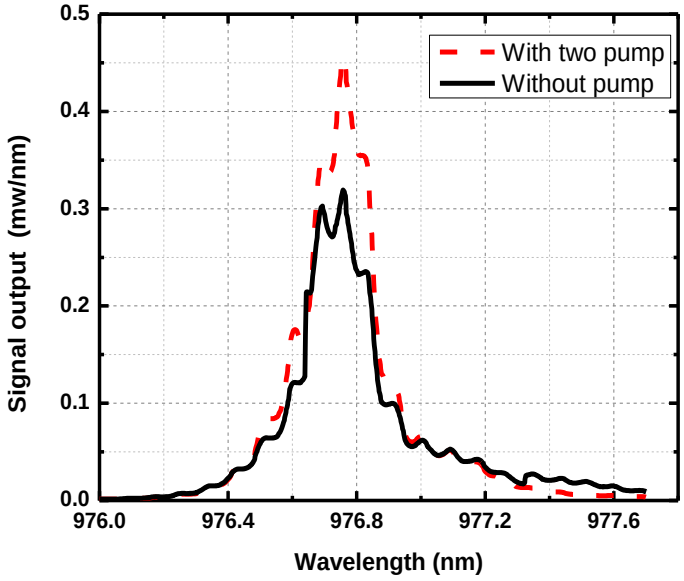


**Figure B.13 Signal spectrum before (black) and after (red) one-pump FOPA when 500 mW of pump power at wavelength 1485 nm is used. The signal output spectrum is taken after 90 m of HNLF.**

After measuring the spectrum of the signal wavelength, same kind of measurement for the pump wavelength is performed. The spectrum of the pump is measured when there is signal at the input and no signal and is shown in Figure B.14. The red curve represents when there is no pump at input and black represents when there is a signal at the input. As seen from the Figure B.14 the pump power decreases at the output when there is signal at the input but doesn't decrease as much as expected which at some level describe why enough gain in the signal is not

seen. The modulation on the pump spectrum is seen due to nonlinear effect such as self-phase modulation and cross-phase modulation inside the HNLF.

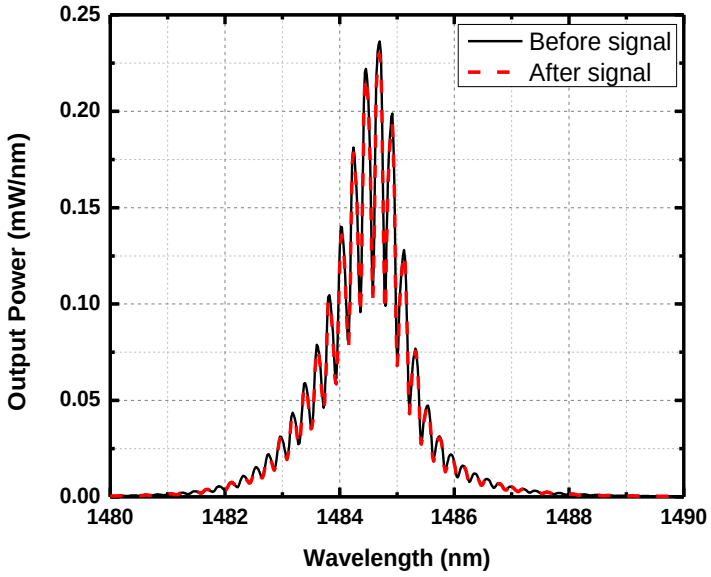


**Figure B.14 Pump spectrum before (black) and after (red) one pump FOPA when there is 10 mW of signal power at wavelength 980 nm at input. The pump output spectrum is taken after 90 m of HNLF.**

The gain in the signal and loss in the pump are seen during both the one- and two-pump cases suggesting that there should be gain in the idler due the energy conservation i.e. if there is loss of photon during parametric process there should be gain of signal and idler photons. During this FWM process the generated idler wavelength is 3097 nm which is the goal of this work. A grating spectrometer was used in order to measure the idler wavelength and hence power. The grating spectrometer has a diffraction grating of groove density of 300 groove/mm blazed at wavelength 3 μm with blaze angle of $26^{o}$. But unfortunately, no light was observed at the output of the spectrometer at the idler wavelength 3097 nm. This is due to the loss through the fiber at

the idler wavelength because the fiber we used for FOPA is made with fused silica. The loss at longer wavelength in fused silica is very high as shown in Figure B.15.

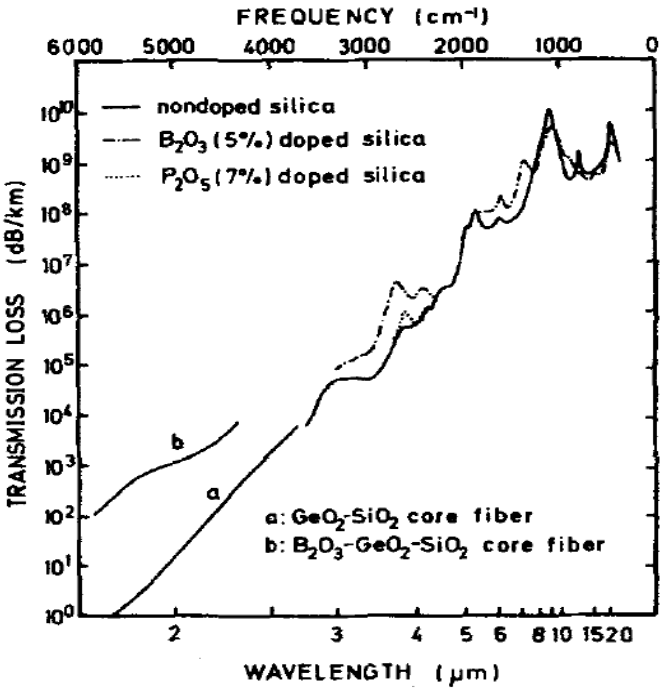


**Figure B.15 Absorption spectra of non-doped fused silica, doped fused silica and fibers. This graph is reproduced from Ref. [65].**

To confirm above conclusion, the loss through the fused silica fiber is measured. He-Ne laser was used as a mid-infrared source which emits the light at 3.39 μm and multi-mode fiber made with fused silica in order to couple more light into the fiber. After the couple measurement, the calculated loss through the fiber is around 121 dB/m at 3.39 μm which is quite high compared with 0.2 dB/km at 1.55 μm.

## B.3 Summary

I have investigated the FOPA both theoretically and experimentally to generate the mid-infrared. The gain in both signal and idler wavelengths is significant after 90 m of HNLF based on theoretical calculation. Experimentally, the gain in signal wavelength was seen but did not observed idler wavelength due to high loss of fused silica fiber at this wavelength.

This work suggests that the mid-infrared generation via FWM in HNLF is not a good solution. Mid-infrared supercontinuum can be generated in other kind of fiber such as fluoride (ZBLAN) fiber while pumping by high power near-infrared laser [125]. But efficiency of the mid-infrared supercontinuum generation can be increased if one can use longer wavelength as a pump source. So, pulsed 2 μm laser is a good candidate as a pumping source.

# Appendix C - Computation of Group Velocity Dispersion of UHNA Fibers

## Calculation of Dispersion of Fused Silica Fiber and High NA Fibers

### Material dispersion

```
A1 = 0.6961663; A2 = 0.4079426; A3 = 0.8974794;
B1 = 0.0684043; B2 = 0.1162414; B3 = 9.896161;
c = 300.0;
```

$$n_0[\omega\_] = \sqrt{1 + \frac{A1\,(\frac{2\pi c}{\omega}/1000)^2}{(\frac{2\pi c}{\omega}/1000)^2 - B1^2} + \frac{A2\,(\frac{2\pi c}{\omega}/1000)^2}{(\frac{2\pi c}{\omega}/1000)^2 - B2^2} + \frac{A3\,(\frac{2\pi c}{\omega}/1000)^2}{(\frac{2\pi c}{\omega}/1000)^2 - B3^2}};$$

```
Plot[n0[ω], {ω, 0.5, 2.5}, Frame → True, FrameLabel → {"Frequency(1/fs)", "Refractive index(n0[ω]"}]
```

### Waveguide dispersion

**Radius and NA should change for different fibers.**

**For UHNA1, r = 1.25 $\mu$m, NA = 0.28**
**For UHNA3, r = 0.9 $\mu$m, NA = 0.35**
**For UHNA1, r = 1.1 $\mu$m, NA = 0.35**
**For UHNA1, r = 1.2 $\mu$m, NA = 0.41**
**For SMF, r = 4.1 $\mu$m, NA = 0.14**

```
NA = 0.35; r = 1100; (*UHNA4 fiber*)
```

$$\Delta n = \frac{NA^2}{2\,n_0[\omega]};$$

$$v[\omega\_] = \frac{r\,\omega}{c}\,n_0[\omega]\,\sqrt{2\,\Delta n};$$

$$b[\omega\_] = 1 - \left(\frac{1+\sqrt{2}}{1+\sqrt[4]{4+v[\omega]^4}}\right)^2;$$

$$n[\omega\_] = n_0[\omega]\,\sqrt{1 + 2\,\Delta n\,b[\omega]};$$

### Calculation of second order dispersion

$$\beta[\omega\_] = \frac{n[\omega]\,\omega}{c};$$

$$\beta 2[\omega\_] = \partial_\omega\,(\partial_\omega\,\beta[\omega]);$$

```
Plot[β2[ω], {ω, 0.5, 2.5}, Frame → True,
 FrameLabel → {Style["Frequency(1/fs)", Bold, 12], Style["β2(fs²/nm)", Bold, 12]},
 PlotStyle → {Black, Thickness[0.007]}, FrameStyle → Directive[Thick], FrameTicksStyle → Directive[12, Bold],
 GridLines → Automatic, GridLinesStyle → Directive[Automatic, Blue]]
```

```
Plot[β2[2 π c/λ], {λ, 800, 3500}, Frame → True,
 FrameLabel → {Style["Wavelength(nm)", Bold, 12], Style["β2(fs²/nm)", Bold, 12]},
 PlotStyle → {Black, Thickness[0.007]}, FrameStyle → Directive[Thick], FrameTicksStyle → Directive[12, Bold],
 GridLines → Automatic, GridLinesStyle → Directive[Automatic, Blue]]
```

### Calculation of third order dispersion

$$\beta 3[\omega\_] = \partial_\omega\,\beta 2[\omega];$$

```
Plot[β3[ω], {ω, 0.5, 2.5}, Frame → True,
 FrameLabel → {Style["Frequency(1/fs)", Bold, 12], Style["β3(fs³/nm)", Bold, 12]},
 PlotStyle → {Black, Thickness[0.007]}, FrameStyle → Directive[Thick], FrameTicksStyle → Directive[12, Bold],
 GridLines → Automatic, GridLinesStyle → Directive[Automatic, Blue]]
```

```
Plot[β3[2 π c/λ], {λ, 800, 3500}, Frame → True,
 FrameLabel → {Style["Wavelength(nm)", Bold, 12], Style["β3(fs³/nm)", Bold, 12]},
 PlotStyle → {Black, Thickness[0.007]}, FrameStyle → Directive[Thick], FrameTicksStyle → Directive[12, Bold],
 GridLines → Automatic, GridLinesStyle → Directive[Automatic, Blue]]
```

# Appendix D - License for Using Figures

## D.1 Nature photonics

**NATURE PUBLISHING GROUP LICENSE TERMS AND CONDITIONS**

Apr 10, 2014

This is a License Agreement between Rajesh Kadel ("You") and Nature Publishing Group ("Nature Publishing Group") provided by Copyright Clearance Center ("CCC"). The license consists of your order details, the terms and conditions provided by Nature Publishing Group, and the payment terms and conditions.

**All payments must be made in full to CCC. For payment instructions, please see information listed at the bottom of this form.**

| | |
|---|---|
| License Number | 3353740188973 |
| License date | Mar 21, 2014 |
| Licensed content publisher | Nature Publishing Group |
| Licensed content publication | Nature Photonics |
| Licensed content title | Mid-infrared frequency combs |
| Licensed content author | Albert Schliesser, Nathalie Picqué, Theodor W. Hänsch |
| Licensed content date | Jun 28, 2012 |
| Volume number | 6 |
| Issue number | 7 |
| Type of Use | reuse in a dissertation / thesis |
| Requestor type | academic/educational |
| Format | print and electronic |
| Portion | figures/tables/illustrations |
| Number of figures/tables/illustrations | 2 |
| High-res required | No |
| Figures | Figure 1 Molecular mid-infrared fingerprints and the principle of the laser frequency comb. |
| Author of this NPG article | No |
| Your reference number | |
| Title of your thesis / | Laser dynamics of a mode-locked thulium/holmium fiber laser in the |

| | |
|---|---|
| dissertation | solitonic and the stretched pulse regimes |
| Expected completion date | May 2014 |
| Estimated size (number of pages) | 135 |
| Total | 0.00 USD |
| Terms and Conditions | |

## Terms and Conditions for Permissions

Nature Publishing Group hereby grants you a non-exclusive license to reproduce this material for this purpose, and for no other use,subject to the conditions below:

1. NPG warrants that it has, to the best of its knowledge, the rights to license reuse of this material. However, you should ensure that the material you are requesting is original to Nature Publishing Group and does not carry the copyright of another entity (as credited in the published version). If the credit line on any part of the material you have requested indicates that it was reprinted or adapted by NPG with permission from another source, then you should also seek permission from that source to reuse the material.
2. Permission granted free of charge for material in print is also usually granted for any electronic version of that work, provided that the material is incidental to the work as a whole and that the electronic version is essentially equivalent to, or substitutes for, the print version.Where print permission has been granted for a fee, separate permission must be obtained for any additional, electronic re-use (unless, as in the case of a full paper, this has already been accounted for during your initial request in the calculation of a print run).NB: In all cases, web-based use of full-text articles must be authorized separately through the 'Use on a Web Site' option when requesting permission.
3. Permission granted for a first edition does not apply to second and subsequent editions and for editions in other languages (except for signatories to the STM Permissions Guidelines, or where the first edition permission was granted for free).
4. Nature Publishing Group's permission must be acknowledged next to the figure, table or abstract in print. In electronic form, this acknowledgement must be visible at the same time as the figure/table/abstract, and must be hyperlinked to the journal's homepage.

5. The credit line should read:
   Reprinted by permission from Macmillan Publishers Ltd: [JOURNAL NAME] (reference citation), copyright (year of publication)
   For AOP papers, the credit line should read:
   Reprinted by permission from Macmillan Publishers Ltd: [JOURNAL NAME], advance online publication, day month year (doi: 10.1038/sj.[JOURNAL ACRONYM].XXXXX)

   **Note: For republication from the *British Journal of Cancer,* the following credit lines apply.**
   Reprinted by permission from Macmillan Publishers Ltd on behalf of Cancer Research UK: [JOURNAL NAME] (reference citation), copyright (year of publication)For AOP papers, the credit line should read:
   Reprinted by permission from Macmillan Publishers Ltd on behalf of Cancer Research UK: [JOURNAL NAME], advance online publication, day month year (doi: 10.1038/sj.[JOURNAL ACRONYM].XXXXX)

6. Adaptations of single figures do not require NPG approval. However, the adaptation should be credited as follows:

   Adapted by permission from Macmillan Publishers Ltd: [JOURNAL NAME] (reference citation), copyright (year of publication)

**Note: For adaptation from the *British Journal of Cancer,* the following credit line applies.**
Adapted by permission from Macmillan Publishers Ltd on behalf of Cancer Research UK: [JOURNAL NAME] (reference citation), copyright (year of publication)

7. Translations of 401 words up to a whole article require NPG approval. Please visit http://www.macmillanmedicalcommunications.com for more information.Translations of up to a 400 words do not require NPG approval. The translation should be credited as follows:

   Translated by permission from Macmillan Publishers Ltd: [JOURNAL NAME] (reference citation), copyright (year of publication).

   **Note: For translation from the *British Journal of Cancer,* the following credit line applies.**
   Translated by permission from Macmillan Publishers Ltd on behalf of Cancer Research UK: [JOURNAL NAME] (reference citation), copyright (year of publication)

We are certain that all parties will benefit from this agreement and wish you the best in the use of this material. Thank you.

Special Terms:

v1.1

**If you would like to pay for this license now, please remit this license along with your payment made payable to "COPYRIGHT CLEARANCE CENTER" otherwise you will be invoiced within 48 hours of the license date. Payment should be in the form of a check or money order referencing your account number and this invoice number RLNK501257538. Once you receive your invoice for this order, you may pay your invoice by credit card. Please follow instructions provided at that time.**

**Make Payment To:**
**Copyright Clearance Center**
**Dept 001**
**P.O. Box 843006**
**Boston, MA 02284-3006**

**For suggestions or comments regarding this order, contact RightsLink Customer Support: customercare@copyright.com or +1-877-622-5543 (toll free in the US) or +1-978-646-2777.**

**Gratis licenses (referencing $0 in the Total field) are free. Please retain this printable license for your reference. No payment is required.**

## D.2 Optical Society of America

Dear Rajesh Kadel,

Thank you for contacting The Optical Society.

OSA considers your requested use of its copyrighted material to be Fair Use under United States Copyright Law. It is requested that a complete citation of the original material be included in any publication.

Let me know if you have any questions.

Kind Regards,

Susannah Lehman

```
Susannah Lehman
March 26, 2014
Authorized Agent, The Optical Society
```

**From:** Kadel, Rajesh [mailto:rkadel@phys.ksu.edu]
**Sent:** Thursday, March 20, 2014 5:55 PM
**To:** pubscopyright
**Subject:** permission for using figures

Hi,

I am writing my PhD thesis and would like to use few figures that already published. I would like to get permission to use some figures.

(1)The figures that I would like to use are Figure 1 and Figure 2 from the following Journal

OPTICS LETTERS / Vol. 19, No. 4 / February 15, 1994

Title: Continuous-wave oscillation of thulium-sensitized holmium-doped silica fiber laser.

Authors: Kyunghwan Oh, T. F. Morse, A. Kilian, L. Reinhart and P. M. Weber.

(2) Other two figures that I would like to use are Figure 2 (a) and (b) from following

OSA/CLEO 2011, PDPA5

Title : *Self-referenced frequency comb from a Tm-fiber via PPLN waveguide supercontinuum generation.*

Authors：C. R. Phillips, J. Jiang, C. Langrock, M. M. Fejer, and M. E. Fermann

I hope I can use them.

Thank you

Rajesh Kadel

Kansas State University

## D.3 Physical Review Letter

### *D.3.1 Features for Authors*

- Free Color Online - There is no charge for color figures in our online journals. (For print journals there is an additional per figure charge. More information.)
- Open Access - Authors of accepted manuscripts may choose to pay an article-processing charge whereby their work is made open access, i.e., available to all readers at no cost and without a subscription, upon publication. Such articles are published under the terms of the Creative Commons Attribution 3.0 License (CC-BY), the most permissive of the CC licenses, which permits authors and others to copy, distribute, transmit, and adapt the work, provided that proper credit is given.
- Online Manuscript Submission - Online submission of manuscripts via the web.
- Online Manuscript Status Check- The Author Status Inquiry System (ASIS) allows authors of manuscripts under consideration by our journals to obtain immediate information on the status of their papers electronically.
    - For papers that have been accepted for publication, information about their status in the production process is available via a service maintained by the production vendor. A link to this service is provided as part of the information provided by ASIS for such papers.

- Native Language Author Name Display - Chinese, Japanese, and Korean authors can choose to have their names displayed in their own language.
- Forms and Memos - Direct access to journal-related forms and memos.

### *D.3.2 Features for Readers*

- Editors' Suggestions - Marked papers that the editors hope will lead readers to explore other areas of physics. Please see our Announcement PRL 98, 010001 (2007).
- Email ToC Alerts - Receive table of contents email alerts as new journal issues are complete.
- RSS Feeds - Subscribe to a variety of Editor-selected cross-journal feeds as well as individual journal RSS feeds.
- Accepted Papers Lists - Access listings of recently accepted papers in advance of publication
- Single Article Purchases - Nonsubscribers can purchase journal articles in PDF format directly from links on the abstract page.
- Article Packs - For APS members, Article Packs allow flexible online access to key research articles spanning all of *Physical Review*.
- Free Access to Some Content:
    - Browsing the Tables of Contents (PDF and HTML), viewing abstracts, or searching for articles does not require a subscription.
    - Open Access - Authors of accepted manuscripts may choose to pay an article-processing charge whereby their work is made open access, i.e., available to all readers at no cost and without a subscription, upon publication. Such articles are published under the terms of the Creative Commons Attribution 3.0 License (CC-BY), the most permissive of the CC licenses, which permits authors and others to copy, distribute, transmit, and adapt the work, provided that proper credit is given